VALIDATION OF ILLUMINANCE VALUES OBTAINED BY HDRI EXTERIOR LUMINANCE MAPPING

Alayne Nyboer

A Project Submitted

In Partial Fulfillment of the Requirements for the Degree of

Master of Science in Architectural Engineering

at

LAWRENCE TECHNOLOGICAL UNIVERSITY

21000 West Ten Mile Road

Southfield, MI 48075

May 14, 2021

ABSTRACT:

High dynamic range imaging (HDRI) is a photography tool used for measuring lighting metrics. Luminance maps created with HDRI is a technique popularly used to study visual environments. However, research using HDRI to evaluate illuminance is lacking. This project investigates whether HDRI can be used to obtain illuminance values in an exterior environment. Previous studies show that HDRI can be used as a luminance mapping tool in a wide range of applications with an accuracy of 10%. Yet no research has been done furthering the process to become an illuminance data acquisition tool in an exterior scene. This research aims to provide validation of using HDR photography to create an illuminance map to evaluate large exterior environments. It also addresses proper HDRI data collection processes to minimize error, commonly made mistakes and aspects requiring special attention. Field measurements and measurement retrieved from HDR images were evaluated and compared. Results from the research indicate the proposed methodology can be used to accurately estimate illuminance values obtained through HDRI in exterior environments.

05/13/2021

Dr. Arpan Guha

Date

Department of Civil and Architectural Engineering

TABLE OF CONTENTS

1.0 Introduction and Background 1
- 1.1 Basis of Lighting Measurements 4
- 1.2 Luminance 4
- 1.3 Illuminance 6
- 1.4 Reflectance 8
- 1.5 High Dynamic Range Imaging (HDRI) 10
- 1.6 Conclusions 13

2.0 Literature Review 14
- 2.1 Miscellaneous Lighting Parameters 20
- 2.2 Luminance 23
- 2.3 Illuminance 30
- 2.4 Conclusions 36

3.0 Methodology 37
- 3.1 Research Objectives 38
- 3.2 Requirements 39
- 3.3 Environmental Considerations and Constraints 40
- 3.4 Camera Set Up 40
- 3.5 Grass Reflectance 41
- 3.6 Image File Format 42
- 3.7 Number of Image Files and Camera Settings 42
- 3.8 Reflectance Standards 44
- 3.9 Merging Low Dynamic Range Images 44
- 3.10 Vignetting Correction 45
- 3.11 Calibrating Final High Dynamic Range Images 46
- 3.12 Luminance Maps 47
- 3.13 Number of Data Points 47
- 3.14 Calculating Illuminance from Luminance 49
- 3.15 Procedure 55

4.0 Data Collection 59
- 4.1 Equipment Evaluation – Indoors 59
- 4.2 Pilot Study – Outdoors 63
- 4.3 Final Data Collection 67

5.0 Conclusions 73

6.0 References 74

LIST OF FIGURES

Figure 1. What is Light? 1
Figure 2. What Does the Human Eye See? 1
Figure 3. Relationships Between the 5 Basic Lighting Parameters 3
Figure 4. 1 Steradian and 1 Solid Angle 4
Figure 5. Luminance 5
Figure 6. Relationship of Lighting Measurements 5
Figure 7. Illuminance 6
Figure 8. Appearance vs Illuminance 7
Figure 9. Table A-2 from IES Lighting Handbook: Lighting Sports and Recreational Areas 7
Figure 10. Specular Reflection vs. Diffuse Reflection 8
Figure 11. Material Samples with Different Reflectance Properties 9
Figure 12. Roadway Reflections 9
Figure 13. Comparison of LDR and HDR Images 10
Figure 14. Studio Scene 12
Figure 15. Notre Dame Scene 12
Figure 16. Different Reflectance Properties in Low Dynamic Range Images 12
Figure 17. Debevec and Malik 1997 20
Figure 18. Camera Models Used in Miscellaneous HDRI Studies 22
Figure 19. Lens Models Used in Miscellaneous HDRI Studies 22
Figure 20. Error in Reflectance for Munsell Chips of Different Hues, Values and Illuminance Levels 24
Figure 21. Outdoor Scene with Grayscale Targets under Overcast Sky and Clear Sky 25
Figure 22. Percent Error for 70 Color Samples with Maximum Chroma 26
Figure 23. Gray Cards Reflected in Chrome Mirror Ball 26
Figure 24. Gray Cards on Roof 26
Figure 25. Camera Models used in Luminance Studies 29
Figure 26. Lens Models used in Luminance Studies 29
Figure 27. Wallpaper Patches for Illuminance Map 31
Figure 28. Camera View Tests for Illuminance Measurements 31
Figure 29. Camera with 180-degree Fisheye Lens and Typical Probe 32
Figure 30. UAV Route and Measurement Grid 33
Figure 31. Radiation that Reaches Luxmeter on UAV 33
Figure 32. Camera Models used in Illuminance Studies 34
Figure 33. Lens Models used in Illuminance Studies 35
Figure 34. Unrecorded Data in Literature Review 36
Figure 35. Reflective Properties of Grass and Natural Vegetation 41
Figure 36. Camera Settings Used in Sequence of Multiple Exposures for HDR Photography 43
Figure 37. Vignetting Function of Lens 45
Figure 38. Suggested Soccer Field Calculation Grid 48
Figure 39. Suggested Football Calculation Grid 48
Figure 40. Calculation of Illuminance from Luminance Values in Hemispherical Fisheye Projection 49
Figure 41. Geometry of Illuminance Calculations 51
Figure 42. Reflection from a Lambertian Surface 52
Figure 43. A Lambertian Emitter Illuminating the Interior of a Sphere 53

Figure 44. Spectral Reflectance of Grass 54
Figure 45. Camera and Tripod Setup for Pilot Study and Final Data Collection 55
Figure 46. Camera View with Reflectance Standard & Grid Centered, Final Data Collection ... 56
Figure 47. Konica Minolta CL-70F Illuminance Meter Recording Measurements at the Center of each Grid in Final Data Collection 57
Figure 48. Equipment Evaluation series of Low Dynamic Range Images 60
Figure 49. Final HDR Image: Equipment Evaluation 61
Figure 50. Equipment Evaluation False Color Image 61
Figure 51. Equipment Evaluation Final HDR Image with Grid Overlay 62
Figure 52. Pilot Study Outdoors Series of Low Dynamic Range Images – Location 1 64
Figure 53. Pilot Study Outdoors Series of Low Dynamic Range Images – Location 2 64
Figure 54. Final HDR Image: Piot Study Outdoors Location 1 65
Figure 55. Final HDR Image: Pilot Study Outdoors Location 2 65
Figure 56. Pilot Study Location 1 False Color Image 66
Figure 57. Pilot Study Location 1 Final HDR Image with Grid Overlay 66
Figure 58. Final Data Collection Series of Low Dynamic Range Images with Grid Present 68
Figure 59. Final Data Collection Series of Low Dynamic Range Images without Grid Present .. 68
Figure 60. Final HDR Image 69
Figure 61. Final Data Collection False Color Image 69

LIST OF TABLES

Table 1. Miscellaneous HDRI Lighting Parameters Comparison Table 15
Table 2a. Luminance HDRI Comparison Table 16
Table 2b. Luminance HDRI Comparison Table 17
Table 2c. Luminance HDRI Comparison Table 18
Table 3. Illuminance HDRI Comparison Table 19
Table 4. Equipment Evaluation HDRI Luminance Map Values from Photosphere 63
Table 5. Pilot Study Location 1 HDRI Luminance Map Values from Photosphere 67
Table 6. Final Data Collection Luminance Map Values from HDRI in Photosphere 70
Table 7. Illuminance Measurements taken from Illuminance Meter on Scene 71
Table 8. Illuminance Calculations using Methodology with HDRI Luminance Values 71
Table 9. Illuminance Percent Errors for Each Grid 72
Table 10. Percent Error Color Grid 72

1.0 INTRODUCTION AND BACKGROUND:

Light is the part of the electromagnetic spectrum that can be perceived by the human eye; visible light is a relatively small portion of the entire electromagnetic spectrum, between 380 and 780 nm as shown in Figure 1. Figure 2 displays the perception of brightness in daytime, as seen with the cones in the human eye, and during nighttime, as seen with the rods in the human eye.

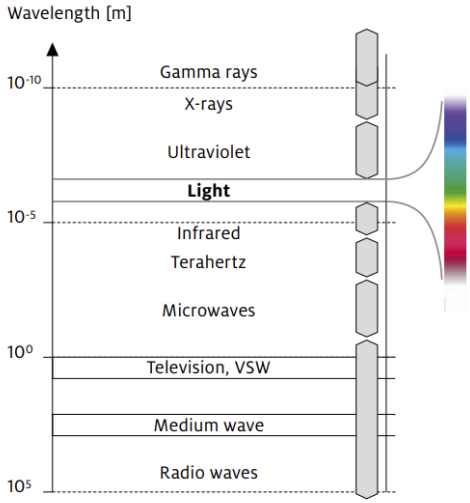

Figure 1. What is Light? (Zumtobel Lighting GmbH 2018)

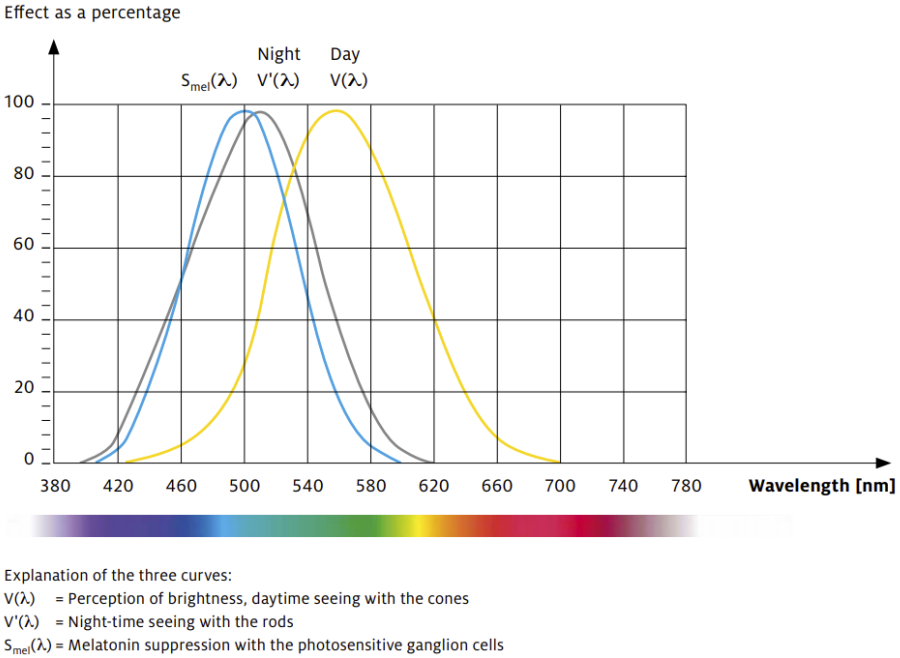

Figure 2. What Does the Human Eye See? (Zumtobel Lighting GmbH 2018)

The practice of human centric lighting expresses the positive effect of light and lighting on the health, well-being and performance of humans and thus has both short-term and long-term benefits (Zumtobel Lighting GmbH 2018). The previous narrative and interpretation of "better" lighting in a space was to simply provide more "light" or illumination in order to achieve "better" lighting. This is no longer the case; experience has shown that inefficiency, eye fatigue, spoiled work and accidents have all been blamed on the lighting system in the particular space. This indicates that there is more to lighting than just a sufficient amount of light in the space.

For humans, light has a triple effect (Zumtobel Lighting GmbH 2018). Lighting for visual functions includes illumination of task areas in conformity with relevant standards, such as the Illuminating Engineering Society's (IES) Lighting Handbook, and a glare-free, convenient lighting system. Lighting for emotional perception can be seen by enhancing architectural features as well as creating scenes and effects, such as in movies. Finally, lighting can have biological effects on humans, such as supporting individual circadian rhythms and either stimulating or relaxing humans (Zumtobel Lighting GmbH 2018).

Lighting design is now a much more detailed process as the focus is now on providing occupants of certain spaces with appropriate and beneficial lighting, rather than simply adequate lighting. The criteria now investigated in the light design process now include; sufficient illumination level, harmonious brightness distribution, glare limitation, reflection avoidance, correct light color, appropriate color rendering, among many others depending on the space type and design goals. In evaluating lighting overall and specific lighting fixtures, five basic metrics are used; luminous flux, luminous intensity, luminous exitance, illuminance and luminance. The relationship between four of these metrics can be seen on the next page in Figure 3. While only illuminance and luminance will be discussed in detailed in this research, understanding the difference between all these metrics is fundamental in order to fully comprehend the study. It can be seen that all metrics are directly related to each other and can be calculated quite simply using other lighting metrics, reflectance values and subject areas.

Luminous flux – Luminous intensity – Illuminance – Luminance

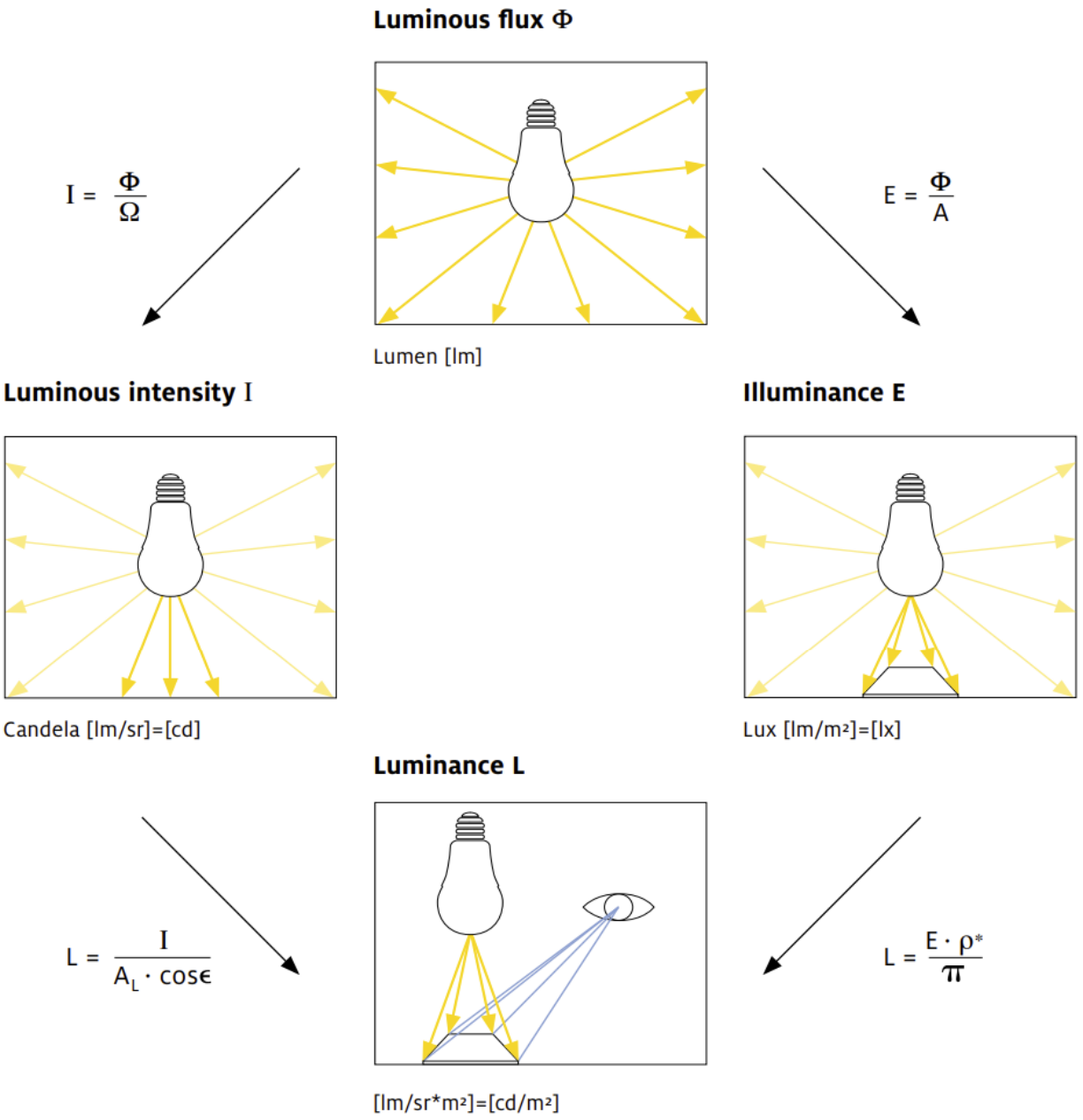

Ω = solid angle into which luminous flux is emitted

A = area hit by luminous flux

$A_L \cdot \cos\epsilon$ = visible areas of light source

ρ = reflectance of area

π = 3.14

* = for diffuse surface areas

Figure 3. Relationships Between the 5 Basic Lighting Parameters (Zumtobel Lighting GmbH 2018)

1.1 *BASIS OF LIGHTING MEASUREMENTS*

One of the key concepts to understanding the relationships between the different measurement geometries of light is that of the steradian (sr), or the solid angle. A steradian can be defined as the solid angle that, with its vertex at the center of the sphere, cuts off a spherical surface area equal to the square of the radius of the sphere (Ryer 1997). A sphere contains 4π steradians and one steradian section of a one-meter radius sphere would equal a spherical surface area of one meter. Figure 4 below illustrates the concept of a cone with a solid angle of one steradian removed from the sphere. The solid angle, Ω, in steradians, is equal to the spherical surface area, A, divided by the radius, r, squared (Ryer 1997).

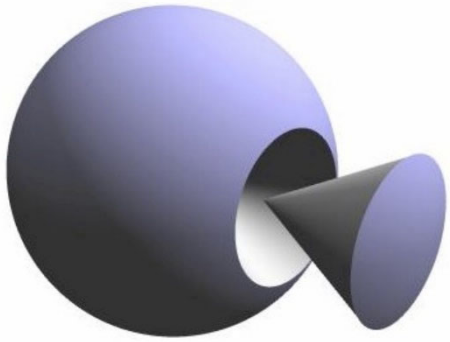

Figure 4. 1 Steradian and 1 Solid Angle (Ryer 1997)

Although understanding the theory of lighting calculation origins, most measurements of light do not require an accurate calculation of the spherical surface area to convert between measurements. Instead, flat area estimates can be substituted for the spherical area when the solid angle is less than 0.03 steradians (Ryer 1997). In other words, the source is at such a small distance from the measurement plane and a planar surface area calculation compared to a steradian measurement calculation results in a percent error of less than one. There are several lighting parameters and measurements including luminous intensity and luminous flux among many others. This research focuses on the relationship between luminance and illuminance.

1.2 *LUMINANCE*

Luminance is a photometric measure of the luminous intensity of light reflected off or passing through a surface in a given direction, usually towards the human eye, per unit projected area. It also indicates how much luminous intensity is perceived by the human eye, meaning luminance can be indicative of how much "brightness" is emitted or reflected off a surface. Of

course, this “brightness” is the subjective impression of the objective luminance measurement standard (Ryer 1997). It’s very possible, and common, for the same amount of luminance to be present on two different objects but the objects appear to have different “brightnesses”, this is a result of the different surface properties of the objects. This will be discussed in the reflectance section. Luminance can be measured in candelas per square meter in the International System of Units (SI) and is independent of distance. Figure 5 below shows a light source and a diffusing surface with an illuminance measurement noted and two luminance measurements labeled on the right. An asb is an obsolete measurement unit for luminance, equal to 1/pi candelas per square meter. Figure 6 shows the relationship between the main lighting metrics and how they are related.

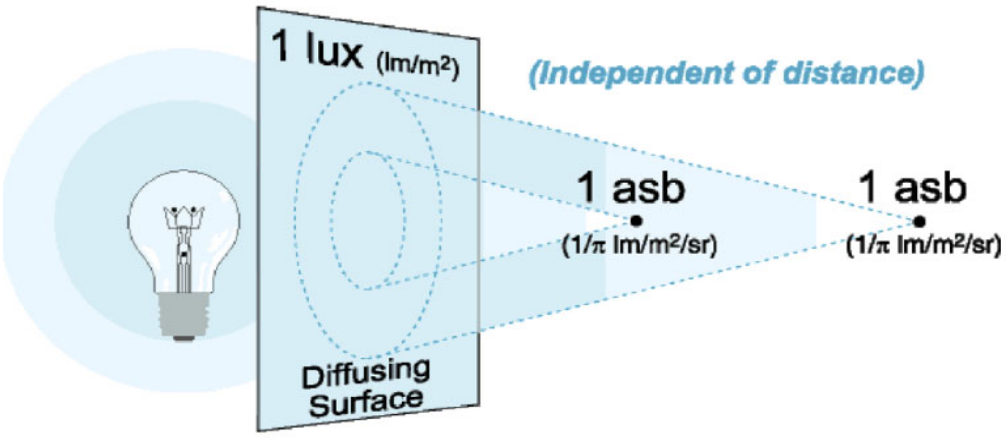

Figure 5. Luminance (Ryer 1997)

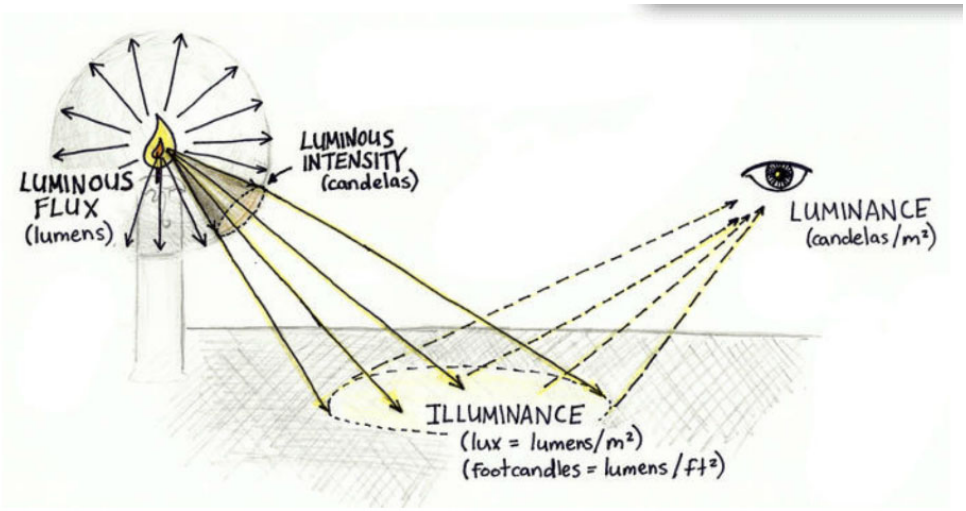

Figure 6. Relationship of Lighting Measurements (Ryer 1997)

1.3 *ILLUMINANCE*

Illuminance is the density of luminous flux on a surface, which shows how "bright" the human eye perceives the surface to be. It's a term that describes the measurement of the amount of light falling onto, "illuminating" and spreading over a given surface. Illuminance can be represented by two units of measure, the footcandle (fc) in the imperial metric system and lux in the SI metric system. The unit of measurement originated as the illumination at the point of a surface that is exactly 1 foot from the point source of 1 candela for a footcandle. Similarly, for lux, it is the illumination at the point of a surface that is exactly 1 meter from the point source of 1 candela. Approximately 1 footcandle equals 10 lux, or one lux equals 0.0929 footcandles. One footcandle is the "brightness" produced by one lumen uniformly distributed over one square foot of a surface (Ryer 1997). Figure 7 below shows a 1 candela point source and the corresponding 1 fc and 1 lux measurements for visual clarification.

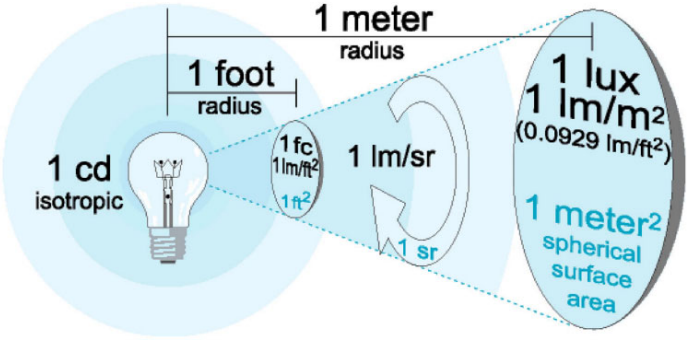

Figure 7. Illuminance (Ryer 1997)

Most people refer to illuminance and brightness interchangeably, which is incorrect as brightness can also be used interchangeably with luminance. Clarifying, illuminance is the density of luminous flux falling onto a surface while brightness is a visual perception and physiological sensation of light as see by the human eye. Figure 8 displays the appearance of a gallery scene and the corresponding illuminance map to show how easily illuminance can be referred to as brightness. Brightness cannot be measured while illuminance and luminance are used for quantitative and lighting quality purposes. Just like luminance, it's extremely likely that the same amount of illuminance is present on two surfaces but the surfaces have different "brightnesses" if the two surfaces have different surface reflectance properties. Illuminance measurements are used as the basis for lighting requirements in the majority of lighting handbooks because it reflects the

amount of "light" on a surface. Different tasks are performed on different surfaces and therefore, the required illumination for each task can be specified based on the surface the task is performed. For example, a table from the Lighting Sports and Recreational Areas portion of the IES Lighting Handbook can be seen below in Figure 9. For golf courses, each area is broken down and the recommended illuminance levels are provided.

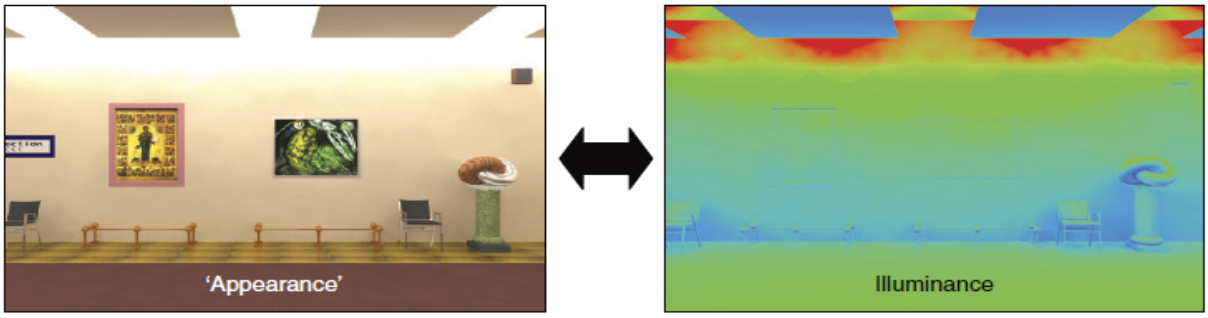

Figure 8. Appearance vs Illuminance. A simulated virtual gallery scene under overcast sky conditions with shaded roof lights and corresponding illuminance map (Mardaljevic et al. 2020)

Recommended Maintained Illuminance Targets[a, b]

TS = Task Surface: Recommended illuminances are at height of task surface above finished grade or floor

APPLICATION TASK/AREA	Class of Play	Horizontal (E_h) Target E_h @ Height AFF: CAT	Lux @ m	(Fc @ Ft)	Max Avg Min	Horizontal (E_h) Uniformity Ratio: Max CV	Ratio	Ratio Basis	Vertical (E_v) Target E_v @ Height AFF: CAT	Lux @ m	(Fc @ Ft)	Max Avg Min	Vertical (E_v) CV: Max CV	Vertical (E_v) Uniformity Ratio: Ratio	Ratio Basis
Football															
	I	T	1,000 @ 0.91	(100 @ 3.0)	Avg	0.13	1.7:1	Max:Min							
	II	R	500 @ 0.91	(50 @ 3.0)	Avg	0.17	2:1	Max:Min							
	III	P	300 @ 0.91	(30 @ 3.0)	Avg	0.21	2.5:1	Max:Min							
	IV	O	200 @ 0.91	(20 @ 3.0)	Avg	0.25	3:1	Max:Min							
Golf															
Golf course															
Tee boxes	IV	K	50 @ 0.00	(5 @ 0.0)	Avg	0.25	3:1	Max:Min							
Fairways	IV	I	30 @ 0.00	(3 @ 0.0)	Avg	0.35	6:1	Max:Min							
Greens	IV	O	200 @ 0.00	(20 @ 0.0)	Avg	0.25	3:1	Max:Min							
Golf driving															
Tee boxes	IV	O	200 @ 0.00	(20 @ 0.0)	Avg	0.25	3:1	Max:Min							
At 183 m (600 ft)									M	100 @ 0.91	(10 @ 3.0)	Avg	0.25	3:1	Max:Min

Figure 9. Table A-2 from IES Lighting Handbook: Lighting Sports and Recreational Areas (DiLaura 2011)

1.4 *REFLECTANCE*

Reflectance, a surface property, is the dimensionless ratio of the total luminous flux incident upon a surface that is reflected. Put simply, reflectance is a surface property that dictates how much of the incident light falling on a surface is reflected back. It is a function of the frequency (or wavelength) of the light, its polarization and the angle of incidence. In comparison to illuminance, reflectance is the amount of light reflected by the object in the scene while illuminance is the amount of luminous flux incident upon the scene. Most things humans see every day do not themselves emit visible light; instead, they reflect incident natural sunlight and artificial light. For example, a typical apple appears red because it has a relatively smooth surface that reflects red light and absorbs other non-red color wavelengths of light. This reflection of light can be classified into two types based on the nature of the interface as seen in Figure 10; specular reflection and diffuse reflection. Specular reflection can be thought of as the mirror-like reflection of light waves from a surface. Specular reflection is the result of light reflection from smooth surfaces such as mirrors or calm bodies of water. In comparison, diffuse reflection is the reflection of light from a surface in a scattered manner, reflecting at all angles rather than just one. Instances of diffuse reflection can be seen in clothing or paper. Looking at a person's surroundings, the majority of visible objects are seen primarily by diffuse reflection from their surfaces. Exceptions to this include glass, reflective liquids, polished/smooth metals, glossy objects and objects that themselves emit light. The same object having different reflectance properties can be seen below in Figure 11, displaying how different reflectance properties can change how humans visualize the object. While all objects in Figure 11 are under the same light source and condition, each has a different reflectance property and therefore, each looks different.

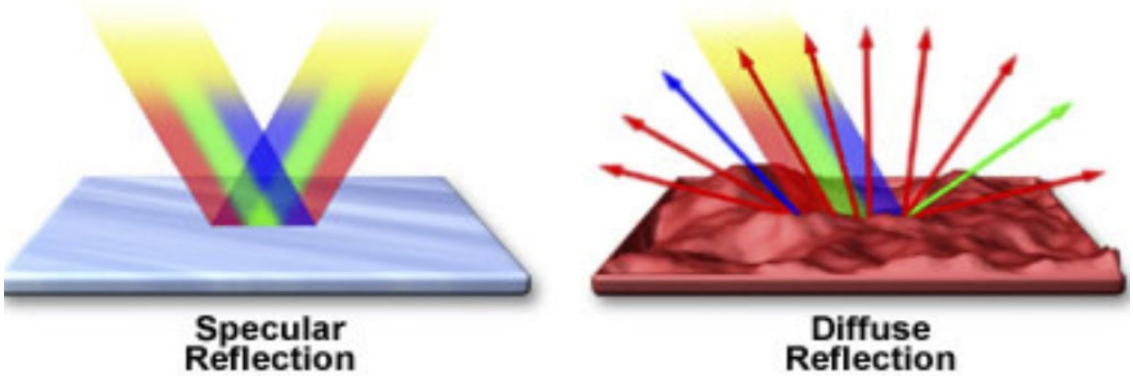

Figure 10. Specular Reflection vs. Diffuse Reflection

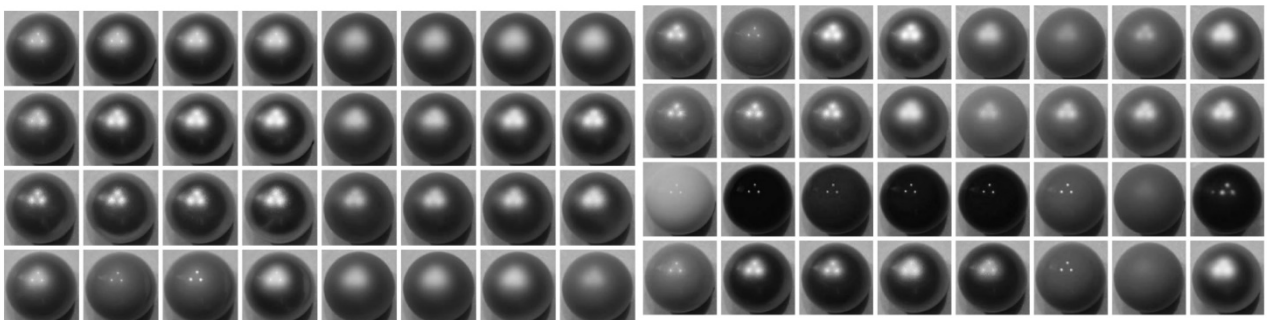

Figure 11. Material Samples with Different Reflectance Properties (Yoo et al. 2009)

A common application of the distinction between specular reflection and diffuse reflection is shown in Figure 12 and pertains to the difficulty of driving at night on a wet roadway versus a dry roadway. More often than not, night driving on a wet roadway results in a glare from oncoming headlights; these glares are due to the specular reflection of the beam of light from the oncoming car. Roadways not in a rainy condition would normally cause diffuse reflection due to their rough surfaces, as seen below. However, if the surface is wet, water can fill in the cracks and crevices to smooth out the surface; rays of light from the headlights of an oncoming car hit this smooth surface and reflect specularly, resulting in a concentrated beam of light hitting your eyes.

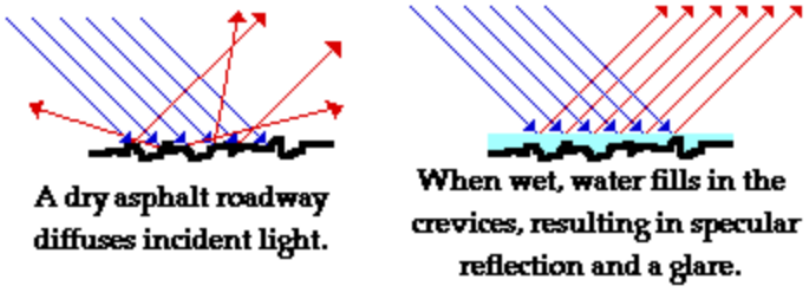

Figure 12. Roadway Reflections

Lambertian reflectance is the property that defines an ideal “matte” or diffusely surface; a Lambertian surface reflects light equally in all directions. This property also leads to the apparent brightness of a Lambertian surface to an observer as the same regardless of the viewer’s angle. As the reflection of various surfaces is described using their bidirectional reflectance distribution function (BRDF) values, all Lambertian surfaces have a constant BRDF value. Lambertian surface models are considered an extreme scenario where the surface roughness equals zero and the intensity of images when viewed through these surfaces changes in proportion with the

illumination directions. As Lambertian reflection is a theoretical concept, there is no naturally occurring true Lambertian surface.

1.5 *HIGH DYNAMIC RANGE IMAGING (HDRI)*

High dynamic range imaging (HDRI) is a technique used in photographic imaging and films to reproduce a greater range of light and color than is produced with general digital photography techniques, thus making the image more photorealistic. Conventional photography techniques only allow differentiation within a certain, limited range. Outside this range, features will appear white in the brighter areas or black in the darker areas. The dynamic range of an image refers to the ratio of the maximum tonal value to the minimum tonal value. Therefore, expanding the range to a "high dynamic range" creates an image considered the closest to simulating what the human eye can see. Any single "low dynamic range" photograph does not accurately represent the dynamic range of the scene photographed. Capturing a series of images, called low dynamic range images (LDRI), taken from the darkest setting to the brightest setting and then fusing the images together creates one single high dynamic range image. The final HDR image contains the true dynamic range of the scene therefore presenting the most accurate and precise data that can be derived for a variety of purposes. A simple comparison of a low dynamic range (LDR) image and a high dynamic range (HDR) image can be seen in Figure 13 below. The LDR image is a standard photograph taken from a consumer grade camera while the HDR image is the result of several LDR photographs, taken in sequential exposure values, fused together. It can be seen that the HDR image represents the true dynamic range of the scene while the LDR image represents only a portion of the dynamic range.

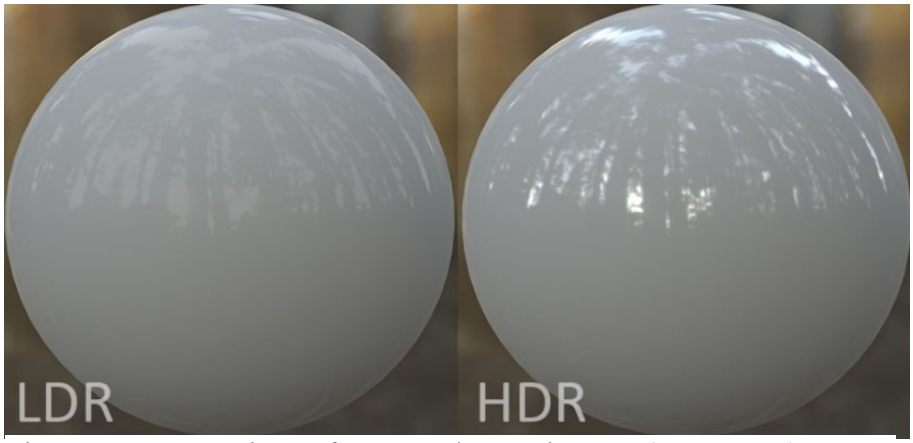

Figure 13. Comparison of LDR and HDR images (Ryer 1997)

A quality HDR image can be created using a variety of techniques but the most widely used and affordable is the sequential exposure change technique. The sequential exposure change technique allows the use of consumer grade digital cameras fitted with wide-angle lens. Either aperture or shutter speeds are varied in sequential order with a low dynamic range image taken at each setting. These two parameters, together or separate, are the only changing variables; the camera is fixed in the same position and focused on the same scene as well as fixed focal length. Of course, different trials may require altering focal lengths to achieve an optimal field of view or visual depth of field. To keep other optical properties consistent, it is advised the camera be controlled by computer to ensure theoretically identical images, with the exception of the varying exposure values. Depending on the scene, the camera can be fixed in any number of ways facing virtually any direction. The time lapses between exposures indicate that HDR photography is ideal for static scenes under constant light and daylight scenes. There is no set standard for the number of LDR images to be fused together or the correlating exposure values, both parameters are up to the researcher. An increase in the amount of data yields an increase in the accuracy or reliability of the results and conclusions. The same is true for high dynamic range imaging; the more low dynamic range images fused together, and thus more exposure values captured, will produce a more precise photograph that can be used for data collection. Three examples of batches of low dynamic range images are shown. Figures 14 and 15 on the next page show the series of low dynamic range images on the left and the final HDR image on the right. All the exposure times and aperture sizes are given in the figure captions. Figure 16 displays how varying shutter speeds and different surface reflectance look in series of low dynamic range images.

Figure 14. Studio Scene

Eight (8) pictures of a static scene taken at different exposure times, photographed with a digital camera with aperture constant f/6.7. The exposure times are, from brightest to darkest, 1/8s, 1/15s, 1/30s, 1/60s, 1/125s, 1/500s, 1/1000s. The high dynamic range image output for the Studio Scene is given at the right. (Robertson et al. 2003)

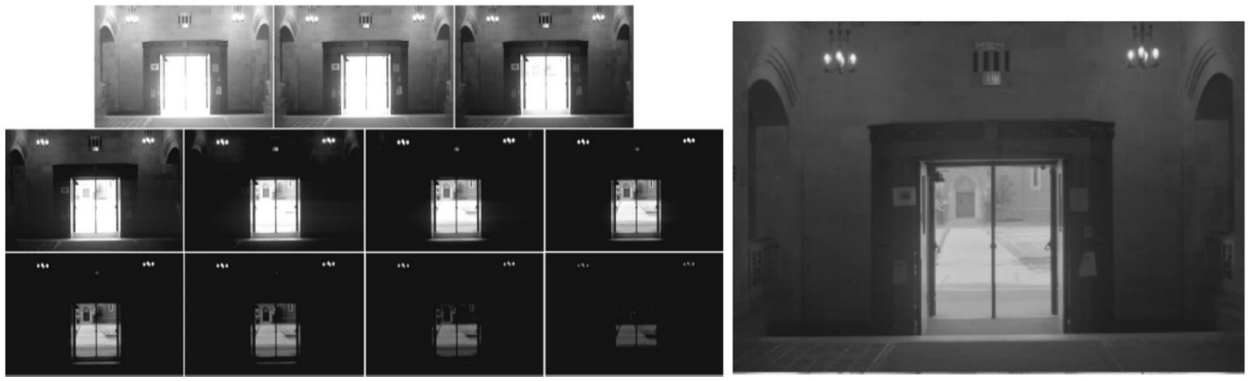

Figure 15. Notre Dame Scene

Eleven (11) pictures from inside a Notre Dame hall taken with a digital camera with aperture constant f/5.6. The exposure times are, from brightest to darkest, 1s, 1/2s, 1/4s, 1/8s, 1/15s, 1/30s, 1/60s, 1/125s, 1/250s, 1/500s, 1/1000s. The high dynamic range image output for the Notre Dame Scene is given at the right (Robertson et al. 2003)

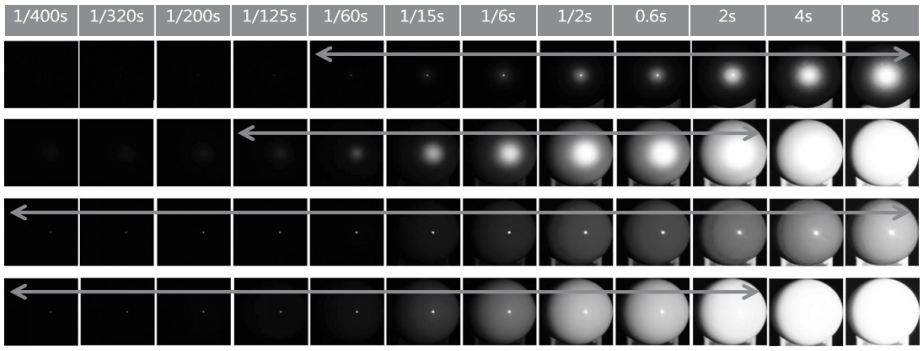

Figure 16. Different Reflectance Properties in Low Dynamic Range Images

Low dynamic range images of Figure 11 with different exposure times (Yoo et al. 2009)

1.6 *CONCLUSIONS*

HDRI is a technique used increasingly to study visual environments with affordable and easily accessible equipment to create luminance maps of the visual field in the camera frame. By taking a series of multiple exposures and merging them together, a more complete range of luminance values are presented in the final image. When calibrated properly, these final HDR images can be used as a data acquisition system for extremely useful information that can be applied to many lighting design or occupant comfort applications. This paper aims to outline a method using HDRI to estimate illuminance values based on the most common equipment and best HDRI practices.

2.0 LITERATURE REVIEW

A compilation of associated and related literature began with a Google Scholar search using the following keywords; illuminance, luminance, and HDRI (high dynamic range imaging). The search results yielded a total of 3,500 results for “illuminance hdr” and 10,600 results for “luminance hdr”. Of the combined 14,100 results, only 70 were deemed related or associated to the research. The process of determining if a useful correlation exists between the previous literature and this presented research is outlined below. If the literature did not meet the following criteria at any point, it was discarded from possible studies to review.

STEP 1: Did the research have a relevant title? Did the title indicate a use of high dynamic range imaging (HDRI) or an analysis of illuminance, luminance or other lighting parameter measurements?

STEP 2: Did the research have a relevant abstract? Did the abstract describe an experimental, analytical, or numerical study using high dynamic range imaging (HDRI) to produce or validate lighting parameter measurements?

STEP 3: Had the literature been cited in other, more recent publications in a positive way? Was the research reputable and reliable, or is the author reputable?

STEP 4: Did the study describe in detail the processes, technologies and resources used as well as providing images and figures for reference and understanding?

If a publication passed all outlined steps, it was deemed useful and included in the literature review. Once fully read and understood, a table was created to record key data points, technology and methodology used for comparison and evaluation purposes. The reviewed literature was further categorized by the main lighting parameter focuses on; illuminance, luminance and miscellaneous.

Table 1. Miscellaneous HDRI Lighting Parameters Comparison Table

YEAR	AUTHOR	PARAMETER OF MEASUREMENT	CONTEXT	CAMERA INFORMATION				HDRI INFORMATION				VIGNETTING CORRECTION	ABSOLUTE CALIBATRION	
				CAMERA MODEL	F-STOP	FISH EYE LENS	LENS MODEL	DYNAMINC RANGE	# OF LDR IMAGES	ISO	HDR CREATION SOFTWARE			
2014	BARAZETTI, L.	N/A	INTERIOR	TEST 1 = NIKON D700, TEST 2 = CANON POWERSHOT S3 IS	N/R	NO	20mm LENS	TEST 1 = EVs (-2EV, -1 EV, 0 EV, +1EV, +2EV), TEST 2 = -4.72EV, -1.82EV, +1.51EV, +4.09EV)	TEST 1 = 5, TEST 2 = 4	N/R	INTEL CORE i7-2760QM, CPU 2.4Hz, 16 GB RAM	N/R	N/R	N/R
1997	DEBEVEC, P., & MALIK, J.	RADIANCE	INTERIOR	TEST 1 = KODAK DCS460, TEST 2 = CANON 35mm SLR	f 8.0	YES	15mm FISHEYE LENS	TEST 1 = 1/30s - 30s, TEST 2 = 30s - 1/1000s	TEST 1 = 11, TEST 2 = 16	N/R	RADIANCE	N/R	N/R	N/R
2009	GAYESKI, N., STOKES, E., & ANDERSEN, M.	RADIANCE	INTERIOR	CCD: KAPPA DX20	f 4.0	YES	FUJINON FE185C057HA	N/R	N/R	N/R	PHOTOSPHERE	CORRECTED	OCEAN OPTICS USB2000 SPECTROMETER	99% REFLECTIVE LABSPHERE SPECTRALON COATED DIFFUSING REFLECTANCE STANDARD.
2009	MARDALJEVIC, J., PAINTER, B., & ANDERSEN, M.	LUMINOUS FLUX	INTERIOR	N/R	N/R	NO	N/R	N/R	N/R	N/R	PHOTOSPHERE	N/R	N/R	N/R
2015	MARDALJEVIC, J., BREMBILLA, E., & DROSOU, N.	REFLECTANCE	INTERIOR	N/R	N/R	N/R	N/R	1/1000s - 1s	N/R	N/R	N/R	N/R	N/R	N/R
2018	POLING, R.M.	LUMINOUS FLUX	INTERIOR	CANON T2i	N/R	YES	4.5mm FISHEYE LENS	N/R	18	N/R	PHOTOSPHERE	CORRECTED	MINOLTA LS-110 LUMINANCE METER	X-RTE MACBETH COLOR CHECKER
2020	POLING, R.M., & CAI, H.	LUMINOUS FLUX	INTERIOR	CANON EOS 550D	N/R	YES	SIGMA 4.5mm F2.8 EX DC HSM CIRCULAR FISHEYE LENS	N/R	18	N/R	PHOTOSPHERE	CORRECTED, SOLID ANGLE EVALUATION	MINOLTA LS-100 LUMINANCE METER	X-RTE MACBETH COLOR CHECKER
2003	ROBERTSON, M.A.	N/A	INTERIOR	TEST 1 = NIKON E2N, TEST 2 = NIKON FM	TEST 1 = f-6.7, TEST 2 = f-5.6	N/R	N/R	TEST 1 = 1/8s, 1/15s, 1/30s, 1/60s, 1/125s, 1/250s, 1/500s, 1/1000s ; TEST 2 = 1s, 1/2s, 1/4s, 1/8s, 1/15s, 1/30s, 1/60s, 1/125s, 1/250s, 1/500s, 1/1000s	TEST 1 = 8, TEST 2 = 11	N/R	N/R	N/R	N/R	N/R
2019	SIELACHOWSKA, M., TYNIECKI, D., ZAJKOWSKI, M.	LUMINOUS FLUX	EXTERIOR	N/R	N/R	N/R	N/R	N/R	N/R	N/R	N/R	N/R	N/R	N/R
2014	VARGHESE, D., WANAT, R., MANTIUK, R.	COLORMETRIC CALIBRATION	INTERIOR	TEST 1 = CANON 550D, TEST 2 = CANON 1000D, TEST 3 = LUMIX DMC-LX7	TEST 1 = f5.7, f8.0; TEST 2 = f5.7, f8.0; TEST 3 = f5.6, f5.0	N/R	N/R	550D & 1000D = 1/16, 1/8, 1/4, 1/32, 1/64; 1/5.2, 1/2.6, 1/1.3, 1/10.4, 1/20.7; 4, 8, 16, 32, 2, 1, 1/2, 1/49.4, 1/197.4, 1/1024; LUMIX = 1/13, 1/50, 1/3.2, 1/13, 1/100, 1/1/6	3, 10	100	PFSTOOLS SOFTWARE	N/R	PHOTOSPECTROMETER (TYPE N/R)	X-RITE COLOR CHECKER CHART

Table 2a. Luminance HDRI Comparison Table

YEAR	AUTHOR	CONTEXT	CAMERA INFORMATION				HDRI INFORMATION				VIGNETTING CORRECTION	ABSOLUTE CALIBATRION	
			CAMERA MODEL	F-STOP	FISH EYE LENS	LENS MODEL	DYNAMINC RANGE	# OF LDR IMAGES	ISO	HDR CREATION SOFTWARE			
2005	ANAOKAR, S., & MOECK, M.	INTERIOR	NIKON COOLPIX 5400	f 7.3 & f 7.9	NO	28-116mm f2.8-4.6 ZOOM LENS	TEST 1 = 1/4000s-1/2s, TEST 2 = 1/500s-1/2s	TEST 1 = 9, TEST 2 = 12	N/R	PHOTOSPHERE	NOT CORRECTED	MINOLTA T-1 ILLUMINANCE METER	MUNSELL VALUE SCALES
2010	ANDERSEN, M., STOKES, E., GAYESKI, N., & BROWNE, C.	INTERIOR	KAPPA DX20 color CCD and Sensors Unlimited SU320 1.7RT near-infrared	N/R	YES	FUJINON	N/R	N/R	N/R	PROPRIETARY MATLAB ALGORITHM	CORRECTED	MINOLTA LS-110 LUMINANCE METER	N/R
2009	BELLIA, L., CESARANO, A., IULIANO, G.F., & SPADA, G.	INTERIOR	CANON EOS 20D	N/R	NO	CANON ULTRASONIC 16-35mm f2.8 ZOOM LENS	1/500s, 1/15s, 1/2s	3	N/R	PROPRIETARY MATLAB ALGORITHM	CORRECTED, SOLID ANGLE EVALUATION	LUMINANCE - CALIBRATION POLYNOMIALS REPORTED	N/R
2002	BELLIA, L., CESARANO, A., MINICHIELLO, F., & SIBILIO, S.	INTERIOR	INDUSTRIAL B/W CCD VIDEO CAMERA	f 3.5 - f 22	NO	50mm	N/R	N/R	N/R	N/R	NOT CORRECTED	LUMINANCE, SPECTRAL RESPONSE	N/R
2005	BELTRAN, L.O., & MOGO, B.M.	INTERIOR	NIKON COOLPIX 5400 and CANON A70	f 3.5 - f 7.9	YES	24mm	1/500s - 8s	8, 9, & 10	N/R	PHOTOSPHERE, HDR-Shop, NUKE and PHOTOGENICS	CORRECTED	MINOLTA LS-110	NONE
2012	CAI, H.	INTERIOR	CANON REBEL T2i	f 4.0 - f 5.6	YES	SIGMA EX DC HSM LENSES: 4.5mm FISHEYE LENS, a 10mm FISHEYE LENS, a 10-20 ZOOM LENS, STANDARD 30mm LENS.	N/R	N/R	N/R	PHOTOSPHERE, RADIANCE	CORRECTED	MINOLTA LS-110 LUMINANCE METER, MINOLTA CL-200A COLOR METER	X-Rite MACBETH CLASSIC COLOR CHECKERS, X-Rite 18% GREY CHECKERS
2013a	CAI, H.	EXTERIOR	CANON REBEL T2i	f 4.0 - f 5.6	YES	10 mm SIGMA EX DC HSM LENS	N/R	N/R	N/R	PHOTOSPHERE, RADIANCE	CORRECTED	MINOLTA LS-110 LUMINANCE METER	X-Rite MACBETH CLASSIC COLOR CHECKERS, X-Rite 18% GREY CHECKERS
2013b	Cai, H.	INTERIOR	CANON EOS REBEL T2i	N/R	YES	TEST 1 = 10mm SIGMA EX DC HSM LENS, TEST 2 = 4.5mm SIGMA f2.8 EX DC HSM LENS	N/R	18	N/R	PHOTOSPHERE, RADIANCE	CORRECTED	MINOLTA LS-110 LUMINANCE METER, MINOLTA CL-200A COLOR METER	X-Rite MACBETH CLASSIC COLOR CHECKERS, X-Rite 18% GREY CHECKERS
2010	CAI, H., & CHUNG, T.M.	INTERIOR	CANON EOS 350D	f 4.0 - f 22	NO	SIGMA 10-20mm f4-5.6	30s, 15s, 8s, 4s, 2s, 1s, 1/2s, 1/4s, 1/8s, 1/15s, 1/30s, 1/60s, 1/125s, 1/250s, 1/500s, 1/1000s, 1/2000s, 1/4000s	18	100	PHOTOSPHERE	CORRECTED, LAMBERTIAN SURFACE	MINOLTA LS-110 LUMINANCE METER	12 GREYSCALE PATCHES G1-G12, MACBETH COLOR CHECKER RENDITION CHART
2012	CAI, H., & CHUNG, T.M.	INTERIOR	CANON EOS REBEL XT	f 5.6	NO	SIGMA ZOOM LENS 10-20MM F4-5.6	N/R	8	100	PHOTOSPHERE, RADIANCE	CORRECTED	N/R	12 GREYSCALE CHECKERS
2014	CAI, H., & LI, L.	EXTERIOR	CANON EOS REBEL T2i with 18-mega pixel CMOS SENSOR	f 5.0	YES	SIGMA EX DC HSM 10mm LENS	1/4000s to 30s	18	N/R	RADIANCE	CORRECTED	MINOLTA LS-110 LUMINANCE METER, MINOLTA CL-200A COLOR METER	X-Rite 18% GREY CHECKER
2010	CHUNG, T., & T.H. NG, R.	INTERIOR	CANON EOS 350D	f 8.0	NO	Sigma 10-20mm f4-5.6	EVs (-4 EV, -3 EV, -2 EV, -1 EV, 0 EV, +1 EV, +2 EV, +3 EV, +4 EV)	4, 18	100	PHOTOSPHERE, RADIANCE	CORRECTED, LAMBERTIAN SURFACE	MINOLTA LS-110 LUMINANCE METER, KONICA MINOLTA T-10m ILLUMINANCE METER	X-Rite COLOR CHECKER CHART

Table 2b. Luminance HDRI Comparison Table

YEAR	AUTHOR	CONTEXT	CAMERA INFORMATION				HDRI INFORMATION				VIGNETTING CORRECTION	ABSOLUTE CALIBATRION	
			CAMERA MODEL	F-STOP	FISH EYE LENS	LENS MODEL	DYNAMINC RANGE	# OF LDR IMAGES	ISO	HDR CREATION SOFTWARE			
2015	CHIOU, Y.-S., & HUANG, P.-C.	INTERIOR	CANON EOS 7D DSLR, CANON EOS D60 DSLR	f 4.5, f 16.0	YES	SIGMA 4.5MM CIRCULAR FISHEYE LENS	N/R	N/R	N/R	N/R	N/R	DELTA OHM LP PHOT 03 BL ILLUMINANCE PYRANOMETER, KONICA MINOLTA CM-2600d PORTABLE SPECTROPHOTOMETER	QPCARD102-4 SHADED GREY CARD
2008	COYNE, S., ISOARDI, G., & HIRING, M.	INTERIOR	NIKON COOLPIX	N/R	YES	N/R	N/R	N/R	N/R	ENTPE PHOTOLUX	N/R	N/R	N/R
2006a	INANICI, M.N.	INTERIOR AND EXTERIOR	NIKON COOLPIX 5400	f 4.0	YES	NIKON FC-E9	2s - 1/4000s	N/R	100	PHOTOSPHERE	CORRECTED	MINOLTA LS-110 LUMINANCE METER	REFLECTANCE SQUARES RANGING 4% to 87% AND THE MACBETH COLORCHECKER
2006b	INANICI, M.N., & NAVVAB, M.	INTERIOR	N/R	N/R	N/R	N/R	N/R	N/R	N/R	N/R	N/R	N/R	N/R
2010	INANICI, M.N.	INTERIOR AND EXTERIOR	EXTERIOR = CANON EOS 5D, INTERIOR CANON EOS 30D	f 4.0 and f 16.0	YES	EXTERIOR = SIGMA 8mm f3.5 EX DG, INTERIOR = CANON EF 20mm f/2.8 LENS	15s - 1/8000s (USING 3-STOP INCREMENTS)	> 10	100	PHOTOSPHERE, RADIANCE	CORRECTED, USING POLYNOMIAL FUNCTION	MINOLTA LS-110 LUMINANCE METER, MINOLTA CM-2002 SPECTROPHOTOMETER	N/R
2005	INKAROJRIT, V.	INTERIOR	NIKON COOLPIX 5400	f 4.0	YES	NIKON FC-E9	(1/2s, 1/15s, 1/125s, 1/1000s, 1/2000s) OR (5 EV, 7.9 EV, 11 EV, 14 EV, 16 EV)	5	100	ENTPE PHOTOLUX	NOT CORRECTED	MINOLTA LS-110 LUMINANCE METER, COSAR 45 REFLECTANCE DENSITOMETER	GRAY-SCALE SQUARES
2007	JACOBS, A., & WILSON, M.	INTERIOR	NIKON COOLPIX 990	N/R	YES	NIKON FC-E8	1/1000s - 2s	12	N/R	HDRGEN	CORRECTED, USING POLYNOMIAL FUNCTION	N/A	N/A
2008	JACOBS, A., WITTKOPF, S., & GROBE, L.	EXTERIOR	NIKON D200	N/R	YES	SIGMA 4.5mm F2.8 EX	N/R	16	N/R	PHOTOSPHERE, HDRGEN	NOT CORRECTED	MINOLTA LS-100 LUMINANCE METER	N/R
2020	KIM, M., KONSTANTZOS, I., & TZEMPELIKOS, A.	INTERIOR AND EXTERIOR	RASPBERRY PI CAMERA MODULE V2 (BASED ON CMOS SENSOR SONY IMX219)	N/R	YES	M12 f-1.8	(28ms, 47ms, 85ms, 198ms, 482ms, 992ms, 1994ms, 3885ms, 7798ms)	9	100	PYTHON, HDRGEN	N/R	CALIBRATED LUMINANCE SPOT METER (TYPE N/R)	N/R
2011	KONIS, K., LEE, E.S., & CLEAR, R.D.	INTERIOR	NIKON COOLPIX 990	N/R	YES	NIKON FC-E8	N/R	6	N/R	RADIANCE	CORRECTED, USING POLYNOMIAL FUNCTION	N/R	N/R
2020	KRUISSELBRINK, T.	INTERIOR	RASPBERRY PI CAMERA BOARD VERSUS 2 WITH SONY IMX219 SENSOR	f 2.0	YES	MINIATURE EQUISOLID-ANGLE LFISHEYE LENS	2s - 1/17,000s	N/R	100	HDRGEN	CORRECTED	N/R	KODAK GRAY CARD
2017	KRUISSELBRINK, T., ARIES, M., & ROSEMANN, A.	EXTERIOR	RASPBERRY PI CAMERA BOARD VERSION 1.3 CMOS	f 2.9	YES	MINIATURE EQUISOLID-ANGLE LFISHEYE LENS	2s - 1/17,000s	N/R	ISO	HDRGEN	CORRECTED	N/R	KODAK GRAY CARD
2019	MAHONEY, E.	INTERIOR	CANON T2i	N/R	YES	SIGMA STANDARD 30mm LENS AND 4.5mm FISHEYE LENS	N/R	18	N/R	PHOTOSPHERE, HDRSCOPE	N/R	MINOLTA LS-100 LUMINANCE METER, MINOLTA T-10M ILLUMINANCE METER	COLOR CHECKERS
2007	MOECK, M.	EXTERIOR	CANON EOS 350D	f 5.6	NO	N/R	N/R	6	100	PHOTOSPHERE	N/R	REPORTED AS ERROR PERCENTS FOR MUNSELL COLOR CHIPS	MUNSELL COLOR CHIPS / VALUE SCALES

Table 2c. Luminance HDRI Comparison Table

YEAR	AUTHOR	CONTEXT	CAMERA INFORMATION				HDRI INFORMATION				VIGNETTING CORRECTION	ABSOLUTE CALIBATRION	
			CAMERA MODEL	F-STOP	FISH EYE LENS	LENS MODEL	DYNAMINC RANGE	# OF LDR IMAGES	ISO	HDR CREATION SOFTWARE			
2000	MOORE, T., GRAVES, H., PERRY, M.J., & CARTER, DJ.J.	INTERIOR	(2) CCD CAMERAS, (1) SENSOR TYPE N/R	N/R	NO	8mm, 17mm and 35mm	N/R	N/A	85, 100, 100	N/R	CORRECTED, USING POLYNOMIAL FUNCTION	LUMINANCE METER (TYPE N/R)	10 GREY SQUARES OF GREY SCALE
2017	NAHRKHALAJI, R.	EXTERIOR	CANON EOS 7D DSLR	N/R	YES	SIGMA 4.5mm F2.8 HSM LENS	N/R	7	N/R	PHOTOSPHERE	CORRECTED	MINOLTA LS-100 LUMINANCE METER, MINOLTA T-10 ILLUMINANCE METER	N/R
2009	NEWSHAM, G.R., & ARSENAULT, C.	INTERIOR	MICRON GRAYSCALE	N/R	NO	N/R	N/R	N/R	N/R	N/R	N/R	HAGNER S2 LUMINANCE METER	N/R
2017	SAFRANEK, S.	INTERIOR	NIKON D200	N/R	YES	SIGMA 24mm F1.8 PRIME LENS	1/4000s - 30s	7	100	PHOTOSPHERE	CORRECTED, MATLAB FUNCTION	N/R	N/R
2013	SUK, J.Y., SCHILER, M., & KENSEK, K.	INTERIOR	NIKON COOLPIX 5400	N/R	YES	NIKON FC-E8	N/R	10	N/R	PHOTOSPHERE	CORRECTED	LUMINANCE METER COOKE CORP. CAL-SPOT 401	N/R
2013	TYUKHOVA, Y., & WATERS, C.	INTERIOR	CANON EOS 7D	f-4.5 and f-16.0	NO	CANON ZOOM LENS EF-28-105mm 1:3.5-4.5 II USM	1/8000s - 30s	N/R	N/R	HDRGEN AND PHOTOSPHERE	N/R	MINOLTA LS-110 LUMINANCE METER	N/R
2020	WOLSKA, A., & SAWICKI, D.	INTERIOR	CANON EOS 550D	f 8.0	YES	SIGMA CIRCULAR 4.5mm F2.8 EX	1s - 1/400s IN VARYING 1-stop, 1/2-stop AND 1/3-stop INCREMENTS	N/R	100	N/R	N/R	N/R	GRAY CARDS
2007	WULLER, D., & GABELE, H.	N/R	NIKON D2X, CANON 350D, NIKON COOLPIX 8400, FUJI FINEPIX F10	N/R	NO	N/R	N/R	N/R	N/R	N/A	N/R	VIA GOSSEN LUMINANCE METER AND TEST CHART	N/R
2018	YUN, S.-I., & KIM, K.-S.	EXTERIOR	CANON EOS 5D	N/R	N/R	N/R	(-2 EV, 0 EV, +2 EV)	3	N/R	PHOTOSPHERE	N/R	LP-PYRA12,02 (GLOBAL HORIZONTAL IRADIANCE AND DIFFUSE HORIZONTAL IRRADIANCE), MINOLTA T-10 ILLUMINANCE METER, MINOLTA LS-110 LUMINANCE METER	145 SKY PATCHES
2007	ZOTTI, G.	EXTERIOR	CANON EOS 5D	f 4.0, f 16.0	YES	SIGMA 8mm f3.5 EX DG	N/R	N/R	N/R	PFS TOOLS	CORRECTED, USING A GLOBE LAMP SHADE AS A DIFFUSER	LUMINANCE/CHROMATIC ABERRATION/COLOR SHIFT	N/R

Table 3. Illuminance HDRI Comparison Table

YEAR	AUTHOR	CONTEXT	CAMERA INFORMATION				HDRI INFORMATION				VIGNETTING CORRECTION	ABSOLUTE CALIBATRION	
			CAMERA MODEL	F-STOP	FISH EYE LENS	LENS MODEL	DYNAMINC RANGE	# OF LDR IMAGES	ISO	HDR CREATION SOFTWARE			
2011	BELLIA, L., MUSTO, M., & SPADA, G.	INTERIOR	CANON EOS 20D	N/R	N/R	N/R	2s, 1/15s, 1.500s	3	N/R	N/R	CORRECTED	MINOLTA T10 LUXMETER	A4 PAPER SHEET
2013	BELLIA, L., & SPADA, G.	INTERIOR	CANON EOS 20D	N/R	NO	CANON ULTRASONIC 16-35mm f2.8 ZOOM LENS	2.0s, 66.6ms, 2.0ms	3	N/R	N/R	N/R	N/R	N/R
2020	MARDALJEVIC, J., CANNON-BROOKES, S., BLADES, N., & LITHGOW, K.	INTERIOR	CANNON 550D DSLR	f 8.0	NO	CANON 10-18mm ZOOM LENS	1/2000s, 1/500s, 1/125s, 1/30s, 1/8s, 1/2s, 2s	7	100	HDRGEN	N/R	DELTA T-DEVICE (ILLUMINANCE)	N/R
2006	MOECK, M. & ANAOKAR, S.	INTERIOR AND EXTERIOR	TEST 1 = NIKON COOLPIX 5400, TEST 2 = OLYMPUS C-5060	TEST 1 = N/R, TEST 2 = f 2.8	NO	TEST 1 = 28-116mm f2.8-4.6 ZOOM LENS, TEST 2 - 27-110mm f2.8-8.0 ZOOM LENS	TEST 1 = 1/2000s - 1s, TEST 2 = 1/30s - 1/5s	TEST 1 = 12, TEST 2 = 6	N/R	PHOTOSPHERE	NOT CORRECTED	TEST 1 = VIA MINOLTA T-1 ILLUMINANCE METER AND MUNSELL VALUE SCALES, TEST 2 = VIA MINOLTA SPOT METER	N/R
2015	NATH, D., MAZUMDAR, S., CHANDRA, J.K., & BAG, A.K.	EXTERIOR	N/R	N/R	N/R	N/R	N/R	N/R	N/R	N/R	N/R	N/R	N/R
2006	STUMPFEL, J., JONES, A., WENGER, A., TCHOU, C., HAWKINS, T., & DEBEVEC, P.	EXTERIOR - SKY MAPPING	CANON EOS 1DS AND SONY VX1000	f-4.0 and f-16.0	YES	N/R	1/8000s - 1s	7	N/R	N/R	CORRECTED	PHOTORESEARCH PR-650 SPECTRORADIOMETER	MACBETH COLOR CHART
2020	TABAKA, P.	EXTERIOR	UAV: MATRICE 60 PRO (SZ DJI TECHNOLOGY CO.)	N/R	N/R	N/R	N/R	N/R	N/R	N/R	N/R	ILLUMINANCE METER (TYPE N/R)	N/R

2.1 *MISCELLANEOUS LIGHTING PARAMETERS*

While the majority of associated publications focused of luminance and illuminance, ten (10) studies, or 14% of the total literature review, analyzed or experimented with HDRI and miscellaneous lighting parameters; including radiance, luminous flux, reflectance and colorimetric calibration. It must be noted that only one of these studies was conducted outdoors.

Debevec and Malik, at the time, offer an advanced method of increasing dynamic range of images using multiple exposures (Debevec and Malik 1997). Rather than assuming a linear camera response, they assume an arbitrary response that is determined as part of the algorithm where the final output pixel is given as a weighted average of the input pixels taken at different exposures (Robertson 2003). The algorithm gives higher weight to input data that are nearer to the mean of the input pixel range and less weight to the input data that are near the extremes of the input pixel range. Several limitations were identified with regards to this method, the most significant amongst them was using data from only one input source rather than using all input data. It would make more sense to calculate an estimate that takes advantage of all available data. Following Debevec and Malik, Robertson proposed a new method of increasing the dynamic range of images by using multiple exposures; an extension of a method proposed by the same researcher in 1999 (Robertson

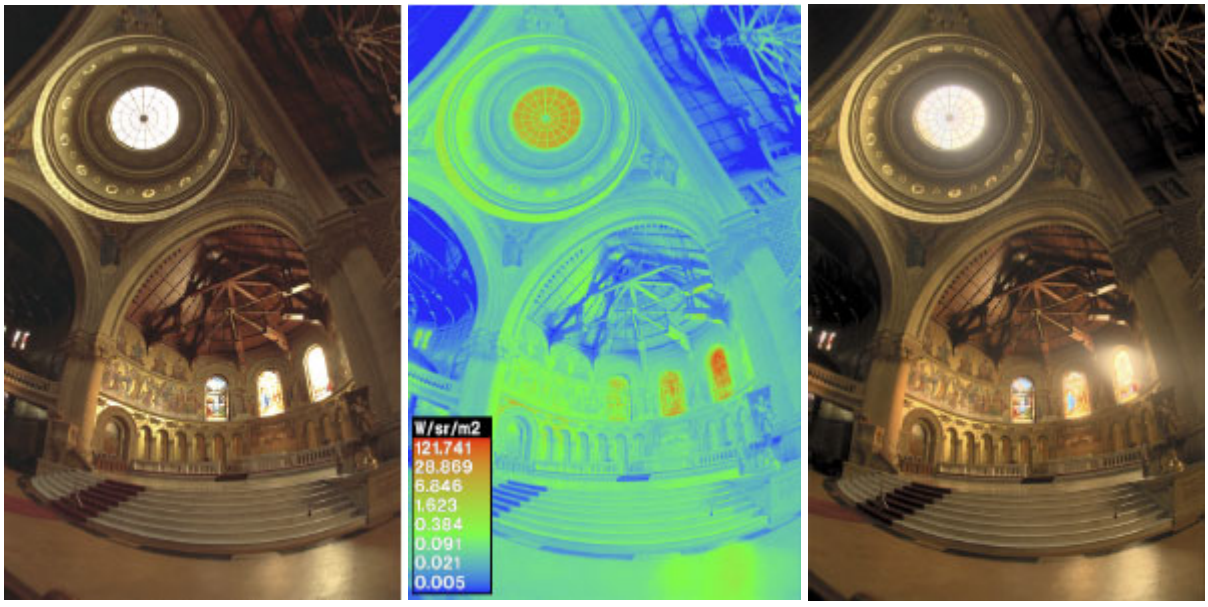

Figure 17. One of the low dynamic range images (left), the false color image showing relative radiance values for a grayscale version of the radiance map (middle), a rendering of the radiance map using histogram compression and simulating glare, contrast sensitivity and retinal response (Debevec and Malik 1997).

et al. 1999). This new method is based on a probabilistic formulation that estimates the response function of the camera and consequently computes HDR images with decreased noise due to averaging of data from all input images (Robertson 2003).

Similar to the use of digital cameras for studying luminance and radiance distributions in rooms, digital cameras can be used as quasi-spectral radiometers following the development of methods to measure bi-directional scatting distribution functions. This can be expanded even further by using filters to assess quasi-spectral transmission and reflection properties of surfaces (Gayeski et al. 2009). By filtering incident light into selected wavelength intervals, accurate estimates of radiances can be made to study to properties of angularly and spectrally selective complex fenestration systems, as complex fenestration systems are increasingly being used to distribute solar radiation purposefully in buildings. Radiance estimates from digital cameras are the basis of this methodology (Gayeski et al. 2009). Colorimetric calibration of HDR images captured using the multi-exposure technique was introduced in other research (Varghese et al. 2014, Inanici 2006a, Anaokar and Moeck 2005, Moeck 2007, Tyukhova 2012).

Four (4) studies used HDR photography to estimate luminous flux of the environment in question (Mardaljevic et al. 2009, Poling 2018, Poling and Cai 2020, Sielachowska et al. 2019). Measuring arbitrarily complex luminous fluxes across large areas is possible from HDR imaging technology achieved using a digital camera and printer-grade white paper. This same approach, named the transmission illuminance proxy – high dynamic range imaging (TIP-HDRI), could be used to determine the direct and indirect components of illuminance (Mardaljevic et al. 2009). Building on previous research, Poling and Cai proved HDR imaging to estimate luminous flux with three supplemental field measurements; luminance of a reference target for photometric calibration, XYZ coordinates of reference point and foveal illuminance at the camera lens perpendicular to the viewing direction for a calibration coefficient (Poling and Cai 2020). Another study used a photometer attached to an unmanned aerial vehicle to measure the distribution of luminous flux emitted by sports facilities. This method was proposed following a method developed to control the photometric probe and calibrate the measurements (Sielachowska et al. 2019).

A number of studies have been conducted to validate lighting measurements obtained through HDRI as HDRI is a valuable tool for lighting research, offering a variety of options for

lighting analysis such as luminance evaluation, illuminance derivation, glare analysis, image-based lighting, luminaire performance testing and many others (Tyukhova 2012). Research on how to minimize errors in HDRI have also been published (Cai and Chung 2011, Cai et al. 2015, Moeck 2007, Reinard et al. 2010, Safranek 2017, Safranek and Davis 2020).

In addition to the numerous methods and subjects proposed by miscellaneous lighting parameter studies, the usage statistics for both the camera models and lens models were analyzed and can be seen below in Figures 18 and 19. In Figure 18, it can be seen that only two studies used

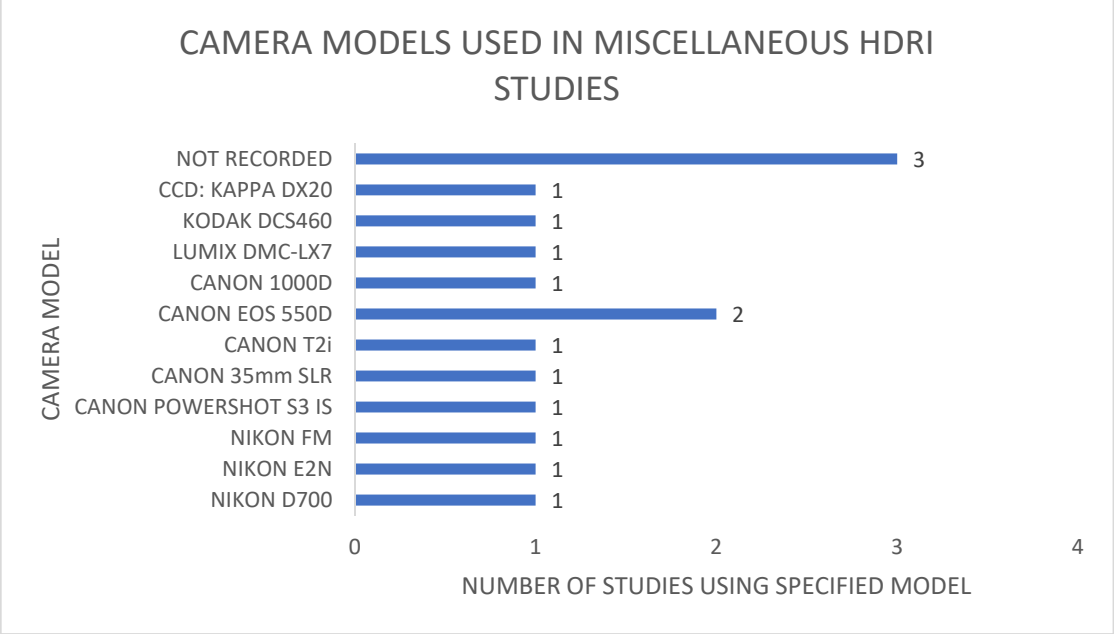

Figure 18. Camera Models Used in Miscellaneous HDRI Studies

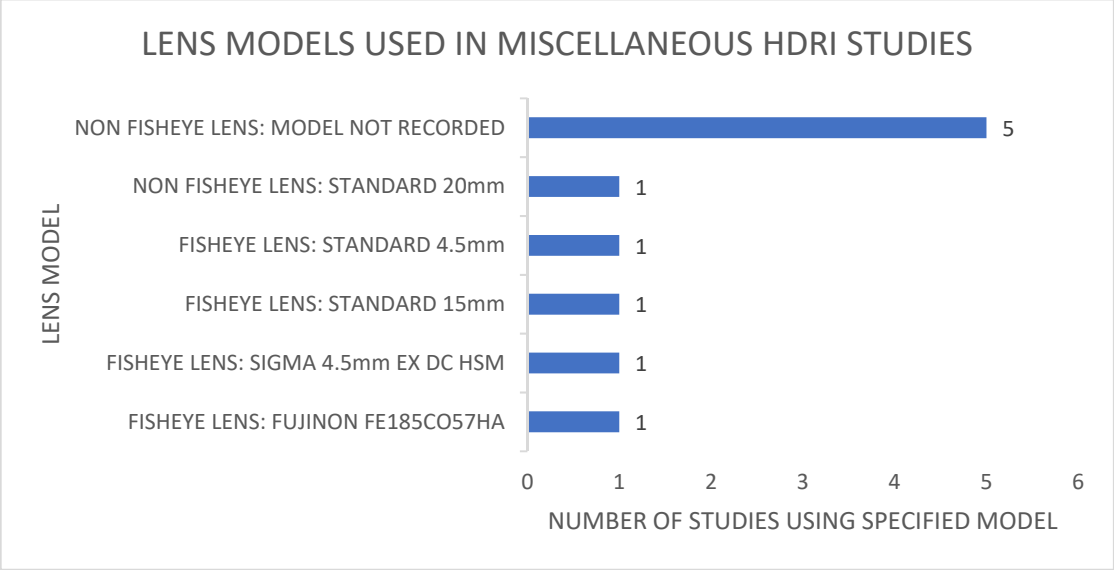

Figure 19. Lens Models Used in Miscellaneous HDRI Studies

the same camera (Poling and Cai 2020, Varghese et al 2014), while every other study used a different combination of camera and lens. While no specific conclusions can be drawn from this, it shows that almost any consumer grade digital camera and lens can be used in the HDR imaging process to derive accurate lighting measurements. In addition, while none of these studies directly measure luminance or illuminance, the research is helpful is developing future methods to do so. This research is directly linked and cited in other luminance and illuminance research.

2.2 *LUMINANCE*

Many research papers have been published regarding high dynamic range photography and the ability to derive accurate luminance values from HDR images. For decades, luminance and the patterns of luminance in architectural environments have been studied in relation to; predicting perceptions of beam patterns produced by accent lighting systems, human responses based on visual processes and spatial frequency analyses, among many other topics (Safranek and Davis, 2020). Upon the discovery of utilizing HDR imaging to measure luminance, applications of this method have been extended to glare evaluations and the creation of potential new glare metrics (Cai 2013b; Cai and Chung 2012; Suk et al. 2013). Glare research, from electric lighting and daylighting, seems to be the most common application of high dynamic range imaging for luminance measurement.

A luminance gradient was introduced as a metric for evaluating common non-uniform luminous environments, measuring the largest change rate and polarity of spatial luminance variation on a large scale in high resolution (Cai 2013b). This luminance gradient bridges the gap between the conventional luminance evaluation between a target and its immediate background or ambient background. This methodology cannot be used to evaluated the spatial and temporal luminance changes of common non-uniform luminous environments for two reasons; the luminance contrasts obtained from multiple points can't accurately reflect spatial changes of light levels in high resolution and conventional meter-based luminance measurement is point by point (Cai 2013b). Without a luminous gradient, varying daylit luminous environments cannot be measured accurately. Using a MATLAB command, a luminance gradient was calculated at pixel level after HDR images were calibrated using the software Photosphere. This luminance gradient

has been pivotal in advancing HDR photography and imaging to assist in lighting designs and daylighting analysis for non-uniform luminous environments.

Research in 2006 tested the accuracy of high-resolution luminance maps generated by Photosphere software (Anaokar and Moeck 2006). Errors were estimated due to the usage of various Munsell color chips, spectral power distribution of light sources, optical vignetting of the camera and spatial resolution of the object. Twelve images were obtained with varying shutter speeds and then fused in Photosphere, the illuminance values of each cards were taken on site and luminance was calculated using a simple equation. This luminance was used to calibrate the image, then used to compute the reflectance of each sample. These computed values were compared to the actual coefficients of reflectance. Results of the experiment reveal cool hues (blue and green) have the largest error when compared to warm hues (red and yellow) and the error in reflectance increases with saturation and with the decrease in Munsell value. Figure 20 displays the percent error in reflectance for Munsell chips of different hues under high illuminance (above) and low illuminance (below). In addition, images fused in Photosphere show higher luminance for colors with a low value, or darker colors of the same hue (Anaokar and Moeck 2006). To overcome the issue of large errors for surfaces with reflectance less than 20%, spectral responsivity calibration is suggested (Jacobs 2007).

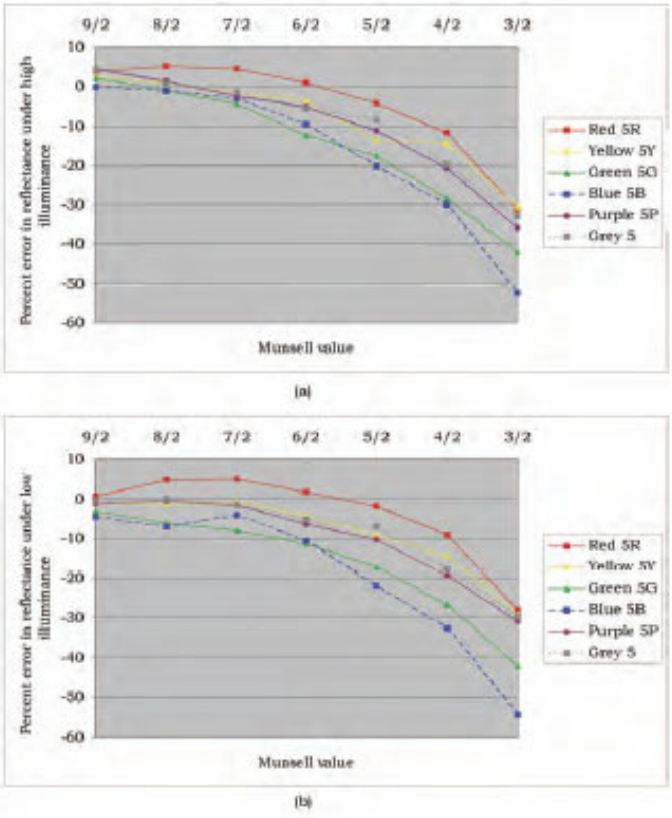

Figure 20. Error in Reflectance for Munsell Chips of Different Hues, Values and Illuminance Levels (Anaokar and Moeck 2006)

An in-depth validation of HDRI as a luminance data acquisition system was again studied in 2006 (Inanici 2006). Multiple exposure photographs were taken with a digital camera, processed using Photosphere and referenced with a calibrated Minolta LS-110 luminance meter. The goal of this study was to compare physically measured luminance values with the

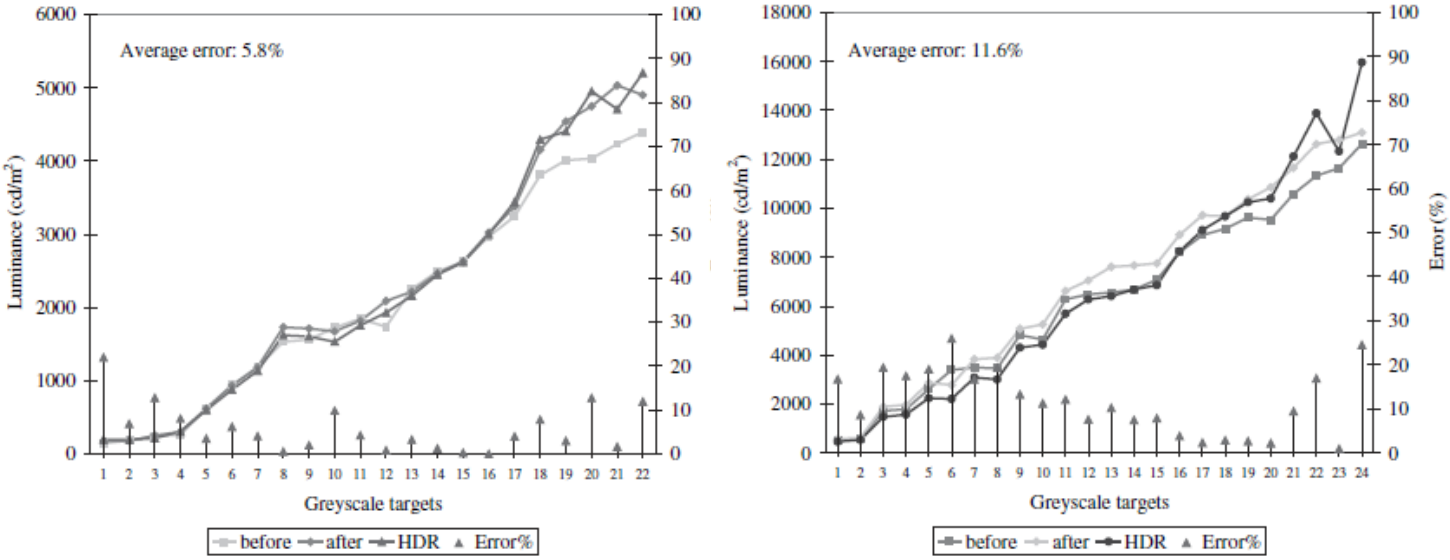

Figure 21. Outdoor Scene with Grayscale Targets under Overcast Sky (left) and Clear Sky (right) (Inanici 2006)

luminance values derived from HDR photography. To further this research, measurements were taken indoors and outdoors with various lighting conditions. A total of 456 targets (different reflectance, grey-square targets and colored Macbeth ColorChecker) under various light sources yielded an average percent error of 7.3% for all targets, 5.8% for greyscale and 9.3% for colored (Inanici 2006). It can be seen in Figure 21 that clear sky scenes yield larger percent errors. Increased error was observed for darker greyscale targets as luminance of the darker regions were over-estimated due to general lighting scattering in the lens and the luminance of saturated color samples showed increased error as well (Tyukhova 2012). This research shows that HDRI techniques give reliable results in capturing a wide range of luminances with an accuracy of 10% (Inanici 2006). It is important to note that these errors are derived from Photosphere's assigned luminance values on an HDR image; absolute validity of this methodology requires calibration in Photosphere from the luminance meter. Photosphere's production of luminance values is relatively accurate on its own, but can be 100% reliable when luminance meter readings from the scene are used to calibrate Photosphere's results.

The accuracy of luminance measurements using a camera with CMOS (Complementary Metal Oxide Semiconductor) sensor was investigated in 2007 (Moeck 2007). The author used mirror spheres, as seen in Figure 23, to overcome the disadvantages of fisheye lens, namely cost,

vignetting problems, lens flare and hemispherical field of view. Capturing panoramic maps when studying the importance of dynamic daylit conditions is important as they offer a full field of view around one axis. This research verifies luminance of grey scales and matte color checkers obtained through HDR images and calculates luminance errors of spherical HDR images obtained with a mirror ball. Results reveal that luminances of most hues can be reasonably estimated through HDR photography; more specifically, luminance values of light surfaces are underestimated while that of dark surfaces are overestimated within a reasonable error range. As seen in Figure 22, luminance measurements of dark colors with high chroma, such as dark saturated blues, greens and purples, result in severe error, with the maximum error of the complete series for dark saturated blue being 53% (Moeck 2007). In comparison, yellow and red hues show minimum error. These inaccuracies can be attributed to CMOS color sensors; limited color gamuts of these image sensors limit the measurements of Munsell color samples and the camera's incorrectly approximated functions lead to these errors.

In a study by Chung and NG (2010), variation over time on the calibration factor

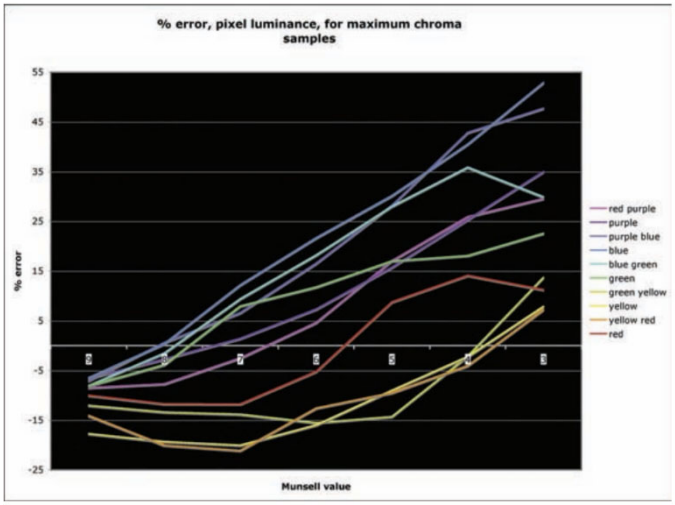

Figure 22. Percent Error for 70 Color Samples with Maximum Chroma, using a gray card with value N5 as the luminance reference (Moeck 2007).

Figure 23. Gray Cards Reflected in Chrome Mirror Ball (Moeck 2007)

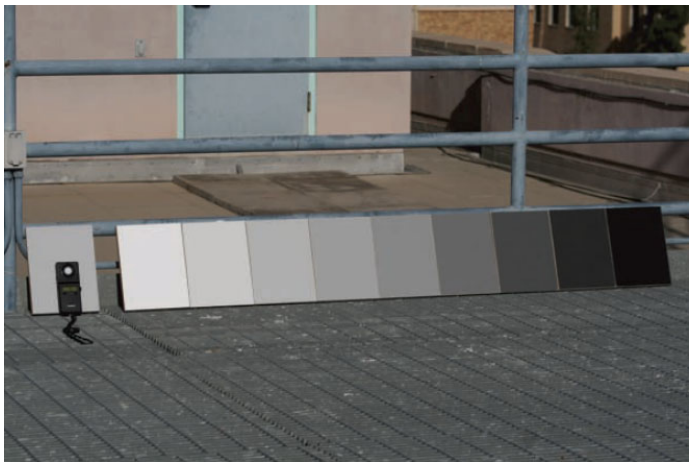

Figure 24. Gray Cards on Roof (Moeck 2007)

for HDR photography was investigated. The calibration factor of an HDR image is determined by dividing luminance value of a specific object in the scene by the same region in the HDR image. In other words, the calibration factor is the ratio of the measured to the HDR-derived luminance value of a pixel in the field of view (Jacobs 2007). The factor is believed to be dependent on the lens aperture and the type of the main lighting source, and should theoretically be around 1 (Jacobs 2007). A calibration factor around 1 means the software used in the post-processing method estimated the luminance values only a small percentage off of the true luminance values of the scene. The calibration factor is used to scale the pixel luminance values to the luminance of the physical scene, ensuring all measurements are precise and accurate moving forward rather. In order to retrieve the luminance of a physical scene, the calibration factor is multiplied by the pixel values in the region of interest in the final HDR image (Tyukhova 2012). Following experiments conducted over 6 days at different times, the calibration factors of each series were computed and analyzed. As a result, the influence of different lighting conditions was not detected in the HDRI's calibration factor of any color (Chung and NG 2010). In conclusion, today's HDR photography software can estimate luminance values generally close to the scene's true luminance values using a final HDR image no matter the various lighting conditions present. In addition, the vignetting effect was analyzed and the proper correction was applied in this research. This correction, a digital filter, prevented luminance reduction at the corners of the image.

The quality of luminance acquisition from HDR images can also be compared after applying vignetting correction and physical calibration (Cai and Chung 2012). This research examines the dependence of quality of the HDR images based on focal lengths and aperture sizes, aiming to find an optimal combination of focal length and aperture size leading to least number of errors. A number of errors can be seen when using cameras with wide-angle zoom or fisheye lenses; vignetting effects, diffraction of light with small apertures, lighting scattering in the lens can be present depending on the f-stop and wavelength of light, chromatic aberration from an imperfect lens or incorrect white balance of the camera, and radial distortion of the lens (Tyukhova 2012). The findings in this study are used in the data collection and methodology procedure of the presented research (Tyukhova 2012).

Other applications of high dynamic range imaging for luminance measurement include evaluating the uniformity of luminance across an LED chip (Tyukhova and Waters 2013), deriving the luminous intensity distribution of a luminaire by evaluating the luminaire's delivered

luminance pattern (Bellia and Spada 2013) and modeling daytime sky luminance (Inanici 2010). In addition, there are a variety of other applications of high dynamic range imaging for luminance measurement and analysis. As the scope of using HDRI for luminance measurement increases, a continued interest in the accuracy of the luminance data produced remains. Unlike conventional spot or imaging luminance meters, which can be validated through accredited testing, HDRI luminance measurements derived from commercial digital photography are often adjusted in the post-processing phase. Several studies have been conducted to validate either the luminance data produced, the best post-processing techniques or the best technology to produce accurate data (Anaokar and Moeck 2005; Inanici 2006a; Moeck 2007; Wuller and Gabele 2007; Jacobs and Wilson 2007; Cai and Chung 2010; Bellia and Spada 2013; Varghese et al. 2014; Safranek 2017; Safranek and Davis 2020).

It can be seen in the Table 2a-c, on pages 16-18, luminance is the most researched lighting parameter in terms of utilizing high dynamic range imaging. Most of these studies researched luminance in an indoor setting; ignoring and disregarding any daylighting effects. 11 of the 36 reviewed luminance publications on luminance and HDRI were conducted in an exterior setting, allowing the validated tactics and methods to be utilized in exterior illuminance studies as well.

When comparing the camera models and lens models used in the reviewed luminance studies (Figures 25 and 26 on the next page), it can be seen that the large number of studies correlates to the large amount of variation in camera and lens models. However, details of both models are mostly provided by the authors of the respective studies, with only 3 of the 36 reviewed publications not disclosing the details of said equipment. In addition to the miscellaneous lighting studies, the luminance studies propose new technology and methodology that can be used in illuminance studies.

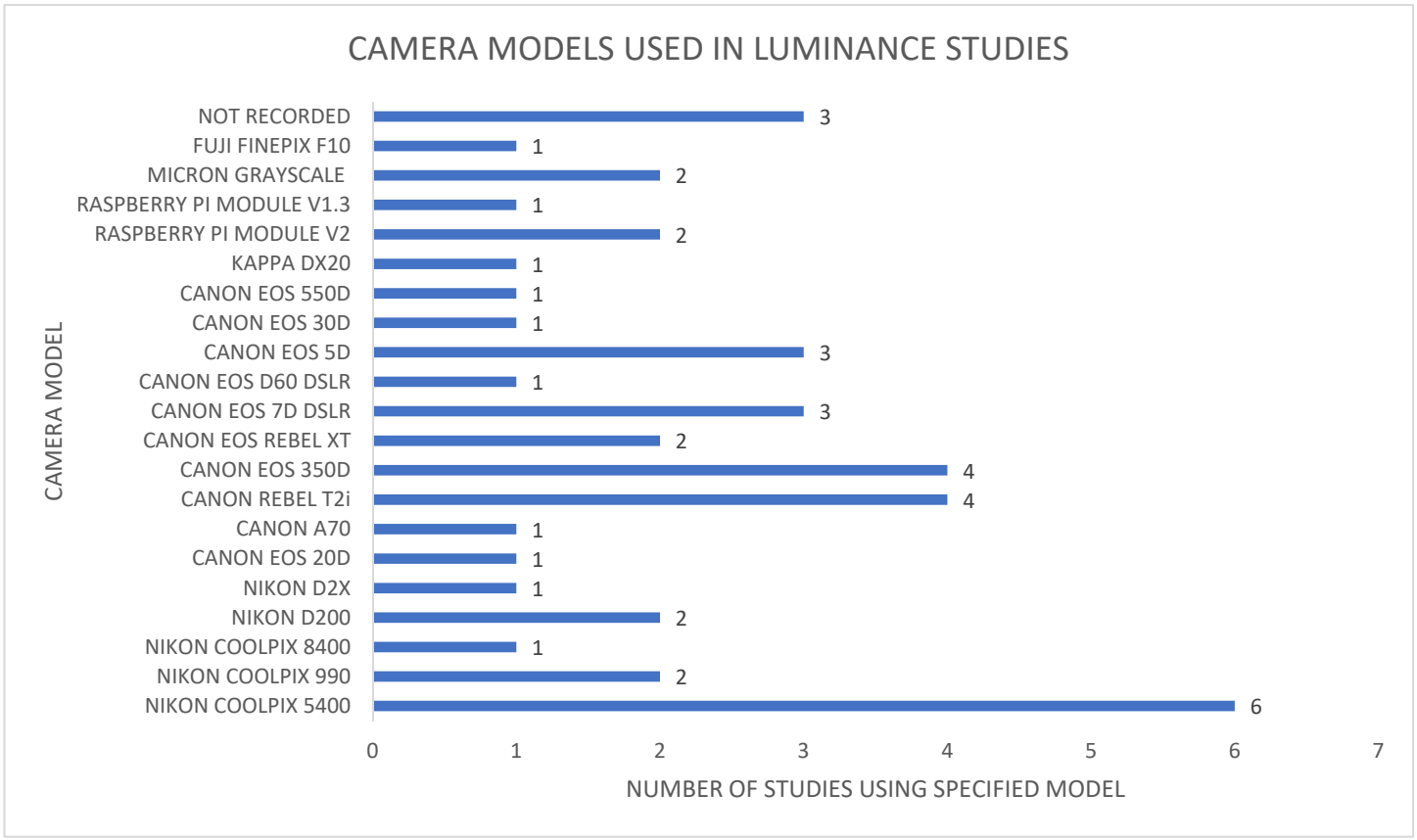

Figure 25. Camera Models Used in Luminance Studies

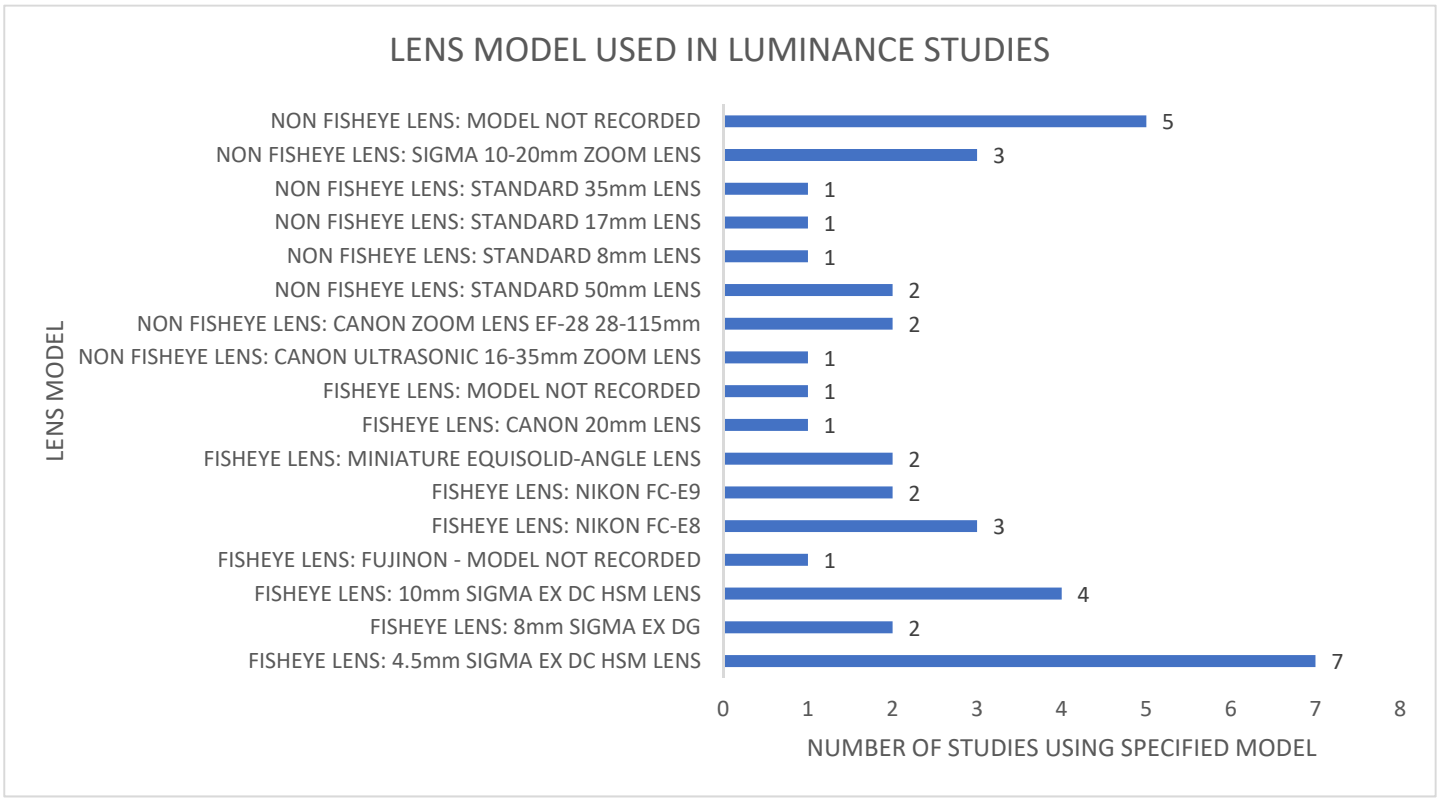

Figure 26. Lens Models Used in Luminance Studies

2.3 *ILLUMINANCE*

Extracting illuminance data from HDRI is relatively less common compared to obtaining luminance data. Some of the applications of utilizing HDRI for illuminance measurement and analysis include; measuring illuminance on task areas (Bellia et al. 2011), mapping the luminous intensity distribution of a light source from the illuminance map by applying the photometric inverse law (Bellia and Spada 2013), validating a technique to measure the arbitrarily complex illuminance values across large areas (Mardaljevic et al. 2009) and measuring the illuminance contributions of architectural features (Moeck and Anaokar 2006).

Mardaljevic et al. 2015 proposed a modest, seemingly overlooked variation of the existing illuminance proxy techniques. This method is based on the premise that the reflectance of a surface can be determined from an HDR image providing that the following conditions are met; the images are taken normal to the surface in question, the surface doesn't contain any significantly specular components, the illuminance field in question doesn't contain steep gradients, no significant lens distortions are present, and a known reflectance value is in the scene in question for HDR calibration purposes. This study limits its research to interior "wall reflectance values" with variation in surface textures and disregards the effects of vignetting. In 2020, Mardaljevic et al. then derived illuminance values from an HDR acquired luminance map at numerous patches of an interior patterned wall, as seen in Figure 27. The patches served as illuminance meters, allowing the entire wall's illuminance values to be derived using an algorithm. A total of 116 patches were identified with each one acting as a proxy for an illuminance meter. Between the patches, interpolation was required as the pattern of the wall made it too difficult to obtain the exact values with HDR photography. The proposed approach described depends on having a sufficient number of patches with known mean reflectance visible in the HDR image and no steep illumination gradients, as stated in previous research (Mardaljevic et al. 2015). For preliminary study, interpolating the illuminance in unknown spaces may suffice, but a better or more refined method should be developed to offer precise accuracy for more intricate patterns.

Bellia et al. 2011 proposed a method to measure the effects of daylighting on illuminance of interior classrooms by taking LDR images at five locations throughout the classroom as shown in Figure 28. The same process was conducted in four more classrooms and both luminance and illuminance values were derived from the single LDR image. Bellia and Spada 2013 then obtained

illuminance maps from a video-luminance meter and a Lambertian screen to back calculate the luminous intensity. While this research could represent a promising tool when control of lighting quality in similar environments is required, further investigation is needed. Directional reflections in points near the windows and the possible inconsistencies when changing camera angle could produce errors affecting the accuracy of obtained measurements.

Figure 27. Wallpaper Patches for Illuminance Map (Mardaljevic et al. 2020)

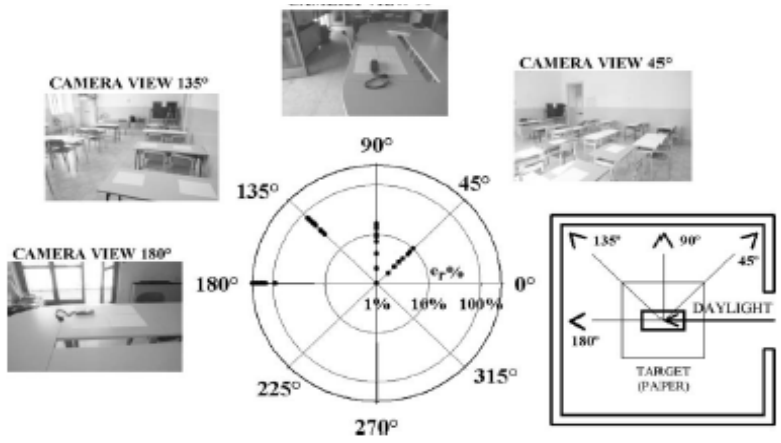

Figure 28. Camera View Tests for Illuminance Measurements (Bellia et al. 2011)

Moeck and Anaokar suggest a method to extract illuminance values from available HDR luminance maps (Moeck and Anaokar 2006). Authors used achromatic Munsell cards to obtain luminances from the luminance map and took physical measurements for further comparison. Illuminance values were extracted by analyzing the quantity of light falling onto objects, colors and features. A way to properly analyze the illuminance contributions of architectural features from luminance maps in presented and applied to a historic landmark for validation.

A study conducted in 2004 stated that HDR images can accurately capture natural illumination including the visible sun (Stumpfel et al. 2004). The authors identified two main challenges with regards to their experiment: selection of the dynamic range and the ability of the camera sensors to accurately capture the true luminance of the sun. Careful selection of shutter speed, aperture size and natural density filter can preserve the full dynamic range of the sun and

surrounding sky. It was determined the full range can be covered in seven exposures with a standard digital camera using a 12-bit linear response sensor (Stumpfel et al. 2004). The research addresses calibration issues including lens vignetting, infrared sensitivity and spectral transmission of the neutral density filter. The camera was set up on the roof with an unobstructed view of the horizon in all directions, as shown in Figure 29, and shutter speeds longer than 2 seconds were deemed unacceptable as this increases the possibility of cloud movement interfering with the data (Stumpfel et al. 2004).

Figure 29. The camera with 180-degree fisheye lens on the roof of the building (left), a typical probe taken with the fisheye lens and neutral density filter (Stumpfel et al. 2004)

Due to the difficulty of accurately modeling a sky luminance distribution because of rapid changes of the daylight environment, 145 luminance measurement points were taken. While the number is large, this data is still insufficient to represent actual sky conditions. In addition, one fixed aperture size does not allow capturing the sun; therefore, two different apertures were used while varying shutter speeds for this research. The low dynamic range images taken at both aperture sizes, a total of 22 images, were then fused together using a specific calibration for this application. Horizontal illuminance was measured at the camera level and used to calibrate. This research showed that image-based sky models can provide reliable results for sky luminance and illuminance distributions (Stumpfel et al. 2004).

The methodology and results of pilot field illuminance measurements using an unmanned aerial vehicle (UAV) were researched in (Tabaka 2020). The main goal of this study was to quantify the luminous flux emitted in the upper hemisphere (towards the sky) from luminaires based on obtained measurement data, as the luminous flux emitted upwards is a source of undesired light pollution. A test luminaire was placed in an open area away from any large city agglomeration and illuminance was measured with the necessary equipment mounted onto the UAV. Unlike other research, no HDR imaging was utilized in this study. Instead, the luxmeter mounted to the UAV recorded all data.

The UAV traveled in the path seen in Figure 30, at a height of 14m above ground, measuring only one quadrant of the luminaire output as the other quadrants would be similar but reflected at some multiple of 90 degrees. After measurement from the luxmeter meter on the UAV were recorded, measurements were also taken on the ground with a trolley, following the same path.

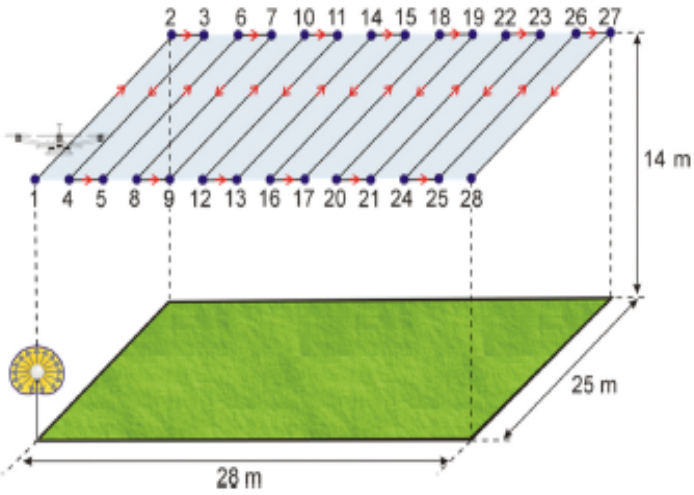

Figure 30. UAV route and measurement grid (Tabaka 2020)

One important limitation of this study is the lack of information on the spectral distribution of radiation emitted towards the sky as the luxmeter only allows luminous flux to be determined from its recorded data. The authors conclude that the phenomenon of light pollution is greatly influenced by spectral characteristics of radiation so a spectrometer should be installed onboard the UAV in future research to account for all forms of radiation as shown in Figure 31 (Tabaka 2020).

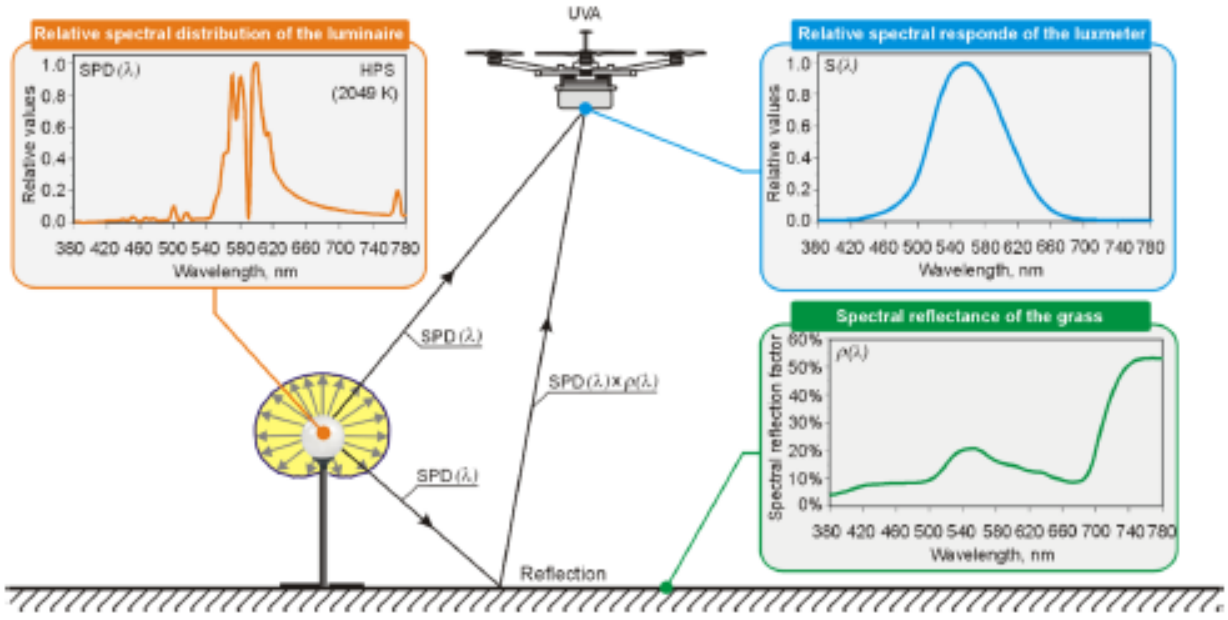

Figure 31. Radiation that Reaches Luxmeter on UAV (Tabaka 2020)

While the previously mentioned studies are validated for their specific research purposes, none are conducted with the 90-degree (normal to measurement plane) camera angle, as seen in the camera setups and subject scenes. Only a few illuminance studies were conducted outdoors; Tabaka 2020, Nath et al. 2015 and Yun and Kim 2018, yet none are set up with this critical angle. While Nath et al 2015 focused on an even illuminance plane in sports arenas, high dynamic range imaging was not used, instead a rough set theory was proposed. Instead of a digital camera, Yun and Kim 2018 utilized a CCD camera pointed straight up to map the sky luminance. While a different type of camera was used, HDR imaging techniques were still applied to measure luminance values which in turn can be used to calculate illuminance values.

In addition to the lack of research done relating illuminance measurements from high dynamic range imaging in exterior scenarios from a 90-degree angle, no research has been completed on the post-processing techniques, best technology or best data-derivation methodology for illuminance data produced from HDRI. One might be able to assume it will be similar to luminance research as the same relative methodology is used for both but further research must validate this. The two figures on the following page, Figures 32 and 33, analyze the two main technological differences in illuminance research. It can be seen that many different models of lenses and cameras are used. While there is much variation, the same lens models and camera models can be seen in miscellaneous lighting parameter studies and luminance studies. Research on illuminance derivation through HDR photography is lacking when compared to HDR luminance research and the proposed research aims to bridge gaps existing between the two fields for exterior lighting applications.

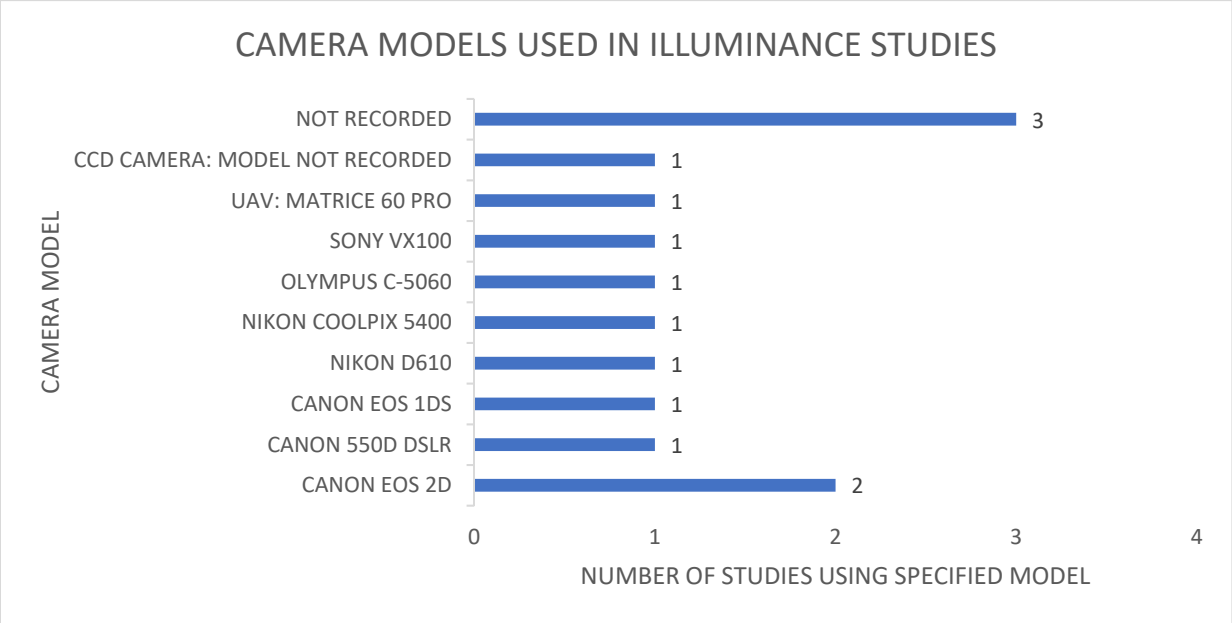

Figure 32. Camera Models Used in Illuminance Studies

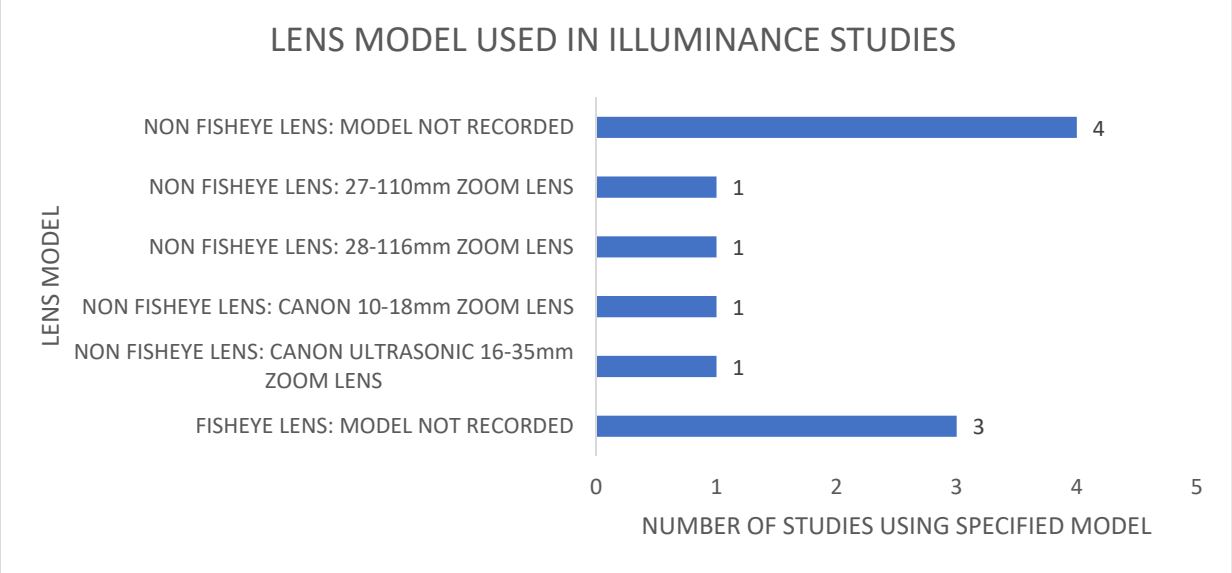

Figure 33. Lens Models Used in Illuminance Studies

2.4 *CONCLUSIONS*

HDR imaging is a promising and reliable technique that can be used for lighting measurements. While the different combinations of camera models and lens model may mean accurate HDRI results can be achieved with any model of either, it also validates that not much research has been done as to what camera and lens combination yields the most accurate results. Further research should be conducted on the best technology and instruments used in HDRI studies in order to provide the most accurate results. Additionally the presence of unrecorded data in the literature review process is cause for concern. Only 2 studies reported all key data points, technology and methodology used (Cai and Chung 2010, Inkarojrit 2005). Some research in the literature review validates a new method, tests new technology or improves existing research methods, but fails to report important data for researchers in the same field. This makes it difficult to use the method or technology proposed in future research as there are too many gaps to be certain.

The extensive literature review verified that while illuminance values have been obtained through HDR imaging, a study has not yet been conducted using the methodology and scenario presented in this research.

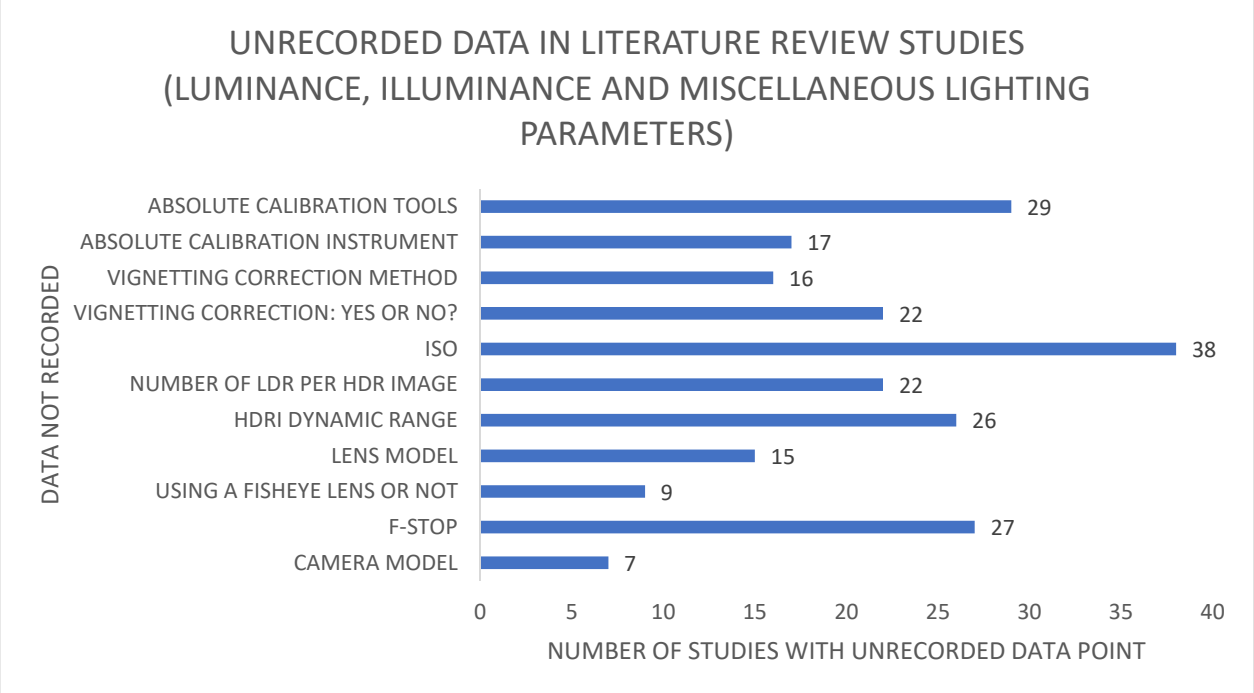

Figure 34. Unrecorded Data in Literature Review

3.0 METHODOLOGY

Not only is high dynamic range imaging used as a technique to simulate accurate lighting and color images, it can also be used as a tool for lighting measurements such as luminance, illuminance and bi-directional reflection distribution functions. The final HDR image must be post-processed to correct small errors or inconsistencies including unwanted voltage bias (readout noise), dark current (thermal noise, ambient temperature dependent) and conductive noise due to non-uniform quantum efficiency on photo sites (Cai et al. 2017). Another inconsistency found in HDR images is fixed-pattern noise, which is caused by hot, stuck and dead pixels that are most likely present and influencing the measurements. All of these types of noise should be filtered out in post-processing software to validate accurate lighting measurements from the final HDR image. Following, the pixel coordinates and RGB values derived from the photographic images can be used for recovering information such as geometry, color and material properties, among the other lighting parameters previously mentioned. Specific software such as Photosphere, Radiance and Photolux can embed HDR images with spatial luminance data of the scene with proven errors limited to 1.5-10% for luminance mapping (Cai et al. 2017).

Collecting luminance data from HDR images involves calibrating the image using real-time luminance measurements on a target with known reflectance. By simultaneously measuring the luminance values of the reference targets and capturing the HDR image components, software is able to linearly calibrate the resulting image with luminance data. A similar technique can be utilized to calibrate illuminance values as well. The illuminance data produced also requires the illuminance meter values taken at the time of the capture in order to calculate the calibration factor and apply it to the image. Illuminance data can also be obtained from the luminance maps or data produced by HDRI.

Several studies have been conducted to find limitations and errors related to HDR photography (Cai et al. 2015, Inanici 2006a, Safranek and Davis 2020). These errors include vignetting, lens distortion and lens flare among some others. These possible errors and correctional techniques were analyzed and studied to ensure this researcher's collected data is validated with proper methodology. There is very little research on what technological instruments – digital camera, fish eye lens, illuminance or luminance meter – are best for accurate results just as there is little investigation on what methodologies or software to use for accurate data. Several methods

exist to derive accurate luminance and illuminance data from HDRI using software and mathematical equations.

3.1 *RESEARCH OBJECTIVES*

The presented and outlined research in the following sections aims to bridge several gaps in the research. The research gaps found in the investigation of HDRI-obtained luminance and illuminance data include:

1. Existing research revolves heavily on luminance, HDRI-produced luminance data, luminance-based applications and best HDRI methodology for obtaining accurate data. Limited research exists on illuminance and HDRI-produced illuminance data. No research exists on the best HDRI methodology for accurate illuminance data or the best technology and software to use.
2. No studies in either illuminance- or luminance-based HDRI applications validate data for an exterior scene from straight above. Though exterior HDRI research has become more common in recent years, none have looked straight down on a scene. Whether illuminance- or luminance-based, all research done with the digital camera fixed downward are focused on a single luminaire, color checkers, grey scales or reflectance standards. An exterior scene, such as an athletic stadium, a public courtyard or an exterior seating area, has not yet been analyzed with HDRI for illuminance data.

The focus of the investigation was placed on validating illuminance values obtained from HDRI of an exterior scene from straight above it. If validated, this technique could replace labor-intensive and time-consuming methods used currently, similar to the way HDRI replaced traditional hand-held measurement devices.

If the HDRI-obtained illuminance values are validated, the methodology will be scaled to fit a larger environment. If proven accurate, this methodology would unlock endless possibilities for related HDRI and lighting parameter research as well as providing a more convenient way to measure illuminance of complicated environments.

The methods implemented in this study were influenced by the suggested best practices in past research (Moeck and Anaokar 2006, Yun and Kim 2018, Inanici 2006a, Cai et al. 2015, Safranek and Davis 2020, Tabaka 2020, Cai and Chung 2010, and Beltran and Mogo 2005). The

process of creating an HDR image while minimizing the many possible errors must be precise and methodical. Several parameters of HDR and this study were evaluated in order to ensure proper measurement protocols were taken and future results could be validated.

3.2 *REQUIREMENTS*

The methodology and data collection processes of this research invovles both software and hardware, which are discussed as follows:

- A digital camera with a circular lens (CCD and CMOS sensors are equivalent competitors in the camera market in today's technologically advanced world (Stanley 2016)).

- A tripod on which to set the camera to ensure the camera remains still during the sequence of multiple exposures.

- A computer or mobile phone to remotely control the camera and process the images (and a means of connecting the device to the camera if not through Wifi or Bluetooth).

- A calibrated spot luminance meter and a reflectance standard of known value to make the photometric adjustment through a spot luminance measure on the reflectance standard (Pierson et al 2021).

- A calibrated illuminance meter or spectrometer to check the validity of the measurements from the calibrated HDR image.

- 1-foot (12-inch) by 1-foot (12-inch) "grid" should be present at the scene for assistance centering the reflectance standard and data locations for easier luminance and illuminance measurements.

- *DSLRRemotePro, DigitSnap, HDRcapOSX*, *or qDSLRdashboard* available for Windows, Linux and macOS or *Canon Camera Connect* application available on mobile phones to remotely control the camera (Pierson et al. 2017).

- *Photosphere* to apply the photometric adjustment, available only for macOS (Ward 1998).

- *Adobe Illustrator* to overlay a grid (in the pilot studies) for later calculations.

3.3 *ENVIRONMENTAL CONSIDERATIONS AND CONSTRAINTS*

In addition to the technology and equipment required for this research, below are more environmental requirements:

- The data collection must be conducted on flat, grass or turf ground.

- The data collection must take place in night sky with the only illumination coming from exterior or stadium lights. Daytime measurements can suffer from lack of consistency due to the dynamic nature of cloud patterns.

- No wind or very little wind can be present at the time of the data collection; grass or turf moving due to the wind will negatively affect the sequence of low dynamic range images and the final HDR image will be blurry in some or all areas.

- The proper functioning of the equipment should be ensured before starting any data collection. As it deteriorates over time, the camera sensor should be checked for stuck, dead or hot pixels that may show up in the images (Jacobs and Wilson 2007).

3.4 *CAMERA SET UP*

To capture a sequence of multiple exposures, there are three main options; manual bracketing, automatic exposure bracketing, and automatic bracketing with a remote control. Manual involves changing exposure manually on the camera in between each low dynamic range image capture. The most common method is the automatic exposure bracketing (AEB), a feature often included in the camera but can generally be limited to only five (5) photos in a sequence. Two issues arise with this technique; not all cameras offer this feature and it is recommended that more than 5 images are used in HDR creation. The last technique, and the one that will be utilized for this research, is automatic bracketing with a remote control. Software such as *DSLRRemotePro, DigitSnap, HDRcapOSX* or *qDSLRdeshboard* can be used to capture a sequence of no more than fifteen (15) sequential exposure bracketed images at once (Pierson et al. 2017). This software, in addition to others, are used so the camera can remain in a fixed position throughout the entire process of capturing low dynamic range images. The application Canon Camera Connect will be used for this research as it has similar functionality as the previously mentioned software. Any change is the photo frame, angle or orientation of the camera will negatively affect the validity of results pulled from those images as luminance measurements are very much dependent on the

viewing direction of the camera lens. Keeping optical properties consistent for noise reduction, the camera locations and lens' aperture and focal length are fixed at a single trial, while only the camera shutter speed changes (Cai et al. 2015). This is where a laptop, or another sort of technology, connected to the camera for remote control is required. In addition to this remote control, the camera should be set up on a tripod to avoid alignment problems during HDR generation (Pierson et al. 2017). To ensure quality calibration procedures in the later data collection and validation processes, a reference luminance measurement was included in the scene captured by the camera. The placement of a reference luminance measurement, a reflectance standard as discussed previously, also minimizes vignetting effects and lens flare effects. The setup used in this research can be seen below.

3.5 *GRASS REFLECTANCE*

As this study is conducted outside, understanding the effects of exterior elements, grass and turf in this research, on the reflectance of the measurement surfaces in this study is vital to prevent unnecessary errors. While grass and soil might appear to be diffused surfaces, the reflectance values can vary quite easily depending on the viewing angle in addition to other, more obvious factors; moisture content, cell structure, the stress and age of vegetation, etc. While some contributing factors cannot be controlled by the researchers, the viewing angle and its effect on the reflectance of exterior vegetation will be one of many factors studied to avoid error in this study. In Figure 35, a curve presented by Hodgson and Overton (1965) characterizes the reflectance of grass according to the viewing angle at which the high dynamic range image is taken. It can be seen that the reflectance of grass is at a maximum at a viewing angle of approximately 35 degrees and a minimum at 90 degrees. Therefore, taking the series of low dynamic range images at 90 degrees, or normal to the measurement plane, will minimize the associated error.

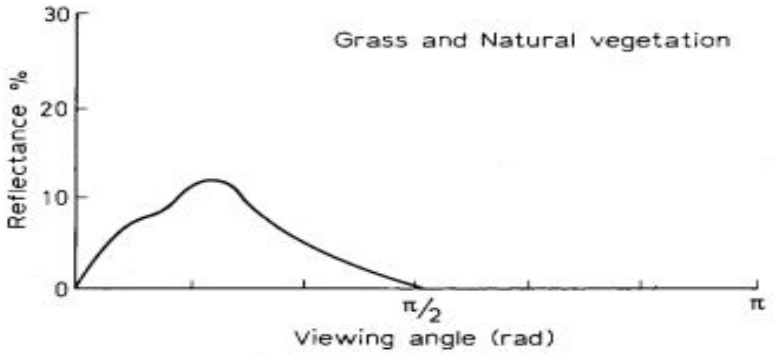

Figure 35. Reflective Properties of Grass and Natural Vegetation (Hodgson and Overton 1965)

3.6 *IMAGE FILE FORMAT*

When comparing image formats and what is best used for a quality high dynamic range image, two categories are discussed; raw (lossless) and compressed (lossy) (Hiscocks 2011). A raw image file stores the captured pixel values exactly as they are generated by the camera sensor, which varies with the different camera manufacturers. Raw images are usually converted to some more universal format, such as a tagged image file format (TIFF), which contains all the information of the original and can be considered a lossless format as well (Hiscocks 2011). While no information is lost, the files are very large for both Raw and TIFF. For example, a Canon raw format (DNG) is typically around 15 Megabytes per image while TIFF formatted file is closer to 60 Megabytes per image. If a TIFF formatted file is processed to monochrome, which is rare when trying to measure lighting parameter values, the size drops to about 20 Megabytes per file, still larger than a DNG. For many applications, including both Photosphere and Radiance, raw format images are overkill as there is redundant information and the file will likely need to be compressed to work with these programs. Compressing an image is "lossy", the other category of image formats, the process cannot be reversed to the original image exactly. The only advantage to compressing an image file is that the size is reduced tremendously, saving storage space and speeding up program processes. A typical JPEG image file is about 71 Kilobytes, a factor of 800 smaller than the comparable TIFF image (Hiscocks 2011).

3.7 *NUMBER OF IMAGE FILES AND CAMERA SETTINGS*

Safranek and Davis (2020) recommends capturing 12-14 low dynamic range images to ensure no crucial information in the scene is excluded in the final HDR image. Similarly, a study in 2011 on improving the quality of HDRI states starting from 4-5 exposures minimum will suffice, but using more exposure values or shutter speeds will significantly increase the quality of HDR images of color, black and luminous surfaces (Cai and Chung 2011). This minimum of 4-5 low dynamic range images can be seen to un-validate a number of the studies in the previous literature review. Cai et al 2015 recommends, for exterior scenes, each scenario should be recorded by capturing multiple, 18 as an example, low dynamic range images which is validated by Pierson's (2017) recommendation that taking the largest bracketed sequence possible (18 images) will ensure all scene information is included. However, to facilitate and accelerate the HDR creation process, only the low dynamic range images that contain useful information should be used; only

using low dynamic range images where the darkest exposure has no RGB value greater than 228 and the lightest exposure has no RGB value below 27 (Pierson et al. 2017).

In addition to the number of low dynamic range images, the range of sequential exposure values also affects the quality of HDR images. Only exposure time, or shutter speed, should be varied in a sequence, since changing the aperture would increase problems with vignetting and shutter speed is a more reliable measure than aperture size (Pierson et al. 2017). While it is acceptable to vary aperture values from one sequence of LDR to another, the aperture value must remain consistent if the LDRs are to be fused together to form a final HDR. It has been researched that large apertures (f/5.6) produce higher quality HDR images than small ones (f/22), whereas no significant differences were found with medium apertures. The least error percentage was obtained at f/5.6 and the most error was found at f/22 for a range of focal lengths. No significant impact on the quality of HDR images photographed at f/5.6 was found; the focal length setting must be carefully selected when choosing a small aperture setting, such as f/22 (Cai and Chung 2011). Finally, the film speed should be set on ISO 100 (Pierson 2017). Pierson et al. (2021) presented a table of recommended camera settings as shown in Figure 36.

Setting	Value
Film speed	ISO 100
White balance	Daylight (5200K)
Exposure mode	Manual
Light metering mode	Insignificant
Focus mode	Manual
Focus value	Infinite
Image quality	Largest
Image type	JPEG or RAW
Picture style	Neutral
Peripheral illumination correction	Disabled
Color space	sRGB

Figure 36. Camera Settings Used in a Sequence of Multiple Exposures for HDR Photography (Pierson et al. 2021)

These settings were be kept constant for the whole calibration process and all luminance maps generated after. Similar to altering the aperture value, modifying the white balance setting during the image capture process alters the color space transitions and the camera response function (Jacobs 2012, Inanici 2006a). Some values might be referenced differently when using different camera brands.

3.8 *REFLECTANCE STANDARDS*

The accurate representation of surface reflectance values is a required component of any lighting evaluation methodology (Mardaljevic et al. 2015). A reflectance standard is a physical reference sample that includes ratio values between the total amount of light radiation reflected by a surface and the total amount of light radiation incident on the surface across the visible spectrum (Wen 2015). Two kinds of reflectance standards exist to represent to two types of reflection; specular reflectance standards and diffuse reflectance standards. In most practices, white and black reflectance standards are utilized for calibration. However, reflectance standards are available in almost any color as well. As mentioned previously, HDRI has become more popular as the technology of consumer grade digital cameras has progressed. In order to obtain luminance, illuminance, as well as other lighting metrics from HDR images, the reflectance properties of the object or scene in question must be known. An HDR image is required to present the wide range of real-world luminance, therefore numerous low dynamic range images must be taken by a digital camera to construct this final HDR image. Unfortunately, all devices dealing with color including a digital camera, a monitor, scanners and printers have a device-dependent color space. In other words, the same red color can be represented by a different RGB value on different devices (Yoo et al. 2009). Therefore, the color space of a digital camera or an HDR camera must be transformed from a device-dependent color space to a color-independent color space. This can be done by placing a reflectance standard or a color-chart in the scene or photo frame. With a known reflectance value, or color calibrations in the case of using a color checker chart, the other unknown measurement values can be calibrated based on this one known data point. Alternatively, reflectance can also be derived from relative measurements of luminance between the sample surface and one or more standard diffuse reflectors under the same lighting condition. Basic methods have been developed on the premise that reflectance can be determined from an HDR image with a reflectance standard or color checker, which can in turn determine various other lighting parameters.

3.9 *MERGING LOW DYNAMIC RANGE IMAGES*

Once a selected sequence of low dynamic range images has been collected, an HDR image can be created using a software such as Photosphere. Photosphere has been validated as one of the

most accurate HDR software currently available and is also the most commonly used (Au and Donn 2003). The most predominant feature of Photosphere is that accurate luminance values can be obtained by simply "selecting a pixel value"; this technology or feature has not been present in other HDR softwares. Photosphere was used for HDR creation in this research. Photosphere is a digital image browsing and cataloging tool, with unique features to create HDR images from bracketed exposure sequences and it supports a number of the standard HDR file formats, as previously discussed (Beltran and Mogo 2005). The HDR creation is completed including automatic lens flare removal and ghost removal. This merging process is based on the principle that each image in the low dynamic range sequence will have different pixels properly exposed, but each pixel will be properly exposed in one or more images. Therefore, a weighting system is used on the pixels of each image to cut out the influence of over- or underexposed pixels and increase the influence of correctly exposed ones in the merging of exposures (Pierson et al. 2021). This is where the importance of consistent scenes comes in; it is imperative that each individual pixel is properly merged. Creating an accurate HDR image comes from a camera response curve created when fusing the photographs, something Photosphere does automatically during this process.

3.10 *VIGNETTING CORRECTION*

The vignetting effect is one of the most documented sources of error in HDR imaging techniques; it is the light falloff that can be observed toward the edges of an image, especially when a fisheye lens is used (Pierson 2017). Vignetting is the gradual decrease of captured luminance towards the edge of an image, where that decrease does not actually exist in the true

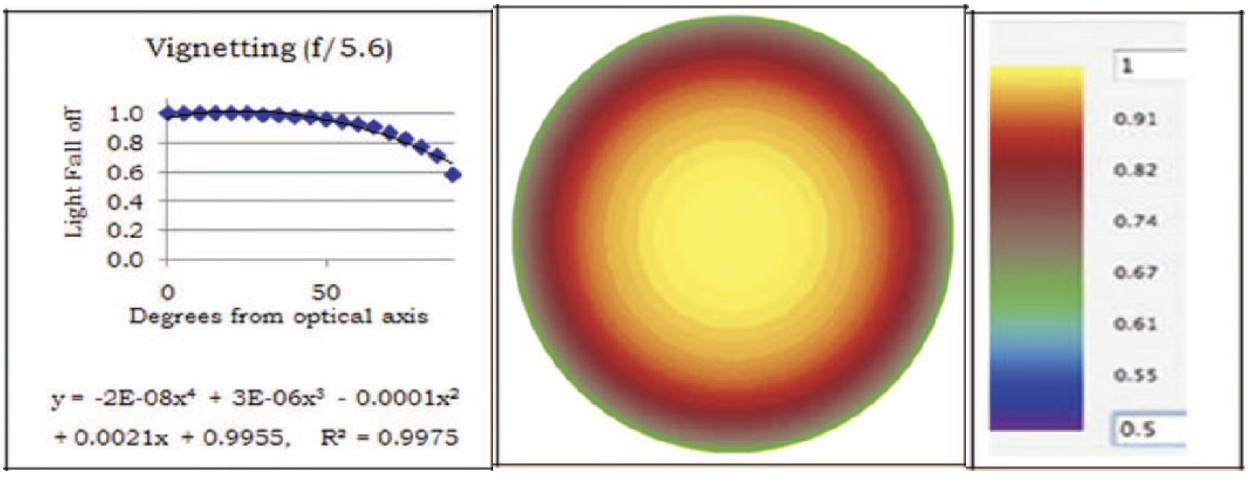

Figure 37. Vignetting Function of Lens (Inanici 2010)

scene being captured (Safranek and Davis 2020). As light enters the lens, optical elements, such as the aperture diaphragm, obstruct off-axes rays, preventing incoming light from entirely filling the aperture and camera sensor. As a result, luminance values for points away from the center of an image measured by HDRI are systematically less than the actual luminance in the scene (Safranek and Davis 2020). The vignetting function of angular distance to the center of the HDR image can be seen in Figure 37, this function is determined as the camera is rotated in 5-degree intervals away from the target; the camera response function for each aperture is determined as a polynomial fit (Inanici 2010). The vignetting function and effects change based on aperture size, f/5.6 is presented as that is the aperture selected in this research. In addition to the vignetting correction function in Photosphere, the researcher will take other precautions to limit the effects as well.

The final data collection of this research will be conducted outside, with the digital camera mounted on a tripod pointed straight down at 90 degrees relative to the ground to limit the reflectance of the grass as seen in Figure 45. The final data collection will contain a square grid, measuring 1-foot by 1-foot along the interior of the sides. Located precisely in the center of this square will be the diffuse reflectance standard, as a reference luminance measurement taken near the center of the scene will limit vignetting effects (Safranek and Davis 2020). Only the pixels in this square grid will be calculated and analyzed. Not only will this eliminate the pixels effected by vignetting even after the Photosphere correction function is applied, it also eliminates the additional reflectance from the grass outside of this imperative 90-degree angle. Pixels around the exterior of the final HDR image are no longer in the 90-degree frame of view and are therefore, contributing unwanted reflectance as well as vignetting effects to the luminance values that will be used to calculate illuminance values. Eliminating these pixels will allow more accurate luminance and illuminance measurements.

3.11 *CALIBRATING FINAL HIGH DYNAMIC RANGE IMAGES*

The digital camera turns an image into a two-dimensional array of pixels with each pixel representing the light intensity at that point (Hiscocks 2011). HDR images contain luminance information and provide more realistic values than conventional low dynamic range images. The HDR imaging technique allows the ability to collect the relative luminance values of every pixel in the lens field of view when a known luminance value is presented in the scene. Consequently,

the luminance values collected at these pixels are proportional to the illuminance values at the same location, a mathematical relationship that will be discussed later in Section 4.14 on page 49. HDR photography has been demonstrated as a useful tool that can capture luminance values overall within 10% accuracy over a wide range of luminance (Coyne et al. 2008). In order to retrieve the real, accurate luminance values of the scene, a calibration adjustment must be applied (Pierson et al. 2017). For this purpose, at least one spot luminance value should be measured in the scene during the low dynamic range image sequence capture. Photosphere offers the ability to calibrate the entire HDR image based on the known area's luminance and a scaling factor. This scaling factor is the ratio of the measured to the HDR-derived luminance value of a pixel in the field of view (Jacobs 2007). The factor is believed to be dependent on the lens aperture and the type of the main lighting source, and should theoretically be around 1 (Jacobs 2007).

3.12 *LUMINANCE MAPS*

Calibrated HDR images can be used to create a luminance map. While moving the cursor over the calibrated HDR image, the luminance values can be seen in the upper right corner of Photosphere corresponding to the location of the cursor. HDR images created in Photosphere can also be transformed into three types of images; false color, iso-contour and human visual sensitivity (Beltran and Mogo 2005). The false color file creates a false color picture of the luminance levels expressed in cd/m^2, the human sensitivity tool adjusts the exposure of the HDR image and mimics human visual perception and the iso-contour tool is similar to false as it draws demarcation lines in equal steps (Beltran and Mogo 2005).

Some limitations of luminance maps obtained from HDR photography pertain to vignetting among some other, less pertinent effects (Inanici 2006b, Moeck and Anaokar 2006). As previously discussed, vignetting will be corrected in the set up and post-processing steps of data collection to ensure accurate luminance maps.

3.13 *NUMBER OF DATA POINTS*

The number of individual data points for this research was decided according to the lighting measurement techniques according to the IES Handbook for sports stadiums. The IES Lighting Handbook sets recommendations for the quantity and quality of illumination. The quantity of illumination is the recommended quantity of light as stated in terms of the maintained average horizontal and/or vertical illuminance levels. The quality of illumination refers to the

recommended quality of illumination as stated in terms of factors such as the uniformity ratio, uniformity gradient and coefficient of variation. In addition, the lighting designer must consider direct and reflected glare, color rendering ability, color contrast and modeling (Kaufman 2020). Not only are the requirements for quantity and quality given, the method of measuring is also included. For this research, both a soccer field and a football field were analyzed.

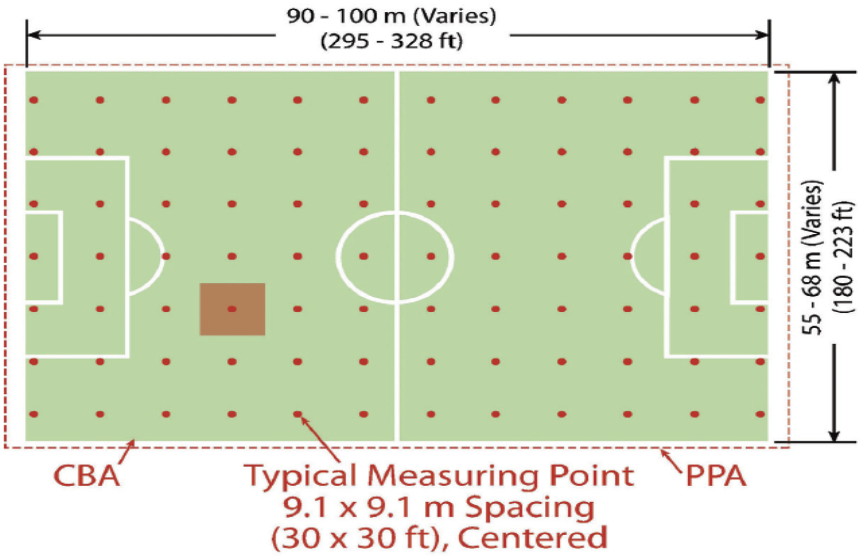

Figure 38. Suggested Soccer Field Calculation Grid (Kaufman 2020)

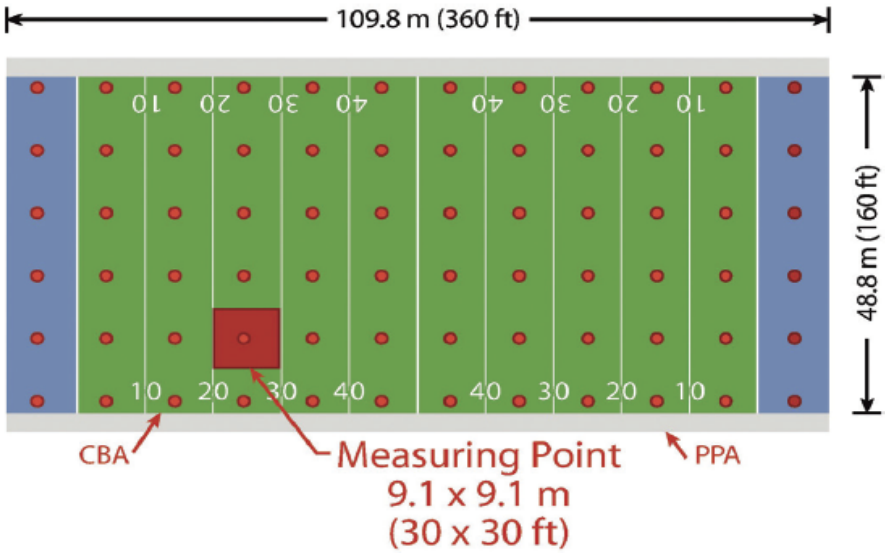

Figure 39. Suggested Football Calculation Grid (Kaufman 2020)

The playing surface of the soccer field, shown in Figure 38, is approximately 68-meters by 100-meters, varying slightly field to field. This surface is split into a grid containing 84 points; on each grid point an illuminance test is made to measure the horizontal illuminance. Horizontal

illuminance measurements are also required at each point; one in each direction to equate four horizontal illuminance measurements at each grid point. Similarly, a football field has the same 30-foot by 30-foot spacing for measurements but only has 72 measurement points due to the difference in field area between the two sports fields, as seen in Figure 39. While the two fields are rectangular in shape and the luminance map from this research must be square to maintain HDR image integrity, conclusions on the spacing of these data points were drawn from the IES Lighting Handbook calculation methodology (Kaufman 2020).

The ratio of a 30-foot (9.1-meter) by 30-foot (9.1-meter) grid from the IES Handbook to the 160-foot (48.8-meter) width of the football field equates to 0.1865; which when multiplied by 12 inches (as the dimension of the grid) equates to 2.23, meaning the maximum spacing between grid lines must be 2.23 inches in order to maintain the same proportion of measurement spots to area/space in question (Kaufman 2020). Spacing gridlines 2 inches apart would exceed this requirement and provide more data points in this research. In the 1-foot (12-inch) by 1-foot (12-inch) grid with grid lines spaced 2 inches apart, 36 data points are provided in this study.

3.14 *CALCULATING ILLUMINANCE FROM LUMINANCE*

Assuming an accurate luminance map, it is possible obtain accurate illuminance (and even further, luminous intensity) distributions with a series of mathematical equations. Several methods exist in the research to derive illuminance from luminance.

Inanici 2010 derived illuminance from the average luminance values in the hemispherical fisheye images as hemispherical fisheye projection is half a sphere projected such that each

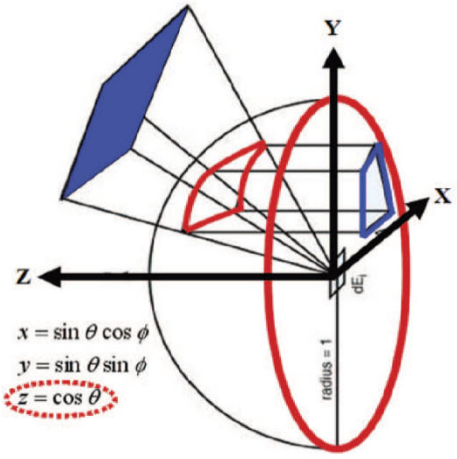

E = Illuminance
L (θ,ϕ): Luminance in the direction of θ,ϕ.

For any hemisphere of luminance L(θ,ϕ), the horizontal illuminance E is calculated as:

$$E = \int_0^{2\pi} \int_0^{\pi/2} L(\theta,\phi) \sin\theta \cos\theta \, d\theta \, d\phi \qquad (1)$$

For a uniform luminance $L(\theta,\phi) = L$

$$E = \pi L \qquad (2)$$

Figure 40. Calculation of Illuminance from Luminance Values in Hemispherical Fisheye Projection (Inanici 2010)

differential area corresponds to the original area multiplied by the cosine of the polar angle (Inanici 2010, Ward and Shakespeare 1997). As a result, illuminance values can be derived from luminance values as shown in Figure 40.

In comparison, Bellia and Spada (2013) utilized a video-luminance-meter to obtain a luminance map and then furthered the research by obtaining illuminance and luminous intensity distributions by means of measurement on a perfectly diffusing (Lambertian) surface. Upon a Lambertian surface, a light beam which strikes a point of an opaque uniformly diffusing surface is reflected in all directions of the half-space following Lambert's law of diffuse reflection (Bellia and Spada 2013); where luminous intensity (I) in candelas is directly related to the cosine of the angle (α) between the viewing direction in question and the normal surface:

$$I(\propto) = I_0 \times \cos \propto \tag{3}$$

Resulting, luminance (L) at this point is constant with viewing direction and depends only on the illuminance (E) and the reflection factor (ρ):

$$L(\propto) = L = \frac{\rho \times E}{\pi} \tag{4}$$

A previous procedure for the measurement of illuminance by means of the video-luminance-meter by positioning Lambertian targets on work planes has been presented in previous research (Bellia et al 2010) by the equation:

$$E_t = \frac{L_t \times \pi}{\rho_t} \tag{5}$$

Illuminances corresponding to all targets can be detected by a single measurement from a single light source placed at a distance from a uniformly diffusing reflecting surface. The illuminance produced by a light source at a point on a surface is given by:

$$E_p = \frac{I \times \cos \propto}{r^2} \tag{6}$$

Similarly, illuminance was derived from luminance maps to find the individual illuminance contributions of each architectural feature of the building in question. This allows a new way of illuminance analysis, measuring the quantity of light due to specific objects, colors and features (Moeck and Anaokar 2006). Once a luminance map was obtained, calculations of illuminance began based on the geometry given in Figure 41.

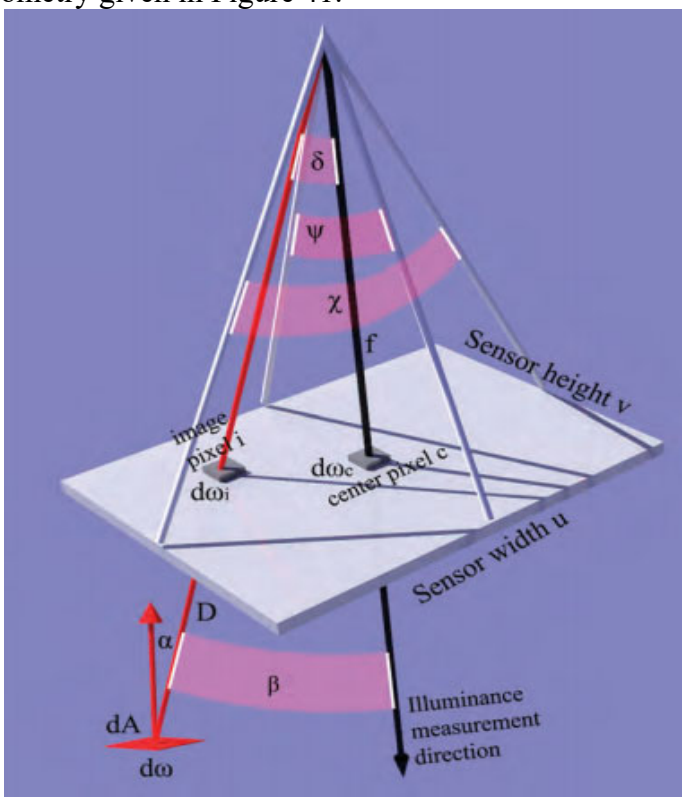

Figure 41. Geometry of Illuminance Calculations (Moeck and Anaokar 2006)

The illuminance E_i due to a scene element represented by pixel "I" is:

$$E_i = L_i \cos\delta \; dw_i \tag{7}$$

Where L_i is the luminance of pixel "i" and the illuminance due to an image is:

$$E = \int L_i \cos\delta \, dw_i \tag{8}$$

The mathematical procedure used in this research will assume the grass or turf in question acts as a Lambertian reflective surface. The differential area (dA) of a Lambertian surface is infinitely small and therefore equivalent to a point source, allowing the flux leaving the surface to be modeled as geometrical rays. The intensity (I_θ) of each ray leaving the surface at an angle (θ)

from the surface normal is given by Lambert's cosine law, where (I_n): is the intensity of the ray leaving in a direction perpendicular to the surface (Ashdown 2002):

$$I_\theta = I_n \times \cos\theta \tag{9}$$

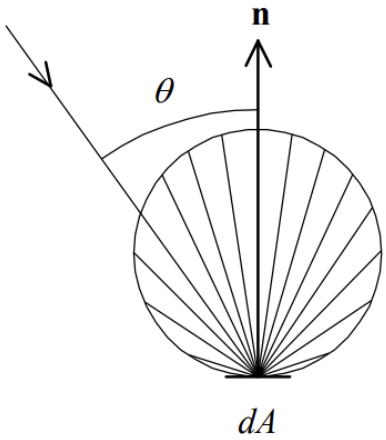

Figure 42. Reflection from a Lambertian Surface (Ashdown 2002)

The derivation of Equation 9 becomes easy when viewing dA from an angle θ. For the differential area dA with a constant radiance or luminance (L), its intensity varies in accordance with its projected area, which is dAcosθ (Ashdown 2002). Following, for any Lambertian surface:

$$L = \frac{dI}{dA\cos\theta} = dI_n/dA \tag{10}$$

The very simple relationship between luminous exitance (M) and luminance (L) for flux leaving a Lambertian surface:

$$M = \pi L \tag{11}$$

Placing a differential Lambertian emitter dA on the inside surface of an imaginary sphere, as seen in Figure 43, the inverse square law provides the illuminance (E) at any point (P) on the inside of the sphere. Where D is the diameter of the sphere, d=Dcosθ, therefore:

$$E = \frac{I_\theta \cos\theta}{(D\cos\theta)^2} = I_\theta/D^2\cos\theta \tag{12}$$

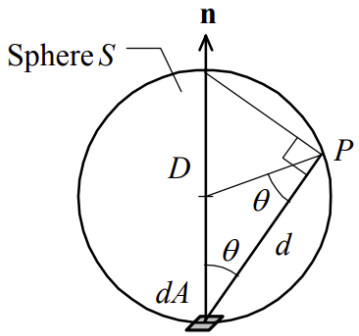

Figure 43. A Lambertian Emitter Illuminating the Interior of a Sphere (Ashdown 2002)

From Lambert's cosine law (Equation 9), stating that the illuminance of any point P on the inside surface of the sphere is a constant:

$$E = \frac{I_\theta \cos\theta}{D^2 \cos\theta} = I_n/D^2 \tag{13}$$

From the definition of illuminance, Φ=EA for constant flux density across a finite surface area A. Since the area of the surface of a sphere with radius r is given by $A=4\pi r^2=\pi D^2$:

$$\Phi = EA = \frac{\pi I_n D^2}{D^2} = \pi I_n \tag{14}$$

Given the definition of luminous exitance and luminance for a Lambertian surface:

$$E = \frac{d\Phi}{dA} = \frac{\pi dI_n}{dA} = \pi L \tag{15}$$

However, the perfectly diffuse reflector (a Lambertian surface) is an abstraction not encountered commonly in real life, especially grass or turf. While some previous research assumed so, this research will account for the reflectivity of the grass/turf in its calculations. A Lambertian surface can be used as a reasonable approximation to allow for simple calculations but accounting for the surface reflectivity only adds one more value in the equation.

The luminance of a diffuse and totally reflecting (Lambertian) surface is given by:

$$L = \frac{1}{\pi}E \qquad \text{in cd/m2} \tag{16}$$

This relationship has already been seen in both previous studies (Inanici 2010, Ashdown 2002). When accounting for surface reflectivity, a diffuse surface that reflects only a fraction, R, of the incident light will show the luminance as (Bruel and Kjaer 1978):

$$L = \frac{R}{\pi} E \qquad \text{in cd/m2} \tag{17}$$

This equation can easily be rearranged to solve for illuminance from known luminance values and surface reflectance values.

The spectral reflectance curve of healthy, green vegetation can be seen below. In general, healthy vegetation absorb electromagnetic energy in the visible region. The wavelengths visible to the human eye are between 380 nm and 780 nm, meaning only that portion of the Figure 44 will be analyzed to find the reflectance of grass. As it varies with the wavelength, an exact coefficient cannot be determined so an estimation of 0.16 will be used in calculations.

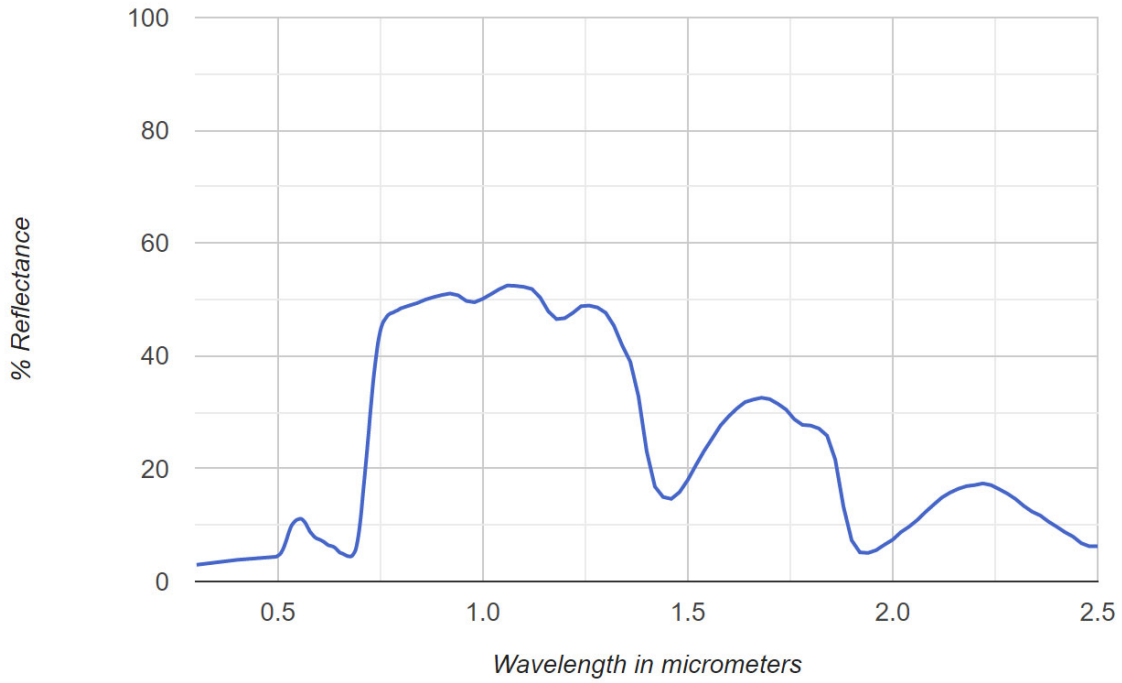

Figure 44. Spectral Reflectance of Grass (Spectral Reflectance 2019)

3.15 *PROCEDURE*

The complete procedure to validate illuminance values from a luminance map acquired by high dynamic range photography is as follows:

1. With the environment and location requirements met, the digital camera was mounted to the top of the tripod and pointed straight down at a 90-degree angle relative to the ground. All legs of the tripod were fully extended so the camera was as high off the ground as possible, as seen in Figure 45. The camera was rotated directly between two legs of the tripod so that the legs were not in the frame of view, as seen in Figure 46.

Figure 45. Camera and Tripod Setup for the Pilot Study (left) and final Data Collection (right)

2. The reflectance standard was placed directly below the camera lens. As the camera provides a box on screen located in the center of the frame of view, lining up the reflectance standard with this box is simple. In addition, the square grid was placed directly underneath the camera with the reflectance standard exactly in the middle. The camera

and tripod combination was configured and oriented in a way that no shadows are present in the square grid, as seen in Figure 46.

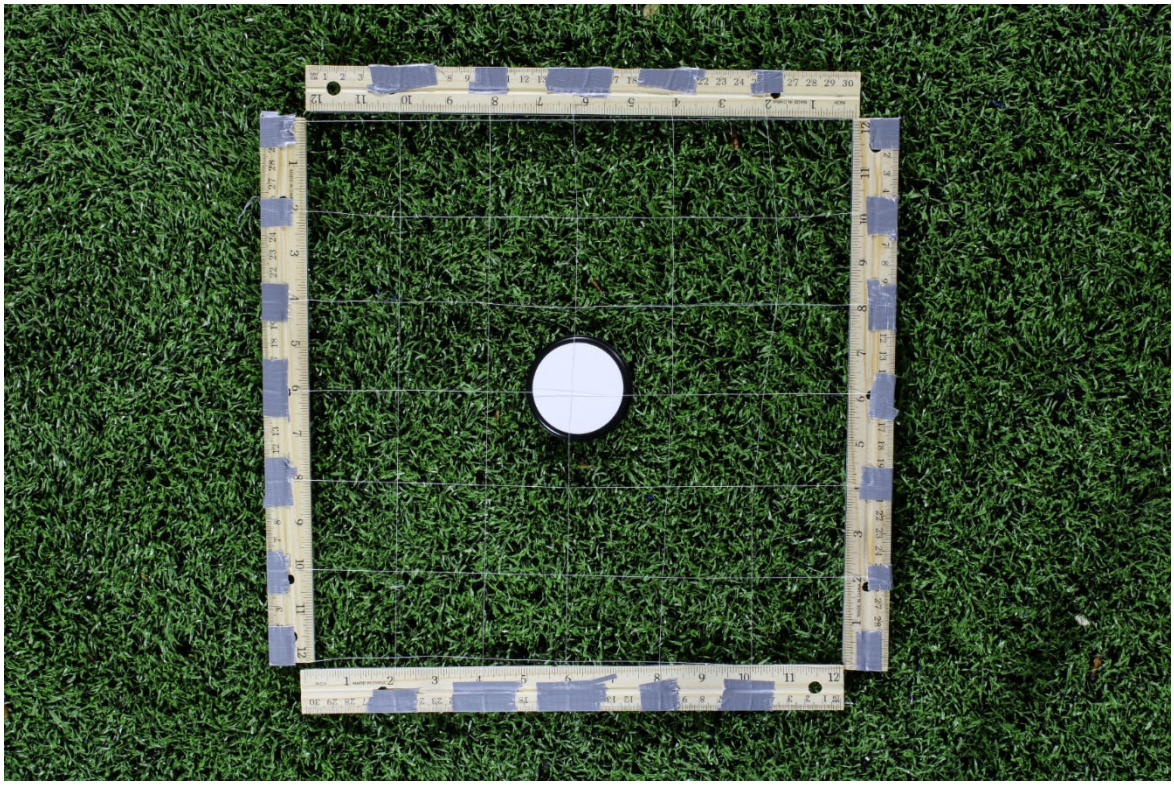

Figure 46. Camera View, with reflectance standard and grid centered, from Final Data Collection

3. The camera and mobile phone were then connected through the Canon Camera Connect mobile app through the directions on the app. Once connected, ‘Remote live view shooting’ was chosen in the app. Before taking any low dynamic range images, it was ensured that the legs of the tripod did not obstruct the camera lens’ view from anything inside the square grid.
4. The settings of the camera were adjusted to aperture f/5.6, ISO 100 and white balance set to daylight for the sequence of low dynamic range images.
5. A single low dynamic range image was then taken at a mid-range shutter speed (1/2s or 1s) to capture the square grid and reflectance standard set up.

6. Reference illuminance measurements were taken using the Konica Minolta CL-70F illuminance meter. The meter was placed in the center of each individual grid tile to record an illuminance measurement, using a 15s measurement setting to allow the researcher to place the meter and then step away to avoid effecting the measurement. Each grid was named in the style ‘A1, A2, A3 …… B1, B2, B3 …….’ for future reference when comparing data points.

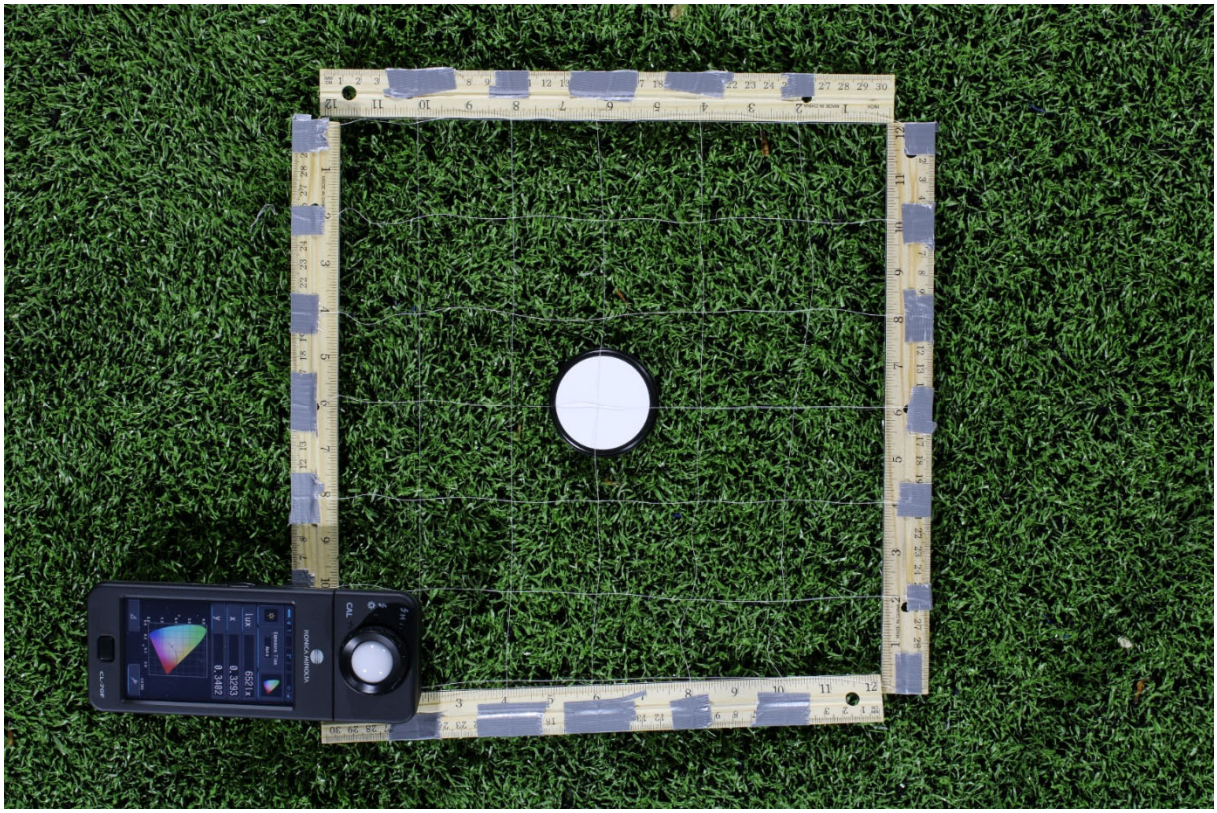

Figure 47. Konica-Minolta CL-70F Illuminance Meter recording measurements at the center of each grid in Final Data Collection

7. Following the illuminance readings at each data point, the square grid was removed and set to the side, out of the camera’s frame of view. This is removed to reduce any additional unnecessary and undesired noise in the images that would affect the luminance and illuminance values.
8. A Minolta LS-100 luminance meter then took a measurement of the reflectance standard. This was done focusing the luminance meter on the reflectance standard until the measurement reading starts to settle around a final number. This final number was be noted

for later calibrations. It is imperative the researcher taking this measurement did not get too close to the reflectance standard to obstruct any nearby illuminance and negatively affect the validity of the luminance meter reading. To make this less time consuming and more accurate, the researcher remained as still as possible when focusing on the reflectance standard.

9. A series of low dynamic ranges images was then taken starting from the shortest shutter speed to the longest. This sequence will be conducted in 1-stop increments to total 18 jpegs with the following shutter speeds: 1/4000s, 1/2000s, 1/1000s, 1/500s, 1/250s, 1/125s, 1/60s, 1/30s, 1/15s, 1/8s, 1/4s, 1/2s, 1s, 2s, 4s, 8s, 15s, 30s. Before moving on, ensure all shutter speeds are accounted for.
10. Steps 1-9 may be repeated if data is being collected in multiple locations.
11. The SD card was then taken from the camera and inserted into a 2013 MacBook Pro with the Photosphere program open. All 18 jpegs were loaded into Photosphere by simply dragging them from the SD card folder to the open Photosphere 'Folder' tab. These individual jpegs were also saved in another folder before being deleted off the SD card.
12. In Photosphere, selecting all useful Jpegs and 'Make HDR' under 'File', an options box emerged and both 'Remove Lens Flare' and 'Remove Ghosts' were chosen. The final HDR only took a few moments to create.
13. Once the final HDR emerges in a new window, it was saved before moving on to the next step. The image was saved in TIFF format and RGBE format.
14. To calibrate the final HDR image, the center of the reflectance standard was selected, then 'Calibrate" under the 'Apply' menu in the upper left was selected. A box emerged allowing the true luminance value to be calibrated. Following, a second box emerged asking if applying a calibration factor to the whole image is correct – yes was selected. This calibration factor should be around 1.
15. Once calibrated, the true luminance measurements at the center of each grid were retrieved by simply moving the cursor to the desired spot. These true luminance values were recorded for each individual grid tile.
16. The final HDR image was then transformed into a false color image by selecting 'Edit' and then 'False Color', this false color image was saved as well.

17. The luminance values obtained from Photosphere's HDR image turned luminance map then followed the mathematical process and equations explained previously to convert into illuminance measurements.
18. The derived illuminance values were then compared to the original Nano-Lambda spectrometer's illuminance readings taken at the scene. A percent error was recorded for each individual data point, using the spectrometer's original reading as the correct measurement.

4.0 DATA COLLECTION

Several series of data were collected to ensure proper methodology. The series are broken down as follows:

4.1 *EQUIPMENT EVALUATION - INDOORS*

An equipment evaluation was conducted indoors in the lighting lab of Lawrence Technological University to test both the methodology and technology that would be used later. The lighting lab is not exposed to any daylight, only a combination of several types of LED fixtures illuminate the space. A Canon EOS 2000D digital camera was mounted to a tripod extended as tall as it could reach. The camera was then fixed at the top of the tripod, pointing straight down at 90 degrees relative to the floor. A 99% diffuse reflectance standard was placed in the field of view of the camera for future luminance calibration. A Minolta LS-110 luminance meter was used to measure the luminance at the diffuse reflectance standard, measuring approximately 180 cd/m^2.

The camera was connected through WiFi to the Cannon Camera Connect app on the researcher's iPhone. The app allows photos to be taken remotely while being able to adjust camera settings without the need to dismount and remount the camera following every photo. This step, as previously discussed, is vital to the integrity and consistency of the final HDR image; the most accurate HDR image and thus the most accurate data comes from no movement, "noise" or changes in the LDR photos. For this same reason, the researchers remained still and in the same positions throughout the entire data collection process to present a consistent scene in the photo frame.

A series of 18 low dynamic range images, JPEGs, were taken with the following shutter speed values; 1/4000s, 1/2000s, 1/1000s, 1/500s, 1/250s, 1/125s, 1/60s, 1/30s, 1/15s, 1/8s, 1/4s, 1/2s, 1s, 2s, 4s, 8s, 15s, 30s. The camera aperture was consistently set to f 5.6, ISO 100, daylight white balance and a Cannon EFS 18-55mm lens was used. The square was not placed for this data collection, the reflectance standard was not centered in the frame of view, nor was the final HDR image cropped into a square; these methods would be imposed later in the data collection process as this first pilot study was to ensure the technology functioned properly. The camera's SD card was then loaded into a 2013 MacBook Pro to be used in the HDR image builder Photosphere program.

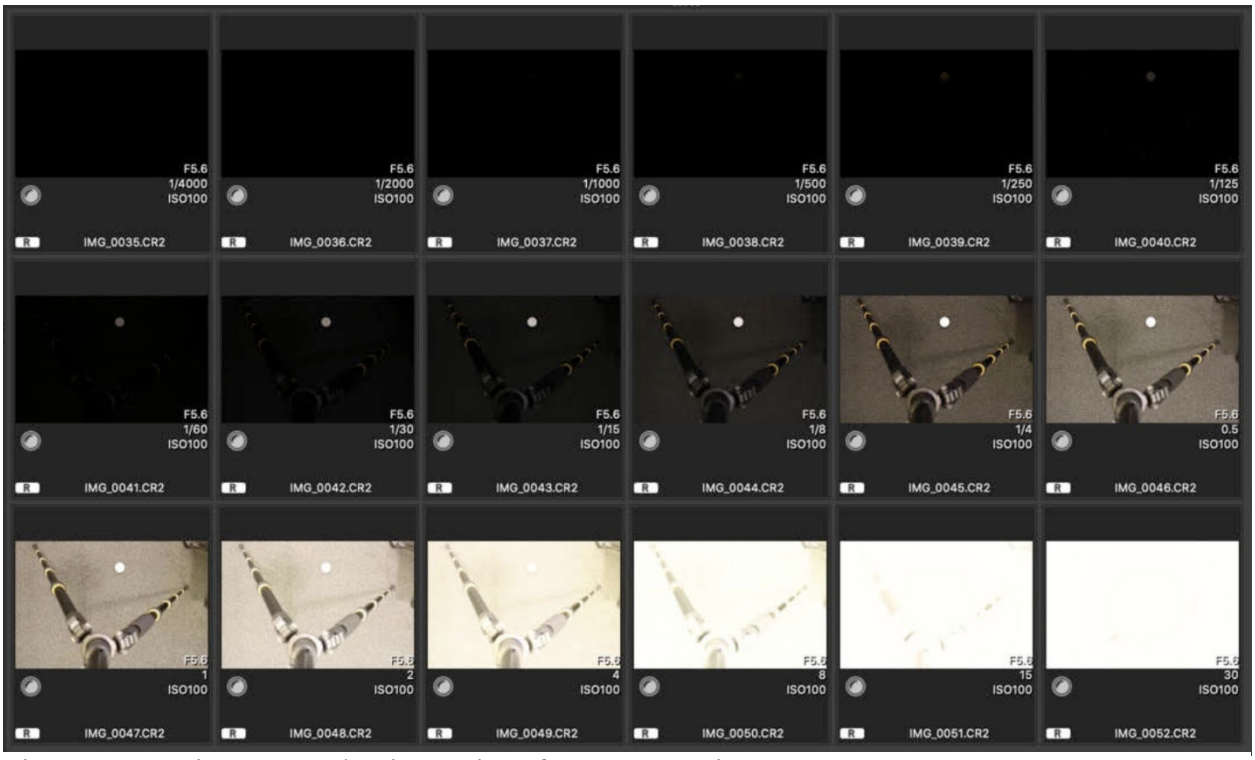

Figure 48. Equipment Evaluation series of Low Dynamic Range Images

The low dynamic range images shown in Figure 48 were fused into a final HDR shown in Figure 49. The HDR creation features utilized in for this final HDR image include automatic lens flare removal and ghost removal. As this is only the first test of the technology and methodology, this photo was not cropped. Therefore, some effects of vignetting may be present.

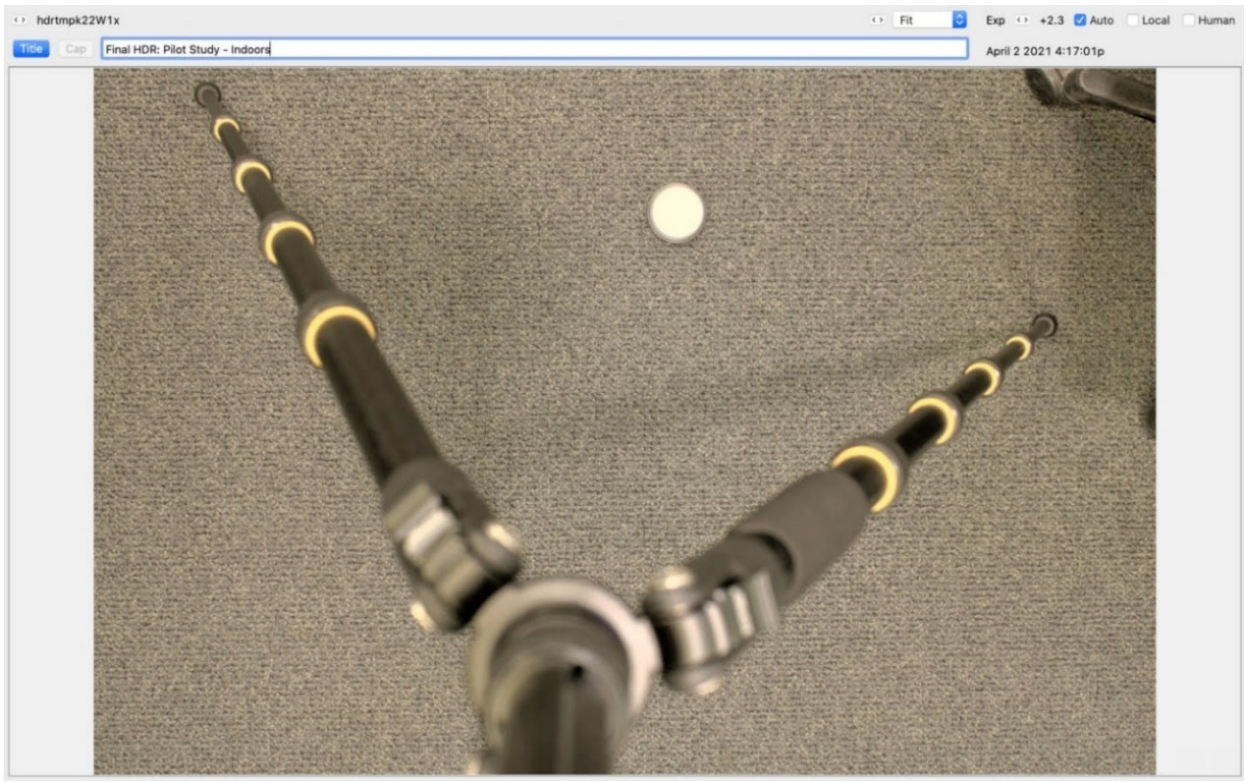

Figure 49. Final HDR Image: Equipment Evaluation

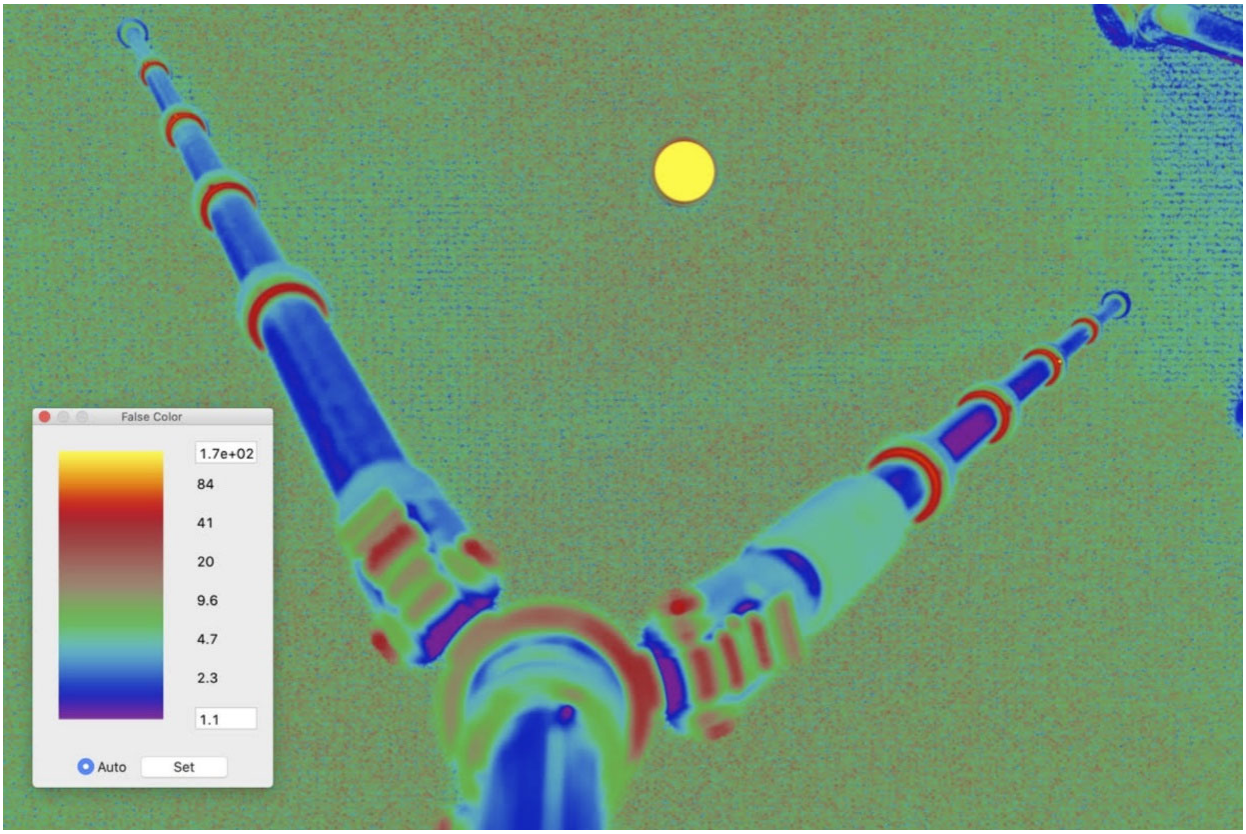

Figure 50. Equipment Evaluation False Color Image

Following the creation of the final HDR image, the image was then calibrated in Photosphere by assigning the luminance of the reflectance standard to be 180 cd/m^2. All other pixels in this final HDR image were then adjusted based on this assignment. The original luminance of the reflectance standard in the HDR image was found to be 172.2 cd/m^2, meaning the entire image was calibrated with a 1.04533 factor. The final HDR image was converted into a false color image as seen in Figure 50. A 2-inch by 2-inch grid was then overlaid on the photo, shown in Figure 51, with measurements based off of the 2-inch diameter of the reflectance standard in the frame of view. The gridline intersection points were then located in Photosphere and the individual luminance measurements were recorded in Table 4.

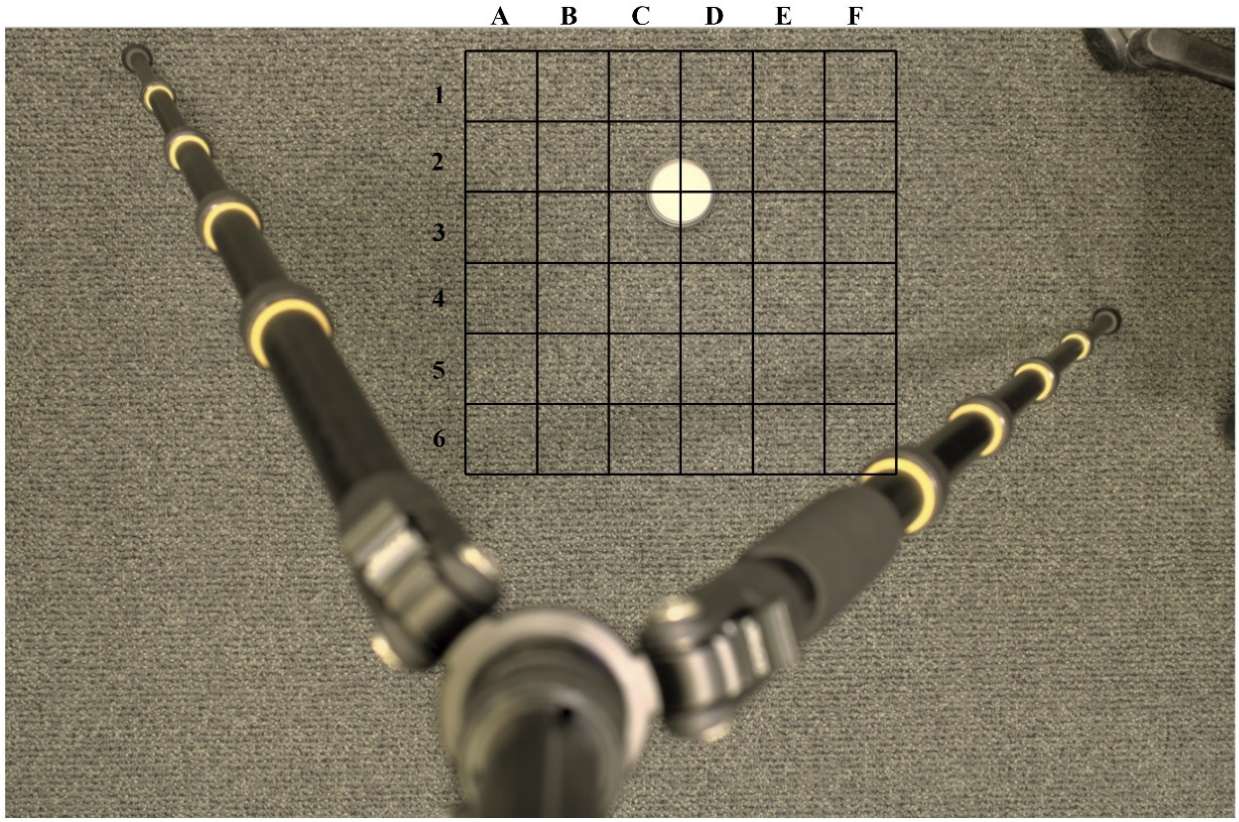

Figure 51. Equipment Evaluation Final HDR Image with Grid Overlay

Table 4. Equipment Evaluation HDRI Luminance Map Values from Photosphere (in cd/m^2)

	A	**B**	**C**	**D**	**E**	**F**
1	12	10.2	11.1	10.3	9.34	10.2
2	10	9.31	16.1	45.3	10.2	9.52
3	8.73	9.35	11.2	9.34	10.8	10.5
4	8.65	8.81	10.9	11.3	10.3	10.2
5	9.08	9.74	10.6	11	8.08	9.74
6	9.15	9.4	9.68	9.41	10.1	8.81

As no illuminance meter was present in the equipment evaluation, no true illuminance values were recorded. The equipment evaluation methodology proved successful and further pilot studies and data collection will mirror this process and continue to validate illuminance values obtained in the HDRI-acquired luminance map.

4.2 *PILOT STUDY – OUTDOORS*

A pilot study was conducted outdoors on grass to verify the previously used technologies and data collection methodologies would still work in a setting closer to the final data collection scenario. Both locations are near the bridge connecting the architecture building and the engineering building on Lawrence Technological University's campus, location 1 was on the engineering building side of the walkway and location 2 was on the architecture building side of the walkway. At both locations, the camera setup in Figure 45 was used. A series of 11 low dynamic range images were taken at location 1 as shown in Figure 52; with shutter speeds 1/4000s, 1/1000s, 1/250s, 1/60s, 1/15s, 1/4s, 1s, 2s, 4s, 8s, 15s and 30s. A series of 10 low dynamic range images were taken at location 2 as shown in Figure 53; with shutter speeds 1/4000s, 1/1000s,

1/250s, 1/60s, 1/15s, 1/4s, 1s, 2s, 4s, 8s and 15s. Following, a final HDR image was made for each location.

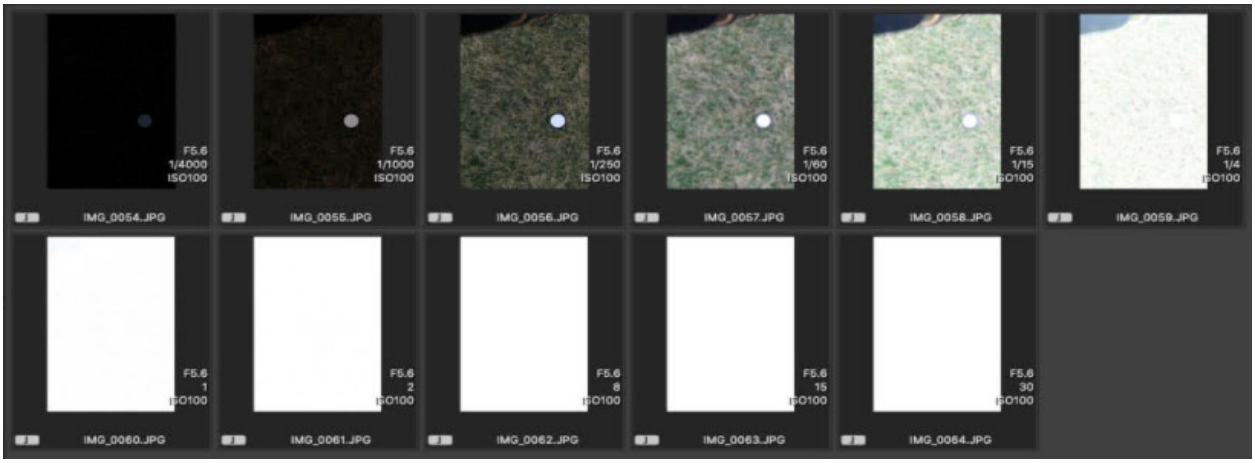

Figure 52. Pilot Study Outdoors Series of Low Dynamic Range Images – Location 1

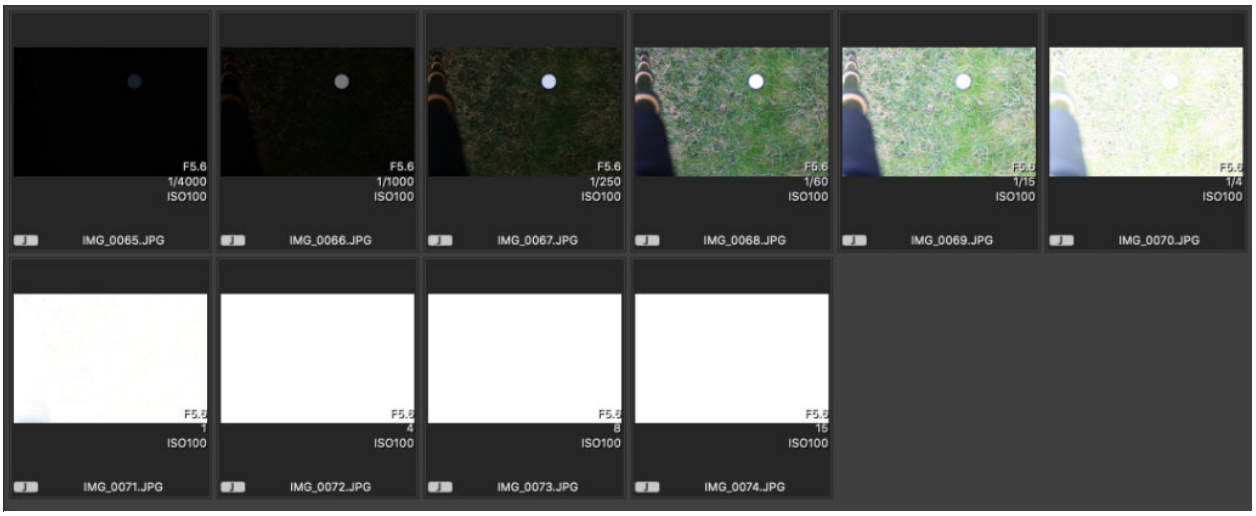

Figure 53. Pilot Study Outdoors Series of Low Dynamic Range Images - Location 2

Figure 54. Final HDR Image: Pilot Study Outdoors Location 1

Figure 55. Final HDR Image: Pilot Study Outdoors Location 2

While location 1's final HDR image, Figure 54, is high quality, location 2's final HDR image, Figure 55, is blurry due to wind blowing the grass while in the process of taking the low dynamic range images. As such, no luminance or illuminance data should be retrieved from this HDR image. Location 1's HDR image will be analyzed further in the same process as the equipment evaluation. Following the creation of the final HDR image, the image was then calibrated in Photosphere by assigning the luminance of the reflectance standard to be 1800 cd/m^2. All other pixels in this final HDR image were then adjusted based on this assignment. The original luminance of the reflectance standard in the HDR image was found to be 1817.05 cd/m^2, meaning the entire image was calibrated with a 0.991 factor. The final HDR image was converted into a false color image as shown in Figure 56. A 2-inch by 2-inch grid was then overlaid on the photo in Figure 57, with measurements based off of the 2-inch diameter of the reflectance standard in the frame of view. In future pilot studies and data collections, the reflectance standard will be located at the very center of the grid and the tripod legs will be kept out of the designated 1-foot by 1-foot measurement square. The individual measurement grids were then located in Photosphere and luminance measurements were retrieved from the final HDR image, shown in Table 5.

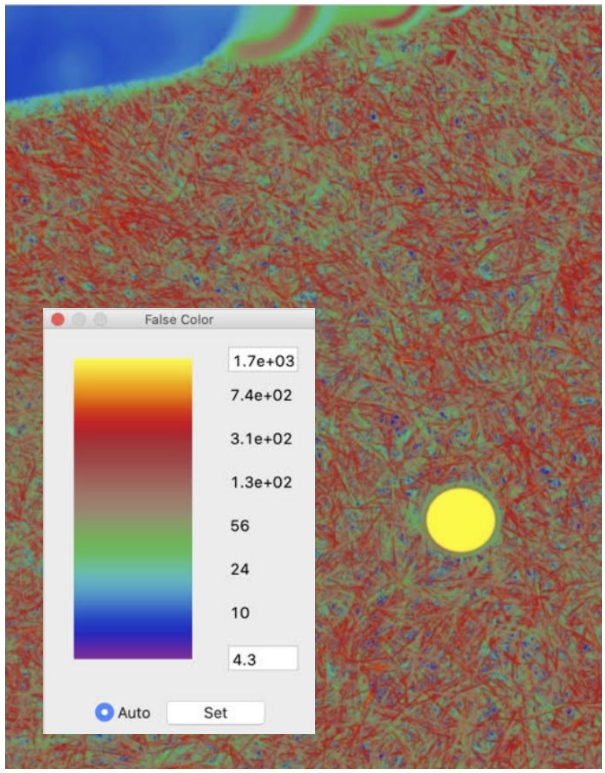

Figure 56. Pilot Study Location 1 False Color Image

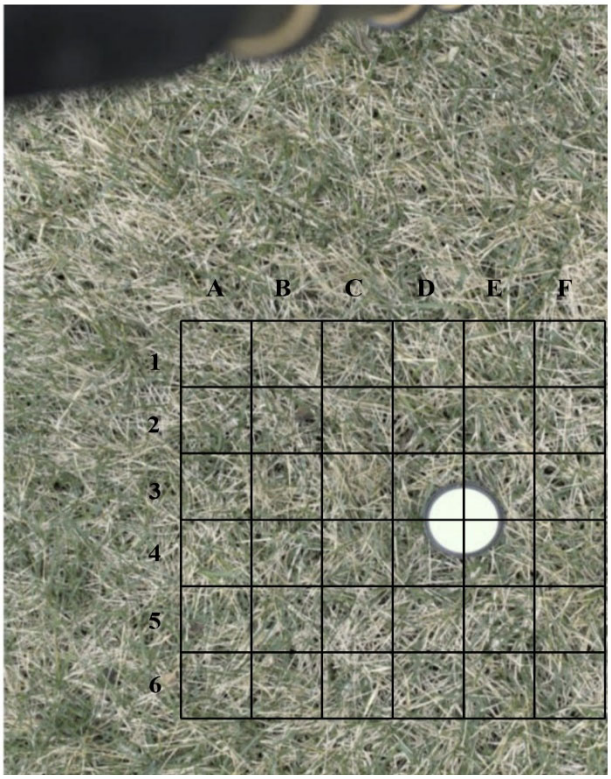

Figure 57. Pilot Study Location 1 Final HDR Image with Grid Overlay

Table 5. Pilot Study Location 1 HDRI Luminance Map Values from Photosphere (in cd/m^2)

	A	B	C	D	E	F
1	216	227	243	253	355	174
2	227	241	252	273	381	179
3	243	260	272	301	384	182
4	288	329	340	379	724	192
5	305	328	325	349	455	229
6	174	166	160	156	169	148

When comparing the luminance maps from the equipment evaluation to the pilot study, it can be seen that there is more variation in the false color image and in the luminance table. This variance is due to the combination of dead and healthy grass. The carpet in the indoor equipment evaluation proved to have more consistency. As no illuminance meter was present in the equipment evaluation, no true illuminance values were recorded. The methodology once again proved successful and future data collection will mirror this process and continue to validate illuminance values obtained in the HDRI-acquired luminance map.

4.3 *FINAL DATA COLLECTION*

The final data collection was conducted at the Lawrence Technological University football stadium at approximately 9:45pm to ensure complete night sky. The LED stadium lights were turned on to full production and the camera and tripod were set up directly between the 40-yard line and the 35-yard line as a mascot logo covers from the 40-yard line to center field. As seen previously in Figure 45, the camera and tripod were set up following the proper protocols. The reflectance standard and grid were centered in the frame as seen previously in Figure 46. A series of 18 low dynamic range images, JPEGs, were taken with the following shutter speed values; 1/4000s, 1/2000s, 1/1000s, 1/500s, 1/250s, 1/125s, 1/60s, 1/30s, 1/15s, 1/8s, 1/4s, 1/2s, 1s, 2s, 4s,

8s, 15s, 30s. The camera aperture was consistently set to f 5.6, ISO 100, daylight white balance and a Cannon EFS 18-55mm lens was used. A series was taken with the grid in place and without the grid in place as well, seen in Figures 58 and 59.

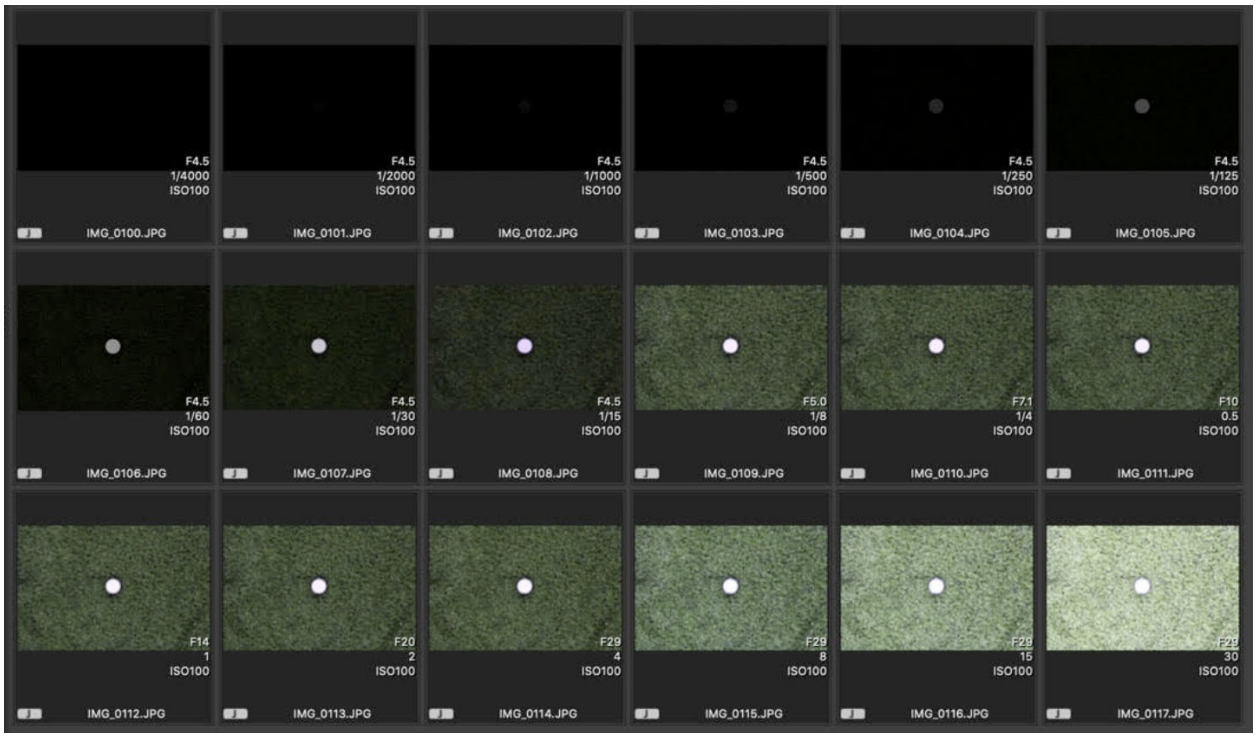

Figure 58. Final data collection series of low dynamic range images with grid present.

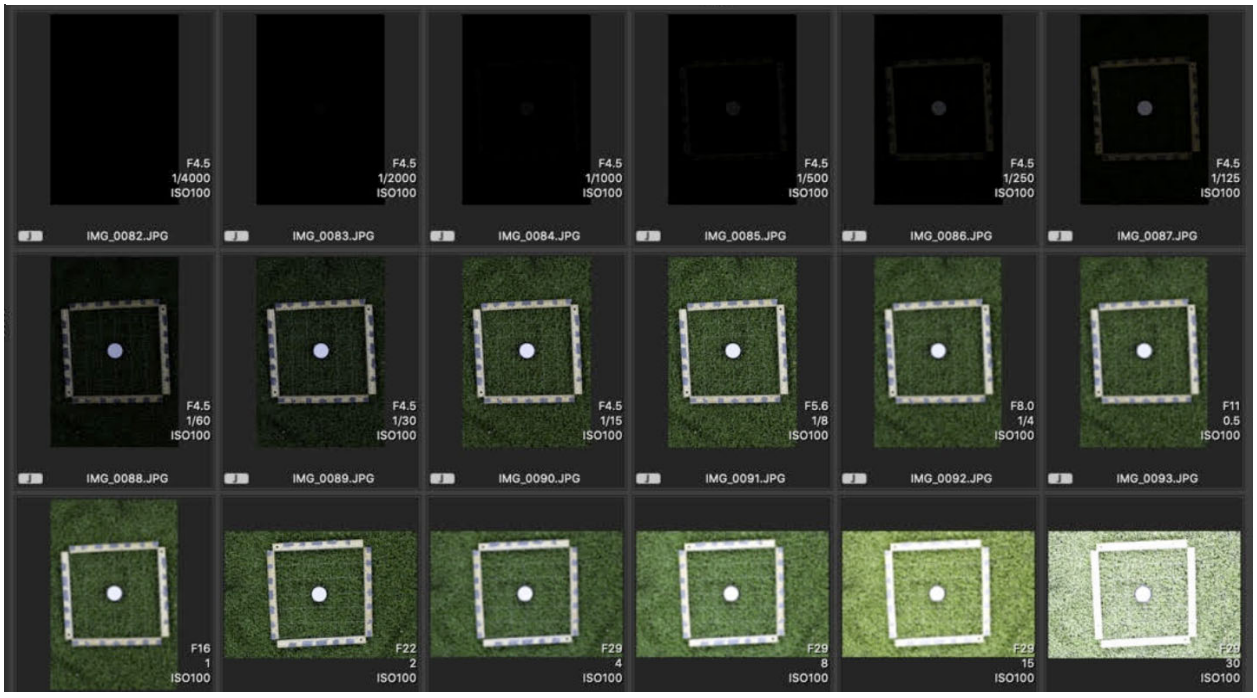

Figure 59. Final data collection series of low dynamic range images without grid present.

Figure 60. Final HDR Image

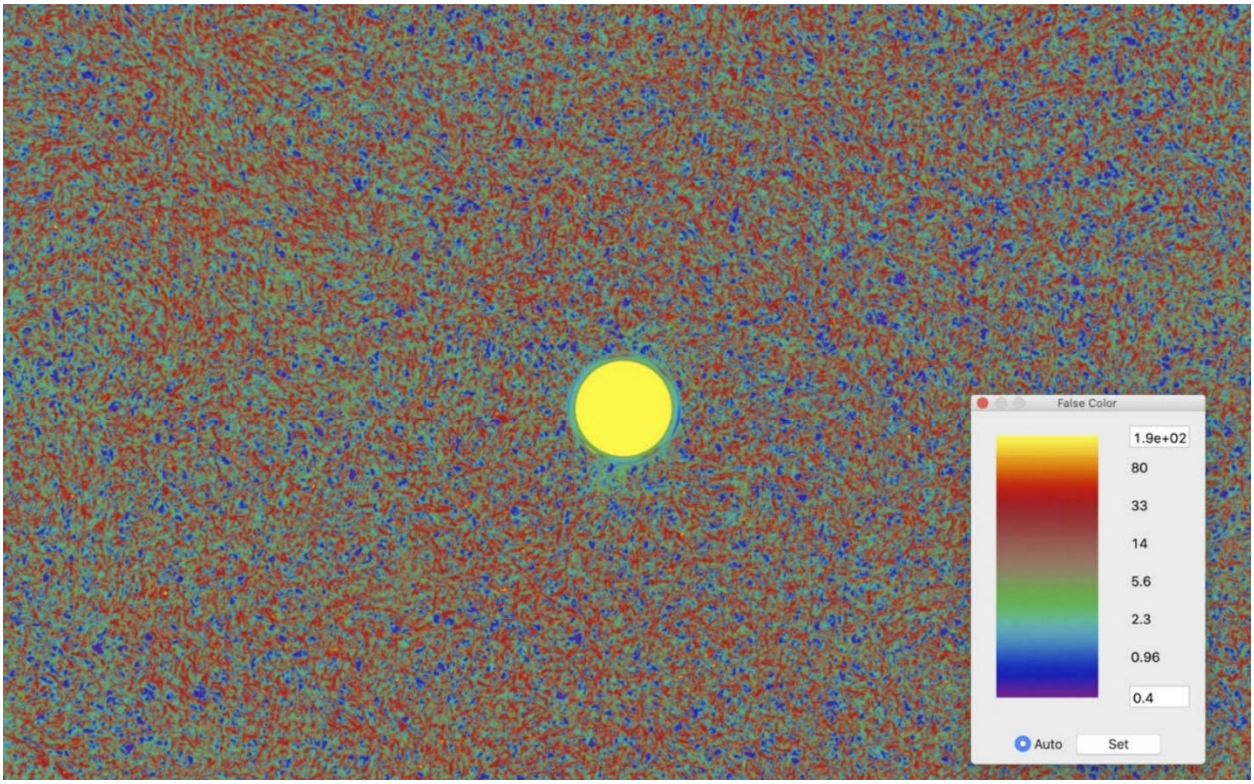

Figure 61. Final Data Collection False Color Image

The low dynamic range images were fused into a final HDR in Figure 60. The HDR creation features utilized in for this final HDR image include automatic lens flare removal and ghost removal. Following the creation of the final HDR image, the image was then calibrated in Photosphere by assigning the luminance of the reflectance standard to be 193.8 cd/m^2. All other pixels in this final HDR image were then adjusted based on this assignment. The original luminance of the reflectance standard in the HDR image was found to be 183.7 cd/m^2, meaning the entire image was calibrated with a 1.061 factor. The final HDR image was also converted into a false color image. The measurement grids were then located in Photosphere and the individual luminance values were retrieved from the final HDR image in Table 6.

Table 6. Final Data Collection Luminance Map Values from HDRI in Photosphere (in cd/m^2)

	A	**B**	**C**	**D**	**E**	**F**
1	30.5	32.7	31.2	31.3	32	31.1
2	30.7	31.4	29.8	31.2	31.7	31.6
3	31.9	33	30	31	32.3	29.5
4	28.4	30.7	29.9	30.6	29.7	28.2
5	29.1	31.2	31.3	31.5	29.9	30.8
6	32.3	32.1	31.5	33.5	33.3	32.4

As illuminance values were recorded at the scene, as seen previously in Figure 47, an illuminance map was compiled as well. Following the retrieval of luminance values in Photosphere, the previously outlined methodology of calculating illuminance from luminance values will be used. Once these illuminance values are derived from the HDRI-acquired luminance values, the percent error from the correct illuminance values, in Table 7, will be calculated.

Table 7. Illuminance Measurements taken from Illuminance Meter on Scene (in lux)

	A	B	C	D	E	F
1	648	649	646	646	647	646
2	648	646	645	645	648	647
3	654	649	647	649	649	649
4	617	646	646	649	651	647
5	583	647	645	650	650	640
6	652	645	651	655	633	650

Table 8. Illuminance Calculations using methodology with HDRI luminance values (in lux)

	A	B	C	D	E	F
1	598.6	641.7	612.3	614.3	628	610.3
2	602.5	616.2	584.8	612.3	622.1	620.2
3	626	647.6	588.8	608.4	633.9	578.9
4	557.4	602.5	586.8	600.5	582.9	553.4
5	571.1	612.3	614.3	618.2	586.8	604.5
6	633.9	610.3	618.2	657.4	653.5	635.9

Using the typical percent error formula, the percent error of each individual grid was calculated by:

$$\delta = \left| \frac{v_A - v_E}{v_E} \right| \cdot 100\% \qquad (18)$$

δ = percent error
v_A = actual value observed
v_E = expected value

Table 9. Illuminance Percent Errors for Each Grid

	A	B	C	D	E	F
1	-8%	-1%	-5%	-5%	-3%	-6%
2	-7%	-5%	-9%	-5%	-4%	-4%
3	-4%	0%	-9%	-6%	-2%	-11%
4	-10%	-7%	-9%	-7%	-10%	-14%
5	-2%	-5%	-5%	-5%	-10%	-6%
6	-3%	-5%	-5%	0%	3%	-2%

Table 10. Percent Error for Each Grid (green = < 5%, yellow = 5% < value < 10%, red = >10%)

	A	B	C	D	E	F
1	-8%	-1%	-5%	-5%	-3%	-6%
2	-7%	-5%	-9%	-5%	-4%	-4%
3	-4%	0%	-9%	-6%	-2%	-11%
4	-10%	-7%	-9%	-7%	-10%	-14%
5	-2%	-5%	-5%	-5%	-10%	-6%
6	-3%	-5%	-5%	0%	3%	-2%

It can be seen in both Table 9 and Table 10 that 34/36 grid measurement points proved less than 10% error, validating the accuracy of the proposed method in estimating illuminance values obtained from an HDR image in an exterior scene.

5.0 CONCLUSIONS AND FUTURE WORK

High dynamic range imaging is typically used for measurement of luminance and assistance in glare analysis. This study proved that HDR photography can also be used to estimate illuminance values obtained from an HDR image from an exterior scene. The camera-aided method developed and tested in this research successfully showed that an HDR image can determine the amount incident on an exterior surface made up on grass or turf. This method differs from other related work in that it estimates the illuminance values from a high dynamic range image taken from straight above it in an exterior scene with grass and turf. Other papers have researched the use of high dynamic range imaging to estimate luminance values and a select few have examined illuminance values. These papers, however, do not take place in an exterior scene.

Some of the larger errors presented in this research could be due to any number of possible confounding variables and conditions; the presence of small shadows in the camera frame of view, a possible larger concentration of turf pellets present in certain areas of the grid, the previously mentioned grass inconsistencies, among many other possibilities. The research is limited to only grass and turf, the validation on surfaces such as concrete or brick sidewalks in not examined in this study.

There are multiple takeaways from this research concerning how it can be used in the future, including the potential for more practical and commercial uses. As this methodology was proven accurate on a small scale, it can now be tested for larger applications. The traditional, time-consuming and intensive illuminance measurement process for sports stadiums can now be replaced by taking a series of low dynamic range images of the entire area. A drone flown above the facility can capture images that can later be run through the researched post processing methodology to retrieve lighting measurements of the entire field.

6.0 REFERENCES:

Anaokar, S., & Moeck, M. (2006). Validation of High Dynamic Range Imaging to Luminance Measurement. LEUKOS, 2(2), 133–144.

Andersen, M., Stokes, E., Gayeski, N., & Browne, C. (2010). Using digital imaging to assess spectral solar-optical properties of complex fenestration materials: A new approach in video–goniophotometry. Solar Energy, 84(4), 549–562.

Ashdown, I. (2002). Photometry and Radiometry - A Tour Guide for Computer Graphics Enthusiasts. Radiosity: A Programmer's Perspective.

Au, P., Donn, M., 2003. Hdr luminance measurements: comparing real and simulated data. In: Proceedings of 46th ANZAScA Conference of the Architectural Science Association

Barazzetti, L. (2014). High dynamic range photography without a tripod. *International Journal of Pervasive Computing and Communications*, *10*(2), 140–152.

Bellia, L., Cesarano, A., Iuliano, G.F., and Spada, G. (2009) "HDR luminance mapping analysis system for visual comfort evaluation," 2009 IEEE Instrumentation and Measurement Technology Conference, Singapore, 2009, pp. 957-961.

Bellia, L., Cesarano, A., Minichiello, F., & Sibilio, S. (2002). Setting up a CCD photometer for lighting research and design. *Building and Environment*, *37*(11), 1099–1106.

Bellia, L., Musto, M., & Spada, G. (2011). Illuminance measurements through HDR imaging photometry in scholastic environment. Energy and Buildings, 43(10), 2843–2849.

Bellia, L., & Spada, G. (2013). Photometric characterisation of small sources with high dynamic range illuminance mapping. Lighting Research & Technology, 46(3), 329–340.

Beltrán, L.O., Mogo, B.M. (2005). Assessment of luminance distribution using HDR photography, in: ISES, ISES Solar World Congress 2005, Orlando, FL, 2005.

Bruel and Kjaer (1978) Luminance Reflectances: Explanation and Calculation of Contrast. Bruel and Kjaer Instruments, Inc.

Cai, H. (2012). High dynamic range photogrammetry for synchronous luminance and geometry measurement. Lighting Research & Technology, 45(2), 230–257.

Cai, H. (2013a), “High dynamic range photogrammetry for light and geometry measurement”, AEI 2013: Building Solutions for Architectural Engineering-Proceedings of the 2013 Architectural Engineering National Conference, State College, PA, p. 544.

Cai, H. (2013b). Luminance gradient for evaluating lighting. Lighting Research & Technology,

48(2), 155–175.

Cai, H., & Chung, T. M. (2010). Improving the quality of high dynamic range images. Lighting Research & Technology, 43(1), 87–102.

Cai, H., & Chung, T.M. (2012). Evaluating discomfort glare from non-uniform electric light sources. Lighting Research & Technology, 45(3), 267–294.

Cai, H., & Li, L. (2014). Measuring Light and Geometry Data of Roadway Environments with a Camera. Journal of Transportation Technologies, 04(01), 44–62.

Cai, H., Papamichael, K., Inanici, M., et. al. (2017). "Application of High Dynamic Range Imaging in Daylighting Practice: An Outline for a Motion to Set Up a New HDRI Sub-Committee."

Chung, T., & T.H. NG, R. (2010). Variation of Calibration Factor over Time for High Dynamic Range Photography in a Single Daylit Interior Scene. Journal of Light & Visual Environment, 34(2), 87–93.

Chiou, Y.-S., & Huang, P.-C. (2015). An HDRi-based data acquisition system for the exterior luminous environment in the daylight simulation model. Solar Energy, 111, 104–117.

Coyne, S., Isoardi, G., Hiring, M. (2008) The Use of High Dynamic Range Luminance Mapping, Understanding and Defining of Visual Issues in Post Occupancy Building Assessments, International energy and efficiency in commercial building (IEECB'08), Frankfurt, 10–11 April, 2008.

Debevec, P. and Malik, J. (1997). Recovering high dynamic range radiance maps from photographs. Computer Graphics, 31:369–378

DiLaura, D. L. (2011). The Lighting Handbook: Reference and Application (10th ed.). Illuminating Engineering Society of North America, New York NY.

Gayeski, N., Stokes, E., & Andersen, M. (2009). Using digital cameras as quasi-spectral radiometers to study complex fenestration systems. Lighting Research & Technology, 41(1), 7–25.

Hiscocks PD (2011) Eng P. Measuring luminance with a digital camera. Syscomp Electronic Design Limited; 2011.

Inanici, M. N. (2006a). Evaluation of high dynamic range photography as a luminance data acquisition system. Lighting Research & Technology, 38(2), 123–134.

Inanici, M. N., & Navvab, M. (2006b). The Virtual Lighting Laboratory: Per-pixel Luminance

Data Analysis. LEUKOS, 3(2), 89–104.

Inanici, M.N. (2010). Evaluation of High Dynamic Range Image-Based Sky Models in Lighting Simulation. *LEUKOS*, *7*(2), 69–84.

Inanici M, Galvin J. 2004. Evaluation of high dynamic range photography as a luminance mapping technique. Berkeley (CA): Lawrence Berkeley National Laboratory.

Inkarojrit, V. (2005) Balancing Comfort: Occupants' Control of Window Blinds in Private Offices (Ph.D.), Centre for the Built Environment University of California, Berkeley, Berkeley, CA, 2005.

Jacobs A. 2007. High dynamic range imaging and its application in building research. Adv Build Energy Res. 1(1):177–202.

Jacobs A. 2012. Glare measurement with hdr photography. 11th International Radiance Workshop. Copenhagen, Denmark. 10.1094/PDIS-11-11-0999-PDN

Jacobs, A., & Wilson, M. (2007) "Determining Lens Vignetting with HDR Techniques," in Bulgarian National Lighting Conference Varna, 2007.

Jacobs, A., Wittkopf, S., Grobe, L. (2008) Per-pixel sky luminance with HDR photography. 7th International Radiance Workshop Fribourg, 2008

Kaufman, J. E. (2020). IES lighting handbook: The standard lighting guide. New York: Illuminating Engineering Society.

Kim, M., Konstantzos, I., & Tzempelikos, A. (2020). Real-time daylight glare control using a low-cost, window-mounted HDRI sensor. Building and Environment, 177, 106912. https://doi.org/10.1016/j.buildenv.2020.106912

Konis, K., Lee, E. S., & Clear, R. D. (2011). Visual Comfort Analysis of Innovative Interior and Exterior Shading Systems for Commercial Buildings using High Resolution Luminance Images. LEUKOS, 7(3), 167–188.

Kruisselbrink, T. (2020). Practical and Continuous Luminance Distribution Measurements for Lighting Quality.

Kruisselbrink, T., Aries, M., & Rosemann, A. (2017). A Practical Device for Measuring the Luminance Distribution. International Journal of Sustainable Lighting, 19(1), 75–90.

Kruisselbrink, T., Dangol, R., & Rosemann, A. (2018). Photometric measurements of lighting quality: An overview. Building and Environment, 138, 42–52.

Kumaragurubaran V, Inanici M. (2013) Hdrscope: high dynamic range image processing toolkit

for lighting simulations and analysis. In: Proceedings of IBPSA 2013: 13th conference of International Building Performance Simulation Association, Chambery, France; 2013.

Mahoney, E. (2019) Using Luminance for Design and Evaluation of Energy Efficient and Sustainable Luminous Environments to Supplement Current Illuminance-Based Design Codes. Master's Thesis, University of Kansas, Lawrence, KS, USA, 2019.

Mardaljevic, J., Cannon-Brookes, S., Blades, N., & Lithgow, K. (2020). Reconstruction of cumulative daylight illumination fields from high dynamic range imaging: Theory, deployment and in-situ validation. Lighting Research & Technology, 147715352094575.

Mardaljevic, J., Painter, B., & Andersen, M. (2009). Transmission illuminance proxy HDR imaging: A new technique to quantify luminous flux. Lighting Research & Technology, 41(1), 27–49.

Mardaljevic J, Brembilla E and Drosou N. (2015) Illuminance proxy high dynamic range imaging: a simple method to measure surface reflectance. In: 28th session of the international commission on illumination. Manchester: International Commission on Illumination,

Moeck, M. (2007). Accuracy of Luminance Maps Obtained from High Dynamic Range Images. LEUKOS, 4(2), 99–112.

Moeck, M., & Anaokar, S. (2006). Illuminance Analysis from High Dynamic Range Images. LEUKOS, 2(3), 211–228.

Moore, T., Graves, H., Perry, M. J., & Carter, D. J. (2000). Approximate field measurement of surface luminance using a digital camera. Lighting Research and Technology, 32(1), 1–11.

Nahrkhalaji, R. (2017). Study of Building Surrounding Luminous Environment using High Dynamic Range Image-Based Lighting Model. Doctoral dissertation, The Pennsylvania State University.

Nasrollahi, N., & Shokri, E. (2016). Daylight illuminance in urban environments for visual comfort and energy performance. Renewable and Sustainable Energy Reviews, 66, 861–874. https://doi.org/10.1016/j.rser.2016.08.052

Nath, D., Mazumdar, S., Chandra, J. K., & Bag, A. K. (2015). A rough set-based method for aiming angle tuning of luminaires for outdoor sports lighting. Lighting Research & Technology, 48(2), 126–154.

Newsham, G. R., & Arsenault, C. (2009). A camera as a sensor for lighting and shading control. Lighting Research & Technology, 41(2), 143–163.

Pierson C, Wienold J, Jacobs A, Bodart M. 2017b. Luminance maps from high dynamic range imaging: calibrations and adjustments for visual comfort assessment. Paper presented at: Lux Europa 2017. Ljubljana, Slovenia.

Poling, R.M. (2018) A new method for calculating luminous flux using high dynamic range imaging and its applications (Master's thesis).

Poling, R. M., & Cai, H. (2020). Calculating luminous flux radiated to a camera lens via high dynamic range photogrammetry. Lighting Research & Technology, 147715352092144.

Rea MS, Jeffrey I. 1990. A new luminance and image analysis system for lighting and vision I – Equipment and calibration. LEUKOS. 19(1):64–72.

Reinhard, E., Ward, G., Pattanaik, S., Debevec, P., Heidrich, W., & Myszkowski, K. (Eds.). (2010). High Dynamic Range Imaging: Acquisition, Display, and Image-based Lighting (2. ed.). Burlington, MA: Elsevier (Morgan Kaufmann).

Robertson, M. A. (2003). Estimation-theoretic approach to dynamic range enhancement using multiple exposures. Journal of Electronic Imaging, 12(2), 219.

Robertson, M.A., Borman, S., and Stevenson, R.L. (1997) ''Dynamic range improvement through multiple exposures,'' Int. Conf. Image Process. 3, 159–163 ~1999!.

Ryer, A. (1997). Light Measurement Handbook. International Light.

Safranek, S. (2017) A Comparison of Techniques Used for the Removal of Lens Flare Found in High Dynamic Range Luminance Measurements, University of Colorado Boulder

Safranek, S., & Davis, R.G. (2020) Sources of Error in HDRI for Luminance Measurement: A Review of the Literature, LEUKOS

Sielachowska, M.; Tyniecki, D.; Zajkowski, M. (2019) The Concept of Measuring Luminous Flux Distribution Emitted from Sports Facilities Using Unmanned Aerial Vehicles. In Methods and Techniques of Signal Processing in Physical Measurements; Hanus, R., Mazur, D., Kreischer, C., Eds.; MSM 2018, Lecture Notes in Electrical Engineering; Springer: Cham, Switzerland, 2019; Volume 548.

Spectral Reflectance. (2019). http://gsp.humboldt.edu/OLM/Courses/GSP_216_Online/lesson2-1/reflectance.html#:~:text=Water,infrared%20wavelengths%20range%20and%20beyond.

Stanley MJ. 2016. On the development and error analysis of a high dynamic range imaging system for luminance measurements [Master thesis]. Boulder (CO): University of Colorado Boulder.

Stumpfel, J., Jones, A., Wenger, A., Tchou, C., Hawkins, T., and Debevec, P. (2006) Direct HDR capture of the sun and sky. In ACM SIGGRAPH 2006 Courses (SIGGRAPH '06). Association for Computing Machinery, New York, NY, USA, 5–es.

Suk, J. Y., Schiler, M., & Kensek, K. (2013). Development of new daylight glare analysis methodology using absolute glare factor and relative glare factor. Energy and Buildings, 64, 113–122.

Tabaka, P. (2020). Pilot Measurement of Illuminance in the Context of Light Pollution Performed with an Unmanned Aerial Vehicle. Remote Sensing, 12(13), 2124.

Tural, M. (2011) A diagnostic tool for assessing lighting in buildings: investigating luminance contrast relationships through high-dynamic-range image-based analysis. Doctoral dissertation. Tempe, AZ: Arizona State University; 2011.

Tyukhova, Y., & Waters, C. (2013). An Assessment of High Dynamic Range Luminance Measurements with LED Lighting. LEUKOS, 10(2), 87–99.

Varghese D, Wanat R, Mantiuk R. (2014) Colorimetric calibration of high dynamic range images with a ColorChecker chart. Paper presented at: HDRi 2014 Second International Conference and SME Workshop on HDR imaging 2014:17-22

Ward G, Shakespeare R. 1997. Rendering with Radiance. California: Morgan Kaufman Publishers. 664 p.

Ward G. 1994. The Radiance lighting simulation and rendering system. Proceedings of SIGGRAPH 94, Computer Graphics Proceedings, Annual Conference Series. 459–572.

Ward G. 1987. Radiance. [accessed 2021 March]. https://radiance-online.org//.

Ward G. 1998. Findglare command (Radiance). [accessed 2017 Sept 27]. http://radsite.lbl.gov/radiance/man_html/ findglare.1.html.

Ward G. 1998. hdrgen. [accessed 2021 March]. http://www.anyhere.com/.

Ward G. 2005. Photosphere. http://www.anyhere.com/ Accessed 2010 July 29.

Ward G. 2011. Raw2hdr perl script. [accessed 2021 March]. http://www. anyhere.com/gward/pickup/raw2hdr.tgz .

Ward G. 2016. Fisheye_corr.Cal file. [accessed 2021 March]. https://www.radiance-online.org/cgi-bin/viewcvs.cgi/ray/src/cal/cal/fisheye_corr.cal.

Wen, B. (2015). Reflectance standards. Encyclopedia of Color Science and Technology, 1-4. doi:10.1007/978-3-642-27851-8_360-1

Wienold J, Andersen M. 2016. Evalglare 2.0 – new features faster and more robust hdr-image evaluation. Paper presented at: 15th International Radiance Workshop. Padua, Italy.

Wolska, A., & Sawicki, D. (2020). Practical application of HDRI for discomfort glare assessment at indoor workplaces. Measurement, 151, 107179.

Wuller, D.; Gabele, H. (2007) The usage of digital cameras as luminance meters. In Proceedings of the SPIE Digital Photography III Conference, San Jose, CA, US, Jan 29-30 2007; pp. 650201:1-650201:11.

Yamín Garretón, J., Villalba, A. M., Rodriguez, R. G., & Pattini, A. (2021). Roller blinds characterization assessing discomfort glare, view outside and useful daylight illuminance with the sun in the field of view. Solar Energy, 213, 91–101.

Yun, S.-I., & Kim, K.-S. (2018). Sky Luminance Measurements Using CCD Camera and Comparisons with Calculation Models for Predicting Indoor Illuminance. Sustainability, 10(5), 1556. https://doi.org/10.3390/su10051556

Zotti, G. (2007) "Measuring light pollution with a calibrated high dynamic range all-sky image acquisition system," presented at the DARKSKY2007—7th European Symposium for the Protection of the Night Sky, Bled, Slovenia (2007).

Zumtobel Lighting GmbH (2018) "The Lighting Handbook" – Schqeizer Strasse 30